Catalytic Study of Copper based Catalysts for Steam Reforming of Methanol

vorgelegt von
Diplom-Ingenieur
Herry Purnama
aus Medan

der Fakultät II – Mathematik und Naturwissenschaften-
der Technischen Universität Berlin
zur Erlangung des akademischen Grades
Doktor der Ingenieurwissenschaften
- Dr. Ing. -
genehmigte Dissertation

Promotionsausschuß:

Vorsitzender:	Prof. Dr. M. Lerch, TU Berlin
Berichter:	Prof. Dr. R. Schomäcker, TU Berlin
Berichter:	Prof. Dr. R. Schlögl, Fritz-Haber-Institut, Berlin

Tag der wissenschaftlichen Aussprache: 17. Dezember 2003

Berlin 2003

D 83

Abstract

The aim of this work is to study the catalytic properties of copper based catalysts used in the steam reforming of methanol. This method is known as one of the most favourable catalytic processes for producing hydrogen on-board. The catalysts investigated in this work are CuO/ZrO_2 catalysts, which were prepared using different kinds of preparation methods and a commercial $CuO/ZnO/Al_2O_3$ catalyst which was used as a reference. The results of the studies can be divided into three sections:

(i) The catalytic study reported in chapter 4 is focused on the investigation of the CO formation during steam reforming of methanol on a commercial $CuO/ZnO/Al_2O_3$ catalyst. The reaction schemes considered in this work are the methanol steam reforming (SR) reaction and the reverse water gas-shift (rWGS) reaction. The experimental results of CO partial pressure as a function of contact time at different reaction temperatures show very clearly that CO was formed as a consecutive product. The implications of the reaction scheme, in particular with respect to the production of CO as a secondary product, are discussed in the framework of onboard production of H_2 for fuel cell applications in automobiles. Potential chemical engineering solutions for minimizing CO production are outlined.

(ii) In chapter 5, the catalytic properties of a CuO/ZrO_2 catalyst synthesized by a templating technique were investigated with respect to activity, long term stability, CO formation, and response to oxygen addition to the feed. It is shown that, depending on the time on stream, the temporary addition of oxygen to the feed has a beneficial effect on the activity of the CuO/ZrO_2 catalyst. After activation, the CuO/ZrO_2 catalyst is found to be more active (per copper mass) than the $CuO/ZnO/Al_2O_3$ catalyst, more stable during time on stream, and to produce less CO.

(ii) In chapter 6, the study of the catalytic behaviours has been carried out on the six CuO/ZrO_2 catalysts. The catalysts were synthesized with different preparation methods, i.e. incorporation of CuO in ZrO_2-nanopowder, in mesoporous ZrO_2 and in macroporous ZrO_2. The activity of CuO/ZrO_2 catalysts can be improved by oxygen treatment. The catalysts which have been used in the reaction provide a much larger value of the S_a than the fresh catalysts. This indicates that the new CuO/ZrO_2 catalysts provide much higher stability with respect to the sintering of metal particles in comparison to the commercial $CuO/ZnO/Al_2O_3$ catalyst. The result concerning the increase of S_a correlates well with the increase of the activity of the used catalysts compared to the fresh catalysts. No linear correlation was found between the activity and copper surface area. However, the activity of the catalysts can be correlated with the preparation methods. In comparison to the commercial $CuO/ZnO/Al_2O_3$, the CuO/ZrO_2 catalysts are more active. The CO concentration determined as a function of methanol conversion shows very clearly that less amount of CO was formed over CuO/ZrO_2 catalysts than the commercial $CuO/ZnO/Al_2O_3$ catalyst.

Zusammenfassung

Im Rahmen meiner Promotion wurden die katalytischen Eigenschaften von kupferbasierten Katalysatoren für die Wasserstoff-Gewinnung aus Methanol untersucht. Die Katalysatoren wurden im Rahmen des gemeinsamen Projekts **„Nanochemie für eine zukünftige Automobiletechnik: Möglichkeit der Optimierung von kupferbasierten Katalysatoren für die on-board-Gewinnung von Wasserstoff aus Methanol“** auf verschiedenen Präparationswegen hergestellt. Das Projekt wird von ZEIT-Stiftung gefördert. Der kommerzielle Katalysator für das Steam-Reforming von Methanol ist der $CuO/ZnO/Al_2O_3$-Katalysator, der auch für die Methanolsynthese verwendet wird. Zwei wesentliche Nachteile dieses Katalysators sind die mangelnde Langzeitstabilität und die hohe Bildung von Kohlenmonoxid im Produkt, das hauptsächlich aus Wasserstoff und Kohlendioxid besteht. Es ist bekannt, dass Kohlenmonoxid ein Gift für die Pt-Elektrode in der Brennstoffzelle ist. Ein Ziel dieser Arbeit ist die Untersuchung der Bildung von CO bei der Nutzung des kommerziellen $CuO/ZnOAl_2O_3$ Katalysators, die als Grundlagen für die Entwicklung von neuen optimierten Reforming-Katalysatoren angewendet werden können. Es werden die katalytischen Eigenschaften von Cu/ZrO_2-Katalysatoren untersucht, die nach verschiedenen Methoden (Fällung, mesoporöses Trägermaterial, makroporöses Trägermaterial) hergestellt wurden. Zum Vergleich wurde der kommerzielle $CuO/ZnO/Al_2O_3$-Katalysator herangezogen. Diese Arbeit gliedert sich in 3 wesentliche Abschnitte.

Der erste Teil der Arbeit beinhaltet die ausführliche Untersuchung der CO-Bildung am kommerziellen $CuO/ZnO/Al_2O_3$-Katalysator und die Ermittlung von kinetischen Parametern. Es wird in der Literatur postuliert, dass die Bildung von CO durch die Spaltung von Methanol erfolgt und mit Wasser in der sogenannten Wassergas-Shift-Reaktion zu Kohlendioxid und Wasserstoff weiter reagiert. Die Ergebnisse der Experimente zeigen, dass die CO-Konzentration im Produktstrom mit zunehmender Verweilzeit in sigmoidaler Form zunimmt. Dies deutet darauf hin, dass CO in einer Folgereaktion gebildet wird. Die experimentellen Ergebnisse konnten mit einem kinetischen Modell mit guter Genauigkeit beschrieben werden, das reversible Methanol Steam-Reforming und die reverse Wassergas-Shift-Reaktion berücksichtigt. Es kann auch gezeigt werden, dass die CO-Bildung im Produktstrom durch Stofftransport-Limitierung im Katalysator beeinflusst werden kann. Je größer die Stofftransport-Hemmung in dem Partikel des Katalysators ist, desto größer ist die CO-Konzentration im Produkt. Da CO als Folgeprodukt in der reversen Wassergas-Shift-Reaktion gebildet wird, besteht die Möglichkeit, die CO-Bildung mit Hilfe einer geeigneten technischen Reaktionsführung zu unterdrücken.

In dem zweiten Teil der Arbeit wird der Vergleich der katalytischen Eigenschaften (Aktivität, Langzeitstabilität, CO-Selektivität und Einfluss von Sauerstoff auf die Aktivität) zwischen dem Cu/ZrO_2 Katalysator, der mit Hilfe einer Polymer-Templat-Methode (Cu auf makroporösem ZrO_2-Trägermaterial) hergestellt wurde, und dem kommerziellen $CuO/ZnO/Al_2O_3$-Katalysator durchgeführt. Der Cu/ZrO_2-Katalysator besitzt eine deutlich höhere Aktivität in Bezug auf die Cu-Oberfläche. Die Abhängigkeit der CO-Konzentration vom Methanol-Umsatz zeigte, dass der Cu/ZrO_2-Katalysator bei vergleichbarem Methanol-Umsatz weniger CO produziert. Es wurde auch festgestellt, dass die Langzeitstabilität der beiden Katalysatoren keinen signifikanten Unterschied aufweist. Es kann ferner gezeigt werden, dass Sauerstoff-Pulse ein wichtiger Schritt für die Aktivierung des Cu/ZrO_2-Katalysators sind.

Der dritte Teil der Arbeit umfasst die katalytischen Untersuchungen von sechs CuO/ZrO_2-Katalysatoren bezüglich ihrer Aktivität und Selektivität. Diese Katalysatoren wurden nach vier verschiedenen Präparationsmethoden hergestellt. Die Cu/ZrO_2-Katalysatoren müssen zuerst für eine längere Zeit im Reaktionsgemisch und mit mehrmaligen Sauerstoff-Pulsen aktiviert werden. Nach der Aktivierung nimmt die Cu-Oberfläche der Cu/ZrO_2 Katalysatoren zu, dieses Ergebnis korreliert mit der Zunahme der Aktivität. Die Aktivität in Abhängigkeit von der Cu-Oberfläche gemessen an allen sechs Katalysatoren weist keine lineare Korrelation auf. Die CuO/ZrO_2 Katalysatoren haben höhere Aktivität im Vergleich zum $CuO/ZnO/Al_2O_3$ Katalysator. Die CO-Konzentration im Produkt in Abhängigkeit vom Methanol-Umsatz zeigt, dass die Cu/ZrO_2-Katalysatoren signifikant weniger CO im Vergleich zu dem kommerziellen $CuO/ZnO/Al_2O_3$ Katalysator produzieren.

Acknowledgement/Danksagung

Die vorliegende Arbeit wurde in der Zeit von April 2000 bis Dezember 2003 in einer Zusammenarbeit der Abteilung Anorganische Chemie des Fritz-Haber-Institut der Max-Planck-Gesselschaft in Berlin und den Technische Chemie der Technische Universität Berlin angefertigt. An dieser Stelle möchte ich allen, die zum Gelingen der Arbeit beigetragen haben, meinen herzlichen Dank aussprechen.

Ich möchte Herrn Prof. Dr. R. Schlögl ganz herzlich für die sehr interessante und aktuelle Themenstellung danken.

Bei Herrn Prof. Dr. R. Schomäcker bedanke ich mich für die hervorragende Betreuung, das beständige Interesse am Fortgang der Arbeit.

Herrn Prof. Lerch von der Technischen Universität Berlin danke ich für die Bereitschaft, als Vorsitzender des Prüfungsausschusses zur Verfügung zu stehen.

Dr. Thorsten Ressler danke ich für die ständige Bereitschaft zur Diskussion, Dr. Rolf E. Jentoft und Dr. Frank Girgsdies für ihre freundliche Unterstützung in besonderes für die Korrektur der Arbeit, was Inhalt und Sprache betrifft. Den Doktoranden der Abteilung Anorganische Chemie (Geometrische Struktur) sei für die gute Arbeitsatmosphäre gedankt.

Mein besonderer Dank gilt Herrn Hartmut Berger, mit dem ich zusammen Chemie studierte, der mir sehr viele fachliche Aspekte sowohl während des Studiums als auch während der Promotion verdeutlicht hat.

Herrn Gerald Bode danke ich für die Unterstützung im Bereich der Installation und Einstellung der Software und Hardware des Labor- und Arbeitsrechners. Den Doktoranden des Arbeitskreis Prof. Schomäcker (Technische Chemie, TU Berlin) sei für die gute Kameradschaft gedankt.

Stellvertretend für die Mitarbeiter der Werkstätten der TU Berlin, Institut für Chemie möchte ich Herrn W. Heine, M. Knuth von der Metallwerkstatt und Herrn Grimm von dem Glaswerkstatt. Herrn S. Winter (†) danke ich für die hilfreichen Vorschläge und die Diskussion am Anfang meiner Arbeit.

Meiner Frau Veronica und meinem Sohn Cleve bin ich für die geistliche und geistige Unterstützung und für die Verständnisse sehr dankbar. Diese Arbeit ist Ihnen gewidmet.

Mein größter Dank gilt an meinen Herrn Jesus Christus, der mir Kraft, Weisheit, Gesundheit, Geduld und Freude schenkt, diese Arbeit überhaupt erst ermöglichte.

Table of Contents

1. Introduction

1.1 Motivation and Strategy

Air pollution and continuous global warming are serious environmental problems, which can cause the change of climate and the damage to environment. Pollutants such as carbon monoxide, hydrocarbons, sulphur dioxide and nitrogen oxides are of importance because they influence the formation of smog. Carbon dioxide, methane and certain nitrogen oxides are of global significance. In the urban areas, the transport sector is one of the main contributors to the air pollution. For examples, in Athens, Los Angeles, and Mexico City almost 100% of carbon monoxide emissions come from road vehicles, whereas NO_x-emissions are caused by road transport at between 75% and 85% [1.1]. The suffering of worldwide some 1.1 billion urban citizens from severe air pollution is related to about 700.000 death cases, reported from the World Bank. The other problem caused by the emission of the pollutants is the increase of the global temperature. It is reported that each of the first eight months of 1998 new record highs for global temperatures is recorded [1.2]. Carbon dioxide is thought to be the main contributor for the greenhouse effect. Every gallon of gasoline burned in an automobile produces 20 pounds of carbon dioxide. Transportation sector is responsible for one-third of all carbon dioxide emissions. Efforts to minimise the environmental damage of rapidly growing automobiles use have focused on end-of-pipe technologies such as catalytic converters and particle traps and recently on producing cleaner gasoline. This strategy has shown a significant decrease of the emissions from the newest cars being put on the road, but the strategy has its limitation. In order to provide ultra low emission vehicles or zero emission vehicles use of fuel cell technology is one of the most prominent solutions. Hydrogen is used as fuel to power the fuel cell. The generating of the electricity by the chemical process, combining hydrogen and oxygen to form water, produces no emissions at all. Other advantages of using hydrogen in the fuel cell in comparison to the conventional internal combustion engine are higher energy efficiency, low noise, no formation of soot particle, which can impact the human health. The most promising type of fuel cell for application in the automobile is the low temperature proton exchange membrane (PEFC) fuel cell. The prototype of such passenger cars have been successfully demonstrated by many automobile industries. The on-board supply of hydrogen for the vehicles can generally be divided into three groups:

1. Storage of high pressure hydrogen and liquid hydrogen.
2. Using of metal-hydride as hydrogen storage.

3. Reforming of hydrocarbon, such as methanol, ethanol, dimethylether, gasoline, diesel, etc.

The lack of a hydrogen refuelling infrastructure, combined with the complexity of on-board storage and handling of the hydrogen, are the drawbacks of applying pure hydrogen on-board. Furthermore, the weight and the volume of the hydrogen tank on board are much greater than of gasoline of diesel. This is a problem of the space limitation in the automobile and the increase of weight causes the increase of fuel consumption. The comparison of the weight and the volume of different fuels based on same energy equivalent of 50 litre gasoline are depicted in Figure 1.1 [1.3].

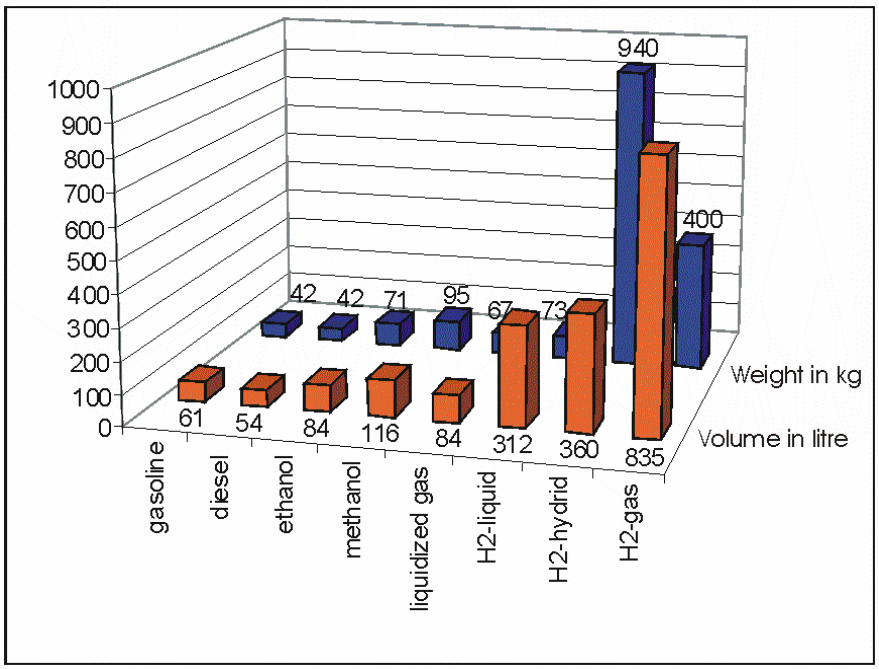

Figure1.1: Weight (tank + fuel) and volume (tank + fuel) of different fuels based on same energy equivalent of 50 litre of gasoline

The alternative to the use of either liquid hydrogen or high pressure hydrogen on board is to carry liquid fuels that have high energy densities and covert them to a hydrogen-rich gas (reformate) via an on-board fuel cell processor. One of the most favourable liquid fuels used to produce hydrogen on board is methanol. This due to the following superior advantages of using methanol in comparison to other liquid fuels in particular with respect to the on board reforming process:

1. low reaction temperature and atmospheric pressure
2. simple molecule with high molar ratio of hydrogen to carbon

3. low CO concentration (CO is poison to the fuel cell performance)
4. no emission of pollutants, such as NO_x, SO_x
5. no formation of soot particles
6. minor effort of changing the fuelling station (from gasoline or diesel)

Another advantage of using methanol as fuel that should also be taken into account is that there are many sources to produce methanol such as natural gas, oil, coal, biomass. In addition, methanol is the third commodity chemical after ammonia and ethylene, with a production excess of 25 million tons [1.4-1.6]. The production of hydrogen from methanol is performed in a reformer reactor. The catalyst used for this reaction is a copper based catalyst. Two main problems using commercial $CuO/ZnO/Al_2O_3$ catalyst for this process are high CO formation and poor long term stability. Using the Polymer Electrolyte Membrane Fuel Cell (PEMFC) as one of the favourable kinds of fuel cells in the passenger car, CO is found to be the poison to the fuel cell which occupies the active surface of Pt electrode. Dams et al. [1.7] performed series concentrations of CO from 30 ppm to 1000 ppm introduced into the gas mixture of hydrogen and carbon dioxide. They found that only CO with 30 ppm showed a satisfactory result of the decrease of the performance over a limited period. The influence of the CO concentrations to the decrease of the voltage has been carried out by Lemons [1.8]. It revealed that the increase of the CO concentration resulted in the monotonically decrease of the voltage determined over a wide range of current density which related directly to the decay of the fuel cell performance, Figure 1.2.

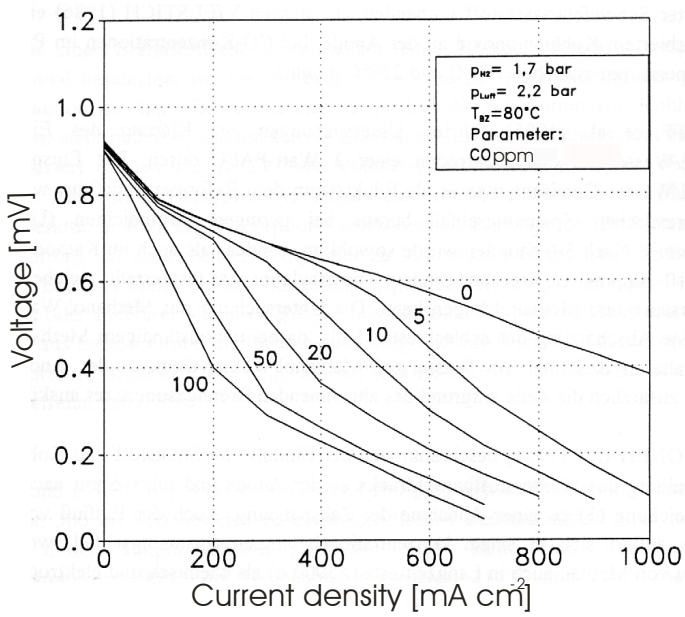

Figure 1.2: Influence of the CO levels to the voltage as a function of current density

Another drawback of using the commercial $CuOZnO/Al_2O_3$ catalyst is the poor long term stability. One of the main factors which cause the decay of the catalyst activity with time on stream is the sintering of the metal particles that result in a decrease of the surface area of the active site. In order to solve these problems, high CO formation and poor long-term stability, many strategies concerning the improvement of the catalyst properties have been followed i.e. synthesis of other metal based catalysts (Pd), synthesis of copper based catalysts promoted with different metal oxides and synthesis of copper based catalysts with various kinds of preparation methods.

The objective of this work is to study the catalytic behaviours of novel Cu/ZrO_2 catalysts which were prepared with different preparation methods. The catalytic properties of these catalysts, such as activity, long term stability, CO selectivity, were studied by means of a fixed bed reactor. In order to evaluate the catalytic properties of the Cu/ZrO_2 catalysts, a commercial $CuO/ZnO/Al_2O_3$ catalyst was used as a reference. A kinetic study of the commercial $CuO/ZnO/Al_2O_3$ catalyst was also performed in this work.

1.2 Hydrogen production from methanol

There are three process alternatives to produce hydrogen through the conversion of methanol:

1. decomposition
2. partial oxidation
3. steam reforming

The decomposition reaction is the most simple process from a chemical point of view as solely methanol is used as feedstock [1.9].

$$CH_3OH \longrightarrow 2\,H_2 + CO \qquad \Delta H_r = 128\ kJ\ mol^{-1} \qquad (1.1)$$

However, the reaction is strongly endothermic which means that it requires a lot of energy for operating. Furthermore, the decomposition yields product gas containing up to 67% hydrogen and 33% carbon monoxide. The high content of CO requires a CO clean-up system if this reaction would be used in the fuel cell system. The CO clean-up system is regarded to be the most complicated part in the fuel cell system. Because of these drawbacks, the decomposition of methanol is found to be unsuitable for fuel cell applications.

In contrast to the decomposition reaction, partial oxidation is a fast and exothermic reaction.

$$CH_3OH + 0.5O_2 \longrightarrow 2\,H_2 + CO_2 \qquad \Delta H_r = -192\ kJ\ mol^{-1} \qquad (1.2)$$

Several studies on this reaction have been published in the last few years [1.10-1.12]. The advantage of this process with respect to the exothermic nature is that an additional energy supply for the reaction is not necessary. However, the exothermic behaviour should be taken into account when designing the reactor. The fast increase of temperature in the reactor can form hot spots, which can cause the deactivation of the oxidation catalyst through sintering of the metal particles. The hydrogen concentration up to 67% in a product stream can be achieved when methanol is partially oxidised with pure oxygen in the feed. The oxygen required for the automobile application would most likely be supplied from air. Due to the high content of nitrogen in the air, this causes dilution of the product gas with nitrogen. As a result, the maximum theoretical hydrogen content in such a system is lowered to 41%. The decrease of the hydrogen content in the product stream influences strongly the performance of the electricity production in fuel cell [1.13].

The steam reforming of methanol (SRM) is known as a reverse reaction of methanol synthesis.

$$CH_3OH + H_2O \longrightarrow 3\,H_2 + CO_2 \qquad \Delta H_r = 50\ kJ\ mol^{-1} \qquad (1.3)$$

SRM is considered to be the most favourable process of hydrogen production in comparison to the decomposition and partial oxidation of methanol. This is because of the ability to produce gas with high hydrogen concentration (75%) and high selectivity for carbon dioxide. SRM is an endothermic reaction. The energy needed for the reaction can be supplied from a catalytic burner device, Figure 1.3. Because of the superiority of this process with respect to high methanol conversion, high hydrogen concentration and mild reaction conditions, studies of this reaction have been carried out intensively by many research groups. [1.14-1.18].

Another additional alternative to produce hydrogen from methanol is to combine the partial oxidation with the steam reforming. The advantage of this process is that heat requirement for the reaction can be supplied by the reaction itself (autothermal reaction). However, the concentration of hydrogen in gas product and methanol conversion is lower than that in the SRM[1.19].

1.3 Methanol steam reforming

The general reaction conditions of SRM are as follows:

- reaction temperature: 250-300°C
- pressure: 1 bar
- 1:1 to 1:1,3 molar ratio of methanol to water

The main products of SRM are hydrogen, carbon dioxide and a low content of carbon monoxide is produced in this process (up to 2 volume % in dry product stream when using a copper based catalyst). The reaction schemes for the formation of carbon monoxide in SRM will be discussed later. Hydrogen production based on SRM for fuel cell drive system consists of the following main devices: a methanol steam reformer, a catalytic burner which provides heat for the reformer and converts all burnable gases in the flue gas into water and carbon dioxide, a gas cleaning unit which reduces CO concentration of the hydrogen-rich product and feeds to the Proton Exchange Fuel Cell (PEFC). A gas storage system is also integrated in the fuel cell system in order to feed the fuel cell during the start-up and speed-up phases. A scheme of the fuel cell drive system based on SRM is shown in Figure 1.3.

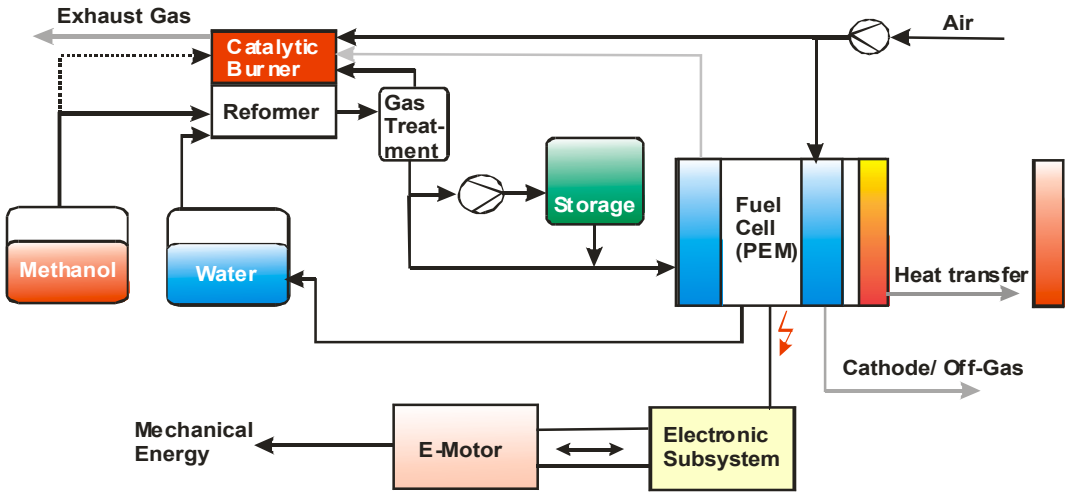

Figure 1.3: Fuel cell drive system [1.20]

1.4. References

[1.1] R. Wurster, PEM fuel cell in stationary and mobile applications pathways to commercialisation, sixth international technical congress-BIEL'99-13th-19th September (1999).

[1.2] G. P. Nowell, The promise of methanol fuel cell vehicles, American Methanol Institute, www.Methanol.org.

[1.3] K. Ledjeff-Hey, F. Mahlendorf, J. Ross, Brennstoffzellen, C. F. Müller Verlag, 2. Auflage, (2001).

[1.4] R. Kumar, S. Ahmed, M. Yu, Preprints, Am. Chem. Soc., Div. Fuel Chem. **38** (1993**)** 1741.

[1.5] R. Kumar, S. Ahmed, M. Krumplet, K.M. Myles, Argone National Laboratory, Report ANL-92/31, Argone, IL, (1992).

[1.6] W. Cheng, H.H. Kung, Methanol Production and Use, Marcel Dekker, New York, (1994).

[1.7] R.A. Dams, S.C. Moore, O.A. Belsey, C.M. Seymour, *"The development of a Methanol Reformer for use with a Proton Exchange Membrane Fuel Cell"*, International Fuel Cell Conference, February 1992, Makuhari/Japan.

[1.8] R.A. Lemons, Journal of Power Sources **29** (1990), 251-264.

[1.9] L. Petterson, K. Sjöström, Combust. Sci. Technol. **80** (1991) 265-303.

[1.10] M. L. Cubeiro, J.L.G. Fierro, Appl. Catal. A **168** (1998) 307-322.

[1.11] S. Velu, K. Suzuki, T. Osaki, Catal. Lett. **62** (1999) 159-167.

[1.12] J. Agrell, K. Hasselbo, K. Jansson, S.G. Järas, M. Boutonnet, Appl. Catal. A **211** (2001) 239-250.

[1.13] S.J. Lee, E.A. Mukerjee, J. Mcbreen, Electrochem. Acta **44** (1999) 3283.

[1.14] C. J. Jiang, D.L. Trimm, M.S. Wainsright, Appl. Catal. A **93** (1993) 245-255.

[1.15] B. Lindström, L.J. Pettersson, J. Power Sources, **106** (2002) 264-273.

[1.16] J. C. Amphlett, R.F. Mann, B.A. Peppely, D. M. Stokes, in: Proceedings of the 26th Intersociety Energy Conversion Engineering Conference, 1991, pp. 642-649.

[1.17] J.P. Breen, J.R.H. Ross, Catal. Today **51** (1999) 521-533.

[1.18] K. Takahashi, N. Takezawa, H. Kobayashi, Appl. Catal. **2** (1982) 363.

[1.19] B. Lindtröm, L.J. Pettersson, P. Govind Menon, Appl. Catal. A **234** (2002) 111-125.

[1.20] R. Peters, B. Emonts, K.A. Friedrich, B. Höhlein, V.M. Schmidt, U. Stimming, Proc. World Car Conf., Riverside, CA, 1997, pp. 407-420.

2. Fundamentals

2.1 Catalysts for methanol steam reforming

The reaction of methanol steam reforming is a heterogeneously catalysed process; with gaseous reactants and solid catalyst. The catalysts used in this reaction are commonly copper based meaning the main active component to be copper. In order to enhance the activity, the copper catalysts are promoted with various kinds of metal oxide. The promoted copper catalysts are normally fixed on support materials. The catalyst support has the function to enlarge the surface area of the active component and also to provide a catalyst stable in reaction condition against sintering of the metal particles. There are many kinds of preparation methods for the copper based catalysts. An overview of the different preparation methods is described in the following.

2.1.1 Preparation methods

2.1.1.1 Co-precipitation method

The most common way of synthesising copper catalysts for SRM is the co-precipitation method. A study on the synthesis of CuO/ZnO catalysts using the co-precipitation method has been performed by B. Bems et al. [2.1]. A general description of the co-precipitation method is given as follows. A $Cu(NO_3)_2/Zn(NO_3)_2$ solution and a co-precipitate solution of Na_2CO_3 are mixed in the reactor at a higher than ambient temperature, i.e. 65 °C. The precipitate formed is aged under continuous stirring. Furthermore the precipitate is then filtered, washed with bi-distilled water and dried at 120 °C in air for several hours. The precursor is then calcined at 350°C. The reaction parameters such as pH, ageing condition, washing have been found to have an influence on the structure of the catalysts and therefore on the activity [2.1, 2.2]. Despite its complexity with respect to the reaction parameters that can influence the catalytic properties, many studies on this preparation method found that it is a promising way to synthesise highly active catalysts. The commercial $CuO/ZnO/Al_2O_3$ catalyst for methanol synthesis, which is also used in SRM is prepared by means of this method. Another co-precipitation method which is called oxalate gel co-precipitation is reported in the work of W. Ning et al. [2.5]. Copper nitrate, zinc nitrate and aluminium nitrate were dissolved in ethanol. Oxalic acid solution was then added to the mixed nitrate solution under vigorous stirring condition. Under gentle stirring, the precipitates were aged at room temperature for 30 min.

After that the precipitates were put in a water bath at 50°C to evaporate the solvent completely. The precipitates were then dried at 110°C overnight and calcined in air. In the work of Y. L. Zhang et al. [2.6], various preparation methods including gel co-precipitation were compared. They found that catalyst prepared by oxalate gel co-precipitation showed a higher BET area and smaller particle size than those prepared by the other methods (supercritical fluid drying, vacuum freezing drying and organic complex decomposing). In addition it also showed the highest activity.

2.1.1.2 Impregnation method

There are two impregnation methods reported in the work of Agaras et al [2.3]. The first method is done by the adding of ($Cu(NO_3)_2$) solution to the support material (alumina spheres) which were put in a rotating vessel. After the impregnation, the samples were dried in an oven at 120°C for 2h. Method 2 is performed as follows. The support material (alumina spheres) contained in a stainless steel basket was added to a well stirred aqueous solution of copper nitrate. The immersion time was varied in order to determine the period in which a constant weight of the immersed support material was reached. The solution was drained and the spheres were slowly dried at ambient temperature (70-80% humidity) overnight. Finally, the spheres were dried in an oven at 120°C for 2h. Impregnation is a simple method of preparing copper catalysts due to the few parameters which have to be controlled during the preparation. However, there are significant differences in the catalytic properties between catalysts prepared using this method and co-precipitation as shown in work of J. P. Shen et al. [2.4]. They reported that the reduction temperature of the impregnation catalyst is much higher than that of the co-precipitation catalyst. This indicates that the dispersion of the copper particles is correspondingly lower. As a result, the catalytic activity of the catalyst prepared using impregnation method is found to be lower than that prepared by co-precipitation.

2.1.1.3 Polymer-Template method

One of the preparation methods of CuO/ZrO_2 catalysts by means of polymer-matrix has been reported by J. H. Schattka [Chem. Mater 14 (2002) 5103]. This synthesis can be divided into two steps, (i) preparation of polymer gel and (ii) Sol-gel nanocoating. For the preparation of the polymer gel, surfactant Tween 60 ® is dissolved in water. The monomers (acrylamide and

glycidylmethacrylate) are added to this homogeneous solution. A crosslinker (ethylene glycol dimethacrylate) is then added to the solution. The Initiator (potassium persulfate) is dissolved in the mixture, which is then poured into test tubes. Polymerisation is carried out at 60°C. After 16 hours the resulting gel is taken out of the test tubes and cut into disks. The surfactant is removed by soxhlet extraction (ethanol, 2 days) and subsequent washing with water. Finally, the gel is transferred into 2-propanol. The following step is the sol-gel nanocoating. Zirconium propoxide and copper (II) acetylacetonate are stirred over night. The polymer gels are initially soaked in this solution over night and then in a hydrolyis solution for 24h. After drying, the polymer gel is removed from the metal oxide by heating the hybrid material over 2 hours to 500°C under a nitrogen atmosphere; then the gas is switched to oxygen and the temperature is maintained for 10 hours. The following figure shows the preparation steps of CuO/ZrO_2 catalyst using this method.

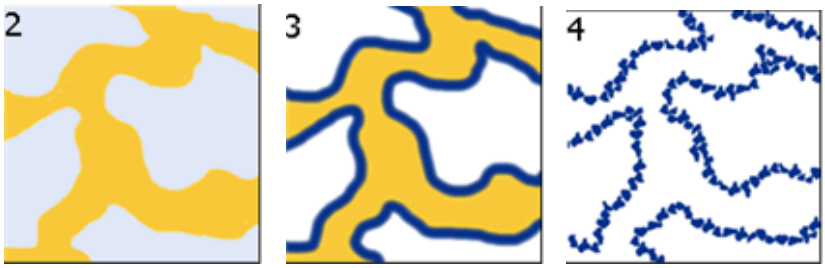

Figure 2.1a: The preparation of macroporous CuO/ZrO2 catalyst by means of polymer-template, (1) a macroporous polymer gel, (2) soaked in zirkonium-copper solution, (3) hydrolysis, (4) sample after the calcinations at 500°C.

2.1.2 Catalysts for steam reforming of methanol

A study of SRM with catalysts based on copper or group VIII metals (Ni, Rh, Pd, and Pt) supported on various oxides (SiO_2, Al_2O_3, ZnO, MgO, La_2O_3, NdO_3, MnO_2, Cr_2O_3, HfO_2, Nb_2O_5) has been performed by Iwasa and co workers [2.7]. The copper and group VIII metal catalysts were prepared by the impregnation method. In comparison to the Cu/SiO_2 catalyst, the hydrogen production rate ($\mu mol(min\ g\text{-}cat)^{-1}$)) of Pt/SiO_2 and Pd/SiO_2 catalysts are about 14 times lower and that of the Ni/SiO_2 catalyst is about 3 times lower. Furthermore, SRM over Pd based catalysts (supported on various oxides) has been carried out. The results reveal that the Pd/ZnO catalyst is the most active concerning the highest hydrogen production rate and providing the highest carbon dioxide selectivity. The authors concluded that copper based catalyst and Pd/ZnO catalyst exhibited high catalytic performance (activity and selectivity) in

SRM. Another group working on the Pd/ZnO catalysts for SRM found that these catalysts showed high activity and low selectivity to CO [2.8]. Two different reduction conditions (reduction at 125°C and 350°C) were studied with respect to activity and formation of CO. The methanol conversion as a function of temperatures (225°C to 300°C) showed that the reduction temperature had no influence on the activity. In contrast, the CO formation from the catalyst reduced at higher temperature is found to be significantly lower than that from the one reduced at lower temperature. The low selectivity for CO found with the catalysts reduced at high temperature is due to the formation of a Pd/Zn alloy. In the work of Iwasa and co workers [2.7], they found that reduction at 125°C was able to reduce the Pd, but not able to initiate the reduction of Zn for the subsequent formation of Pd-Zn alloy. Furthermore in the work of Y. –H. Chin et al., H_2 uptake experiments were carried out on these two catalysts. The results showed that the catalyst reduced at 125°C adsorbed much more hydrogen than that reduced at 350°C. This indicates that the catalyst reduced at 350°C provides a large crystallite Pd-Zn alloy which is in agreement with a XPS analysis performed by Takezawa et al. [2.9]. The presence of Pd-Zn alloy on the catalyst reduced at high temperature was shown using high resolution TEM and XRD. It is well established that metallic Pd is active for the reaction of methanol decomposition [2.10]. Concerning this finding, the presence of metallic Pd is indirectly confirmed by the higher CO formation. An experiment of methanol decomposition on a Pd/SiO_2 catalyst showed that methanol was converted to CO and H_2 with negligible CO_2 produced. The stability of the Pd/ZnO catalyst reduced at 350°C, followed by cooling down at 225°C prior to reaction has also been investigated [2.8]. These experiments were repeated with the same catalyst and no noticeable deactivation was observed. For SRM, metallic Pd is not a suitable catalyst due to the high CO concentration formed during the reaction. However, the Pd/Zn alloy formed at high reduction temperature is an active phase for the SRM reaction and exhibits significantly lower formation of CO. Another enhanced property of Pd/ZnO catalyst is the stability over a wide temperature range. However, the drawback of using the Pd based catalysts for on-board production of hydrogen for fuel cells is the high cost of the Pd which makes the fuel-cell unit, including the reformer much more expensive than the conventional internal combustion engine. Due to this reason, Pd based catalysts do not receive high interest either from the automobile manufacturers or many research groups. This problem can be solved by searching for a catalyst which is based on less expensive metal that is also active and selective for the SRM. Copper based catalysts are those which can fulfil these criteria. The increasing number of studies on copper based catalysts for SRM in the last few years indicates a large interest in a continuous improvement

of the system such as development of preparation methods, wide range study of the structure-activity correlation, application of the catalysts in the fuel cell system. The catalytic behaviour of copper based catalyst promoted with different metal oxides has been investigated by many groups [2.11-2.15]. N. N. Bakhshi and co-workers reported the influence of various promoters on the low-temperature methanol-steam reforming performance of promoted Cu-Al catalysts. The promoters used in their work were Mn, Cr and Zn. Dried coprecipitate Cu-Al catalysts [2.16] containing 24.1 and 27.8 wt % copper were used for the preparation of the promoted catalysts. The preparation of the promoted catalyst was done by impregnation techniques using aqueous solutions of manganese nitrate, zinc nitrate and chromium acetate. The results showed that the promoted Cu-Al catalysts were more active at three reaction temperatures (170-250°C) than the non-promoted Cu-Al catalyst. The Mn promoted catalyst revealed the highest catalytic activity measured at 250°C (99% of methanol conversion) followed by Zn promoted catalyst (96%) and the Cr promoted catalyst (95%). However, it is of less meaning to compare the activity of the catalysts at the high value of methanol conversion. The influence of catalyst properties on the activity and selectivity of SRM over Cu/Zn, Cu/Cr and Cu/Zr on γ-alumina has been investigated by Lindström et al [2.17]. The positive effect of the promoters on the catalyst activity was observed in their study. The comparison of the activity of copper catalysts with different promoters showed that the Cu/Zn catalyst is more active than Cu/Cr and Cu/Zr catalyst. Cu/Zr catalyst was found to be the least active catalyst.
Nevertheless, the study of the CO concentration in the product gas over these three catalysts revealed that Cu/Zr catalyst yields the lowest amount of CO over the entire temperature interval (200-300°C). The metal oxides can be used not only to enhance the activity but also to influence the selectivity. Breen et al. [2.11] reported a study of the catalytic behaviours over Cu/Zn and Cu/Zr catalysts for SRM. The binary catalysts were prepared by co-precipitation at a constant pH of 7.0. The result showed that both, Cu/Zn and Cu/Zr catalysts, are active for the SRM reaction. In addition, the Cu/Zn catalyst is found to be more active than Cu/Zr with respect to the hydrogen production per kg catalyst. However, this does not mean that Cu/Zr is less active then Cu/Zn when the comparison on the methanol conversion per copper surface area is taken into account. At the same copper content in both catalysts (70 % molar ratio of Cu), Cu/Zr catalyst possesses significantly less copper surface area (3.7 m^2g^{-1}) than the Cu/Zn (34.5 m^2g^{-1}). Furthermore they showed that the addition of zinc to the Cu/Zr catalyst resulted in catalysts with considerably higher copper dispersions than those of the Cu/Zr catalysts and it also improved the activity at temperature span from 143 to 345°C. These investigations point out that zinc plays a key role in the improvement of the copper

dispersion which relates to the activity. The influence of alumina on the performance of the catalyst has also been observed. The stability of the catalyst was increased by adding alumina to the Cu/Zn/Zr materials. They assumed that the stability is due to the stabilisation of the active amorphous zirconia phase. This result reveals indirectly that the amorphous zirconia phase is responsible for the catalyst stability. The activity of the catalyst was also increased by adding of alumina. The increase of the activity was found to be correlated with an increase in both the copper and BET surface area. The study of the activity in correlation with the reducibility of the catalyst using TPR analysis showed that the most active catalysts had reduction peaks at lowest temperature. It can be concluded from many investigations reported in the literature that copper based catalysts are suitable for SRM concerning several properties, such as high activity, high selectivity to CO_2, inexpensive materials. An important conclusion from the study of these catalysts is that the performance of the catalysts can be influenced by the preparation method [2.4, 2.5, 2.11, 2.18] as well as preparation conditions, i.e. pH, calcination temperature [2.1, 2.3] and kind of metal oxides used as promoters [2.11, 2.15, 2.17, 2.19].

2.2 Mechanisms of methanol steam reforming

There have been some controversies in the literature concerning the mechanisms for production of hydrogen and carbon dioxide by SRM. The study of the mechanism of the formation of CO as a by-product has received a high attention. There are several schemes suggested in the literature.

1. No formation of CO in the reaction route [2.11, 2.20-2.22].

Some researchers [2.20, 2.24] suggested the SRM process via methyl formate formation, in which no CO takes part in the reaction.

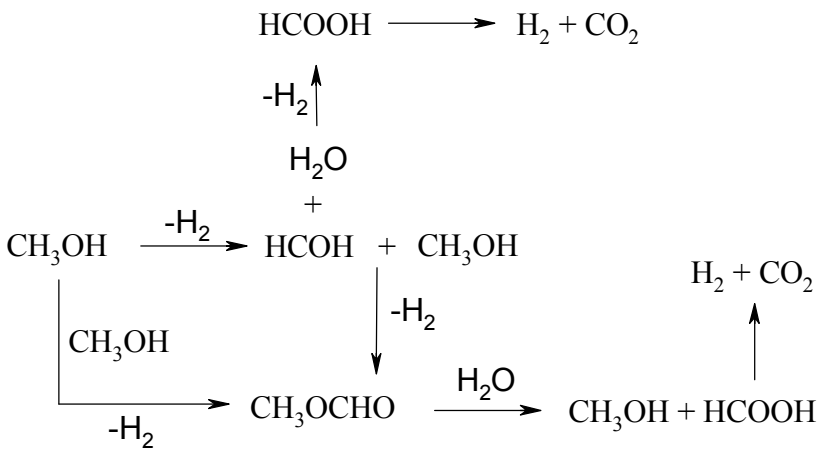

(2.1b)

According to the study performed by Takahashi et al. [2.26], the WGS reaction was found to be blocked in the presence of methanol on Cu/SiO_2. Another argument for excluding WGS in the reaction scheme is that the equilibrium constant $K_p = \frac{P_{CO_2} P_{H_2}}{P_{CO} P_{H_2O}}$ determined in the experiment greatly exceeded those obtained for the WGS reaction [2.26]. A detailed study of the reaction scheme on the Cu/SiO_2 catalyst has been performed by Takezawa et. al. [2.24]. They found that HCHO and CH_3OOCH are involved in the reaction.

By introducing HCHO to the feed of methanol-water mixture, the complete conversion of HCOH to CO_2 and H_2 was observed. The reaction of HCHO and water occurred more rapidly as compared to the steam reforming of methanol. Based on these results they conclude that the production of hydrogen and carbon dioxide over copper based catalysts includes the formation of formaldehyde and HCOOH as intermediate products that can be described as follows:

$$CH_3OH \xrightarrow{-H_2} HCOH \xrightarrow{H_2O} \begin{matrix} HCOOH \\ + \\ H_2 \end{matrix} \longrightarrow H_2 + CO_2 \qquad (2.2)$$

Furthermore, the reaction rate of methyl formate from the reaction of HCHO in both the absence and in the presence of methanol was determined. The rate of methyl formate formation was found to be more enhanced in the presence of methanol at the temperature from 350 K to 450 K. The rate in the presence of methanol was estimated to be (at 393K) 20 times higher than in the absence of methanol. This indicates that the formation of methyl formate from the mixture of HCHO and CH_3OH is much more rapid than the dehydrogenation of methanol to methyl formate. They concluded that the formation of methyl formate over copper based catalysts occurs through a pathway:

$$CH_3OH \xrightarrow{-H_2} HCOH \xrightarrow{CH_3OH} CH_3OCHO + H_2 \qquad (2.3)$$

2. The decomposition of methanol and water gas shift reaction [2.27-2.30]

$$CH_3OH \longrightarrow 2\,H_2 + CO \qquad \Delta H_r = 128\ kJ\ mol^{-1} \qquad (2.4)$$

$$CO + H_2O \longrightarrow H_2 + CO_2 \qquad \Delta H_r = -41.2\ kJ\ mol^{-1} \qquad (2.5)$$

These schemes were suggested by Santacesaria et al. [2.29] who studied the SRM kinetics over a commercial low-temperature $Cu/ZnO/Al_2O_3$ shift catalyst in a continuous stirred-tank reactor. They found that CO concentration was negligible in the product. Based on this result they assumed that CO is produced from decomposition of methanol and followed by water gas-shift reaction, where the decomposition reaction was found to be the rate-determining step. According to this scheme, CO is an intermediate product.

3. The steam reforming of methanol and decomposition of methanol

$$CH_3OH + H_2O \longrightarrow 3\,H_2 + CO_2 \qquad \Delta H_r = 50\ kJ\ mol^{-1} \qquad (2.6)$$

$$CH_3OH \longrightarrow 2\,H_2 + CO \qquad (2.7)$$

A semi-empirical model of the kinetics of the catalyst steam reforming of methanol over $CuO/ZnO/Al_2O_3$ catalyst has been developed by Amphlett et al. [2.32] by using the reaction schemes of irreversible reaction of SRM and decomposition reaction. They found that the water gas-shift reaction could be neglected without substantial loss in accuracy. The rate equations for both reactions can be written as:

$$r_{CH_3OH} = -k_1 C_{CH_3OH} - k_2$$
$$r_{H_2O} = -k_1 C_{CH_3OH}$$
$$r_{CO_2} = k_1 C_{CH_3OH}$$
$$r_{CO} = k_2$$
$$r_{H_2} = 3k_1 C_{CH_3OH} + 2k_2$$

The reaction rate of methanol and water consumption is depending only on the concentration of methanol and not on water concentration. Furthermore, the reaction rate of CO formation is a zero-order rate which means that the formation of CO is not affected by the concentration of methanol or the concentration of water.

4. The steam reforming of methanol, decomposition of methanol and water gas-shift reaction

$$CH_3OH + H_2O \rightleftharpoons 3\,H_2 + CO_2 \quad (2.8)$$

$$CH_3OH \rightleftharpoons 2\,H_2 + CO \quad (2.9)$$

$$CO + H_2O \rightleftharpoons H_2 + CO_2 \quad (2.10)$$

The scheme of SRM process which includes SRM, WGS and decomposition is proposed by Peppley et al. [2.31, 2.32]. They studied the reaction network for SRM over a $Cu/ZnO/Al_2O_3$ catalyst. They claim that in order to fully understand the reaction network, all three reactions must be included in the model. They found that there are two types of catalyst sites that are responsible for the catalyst activity and selectivity, one for the SRM and WGS reactions and another for the decomposition reaction.

5. Steam reforming of methanol and reverse water gas shift reaction

$$CH_3OH + H_2O \rightleftharpoons 3\,H_2 + CO_2 \quad (2.11)$$

$$CO_2 + H_2 \rightleftharpoons H_2O + CO \quad (2.12)$$

A kinetic study of methanol steam reforming on a commercial $CuO/ZnO/Al_2O_3$ catalyst has been performed in our recent work [2.25]. The experimental results of CO partial pressure as a function of contact time at different temperatures show very clearly that CO was formed as a consecutive product. The reaction scheme used is the direct formation of CO_2 and hydrogen by SR reaction and formation of CO as consecutive product by reverse WGS reaction. A simulation employing this scheme is able to fit the experimental data well over a wide temperature range (230-300°C). In the work of Breen and co workers [2.11], they observed that CO is formed at high methanol conversions and long contact times. No CO was formed at

all at low contact times. This indicates that CO is a secondary product, formed by reverse WGS reaction. This result agrees well with the work of Agrell et. al [2.33]. They found that the level of CO decreases with decreasing contact time.

.

2.3 Determination of kinetic parameters

Plug-flow reactors (PFR) containing a fixed-bed of catalyst are primarily used to determine rate law parameters for heterogeneous reaction (liquid-phase and gas-phase reactions). A typical profile of concentration with respect to the position in the tube is shown in Figure 2.1. The characteristics of a PFR can be described as follows:

(1) It is a continuous flow through the tube, both input and output streams.

(2) There is no axial back mixing in the tube.

(3) The properties of the gas, including its velocity, are uniform within the radial plane (no radial gradient in concentration, temperature, or reaction rate).

(4) The properties of the flowing system may change continuously in the direction of flow.

(5) The heat transfer may occur through the wall of the tube in the system.

Some consequences obtained from the model described above are:

(1) In the axial direction, no exchange of material occurs with the portion ahead of it or behind of it

(2) Each element of gas has the same contact time.

(3) There may be a change of the gas volume in the flow direction because of changes in T, P and total number of moles.

The simple model to describe plug flow and laminar flow characteristics in the tube is illustrated in Figure 2.1.

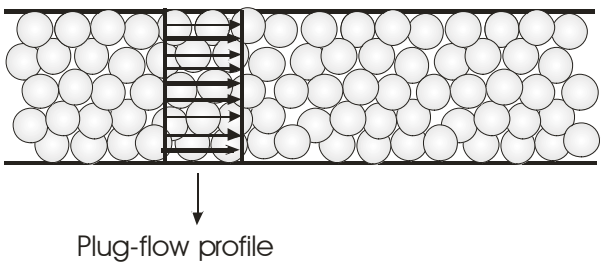

Figure 2.1: Plug-flow profile in fixed-bed reactor

There are certain criteria reported in the literature [2.34] for fixed-bed reactors which ensure that flow condition in the reactor are close to isothermal operation and plug flow condition (elimination of backmixing and minimization of channelling) can be achieved. These criteria are: the ratio of height of catalyst bed to catalyst particle size (L/D_p) is greater than 50 and that of internal diameter of reactor to catalyst particle size (D_r/D_p) greater than 10.

There are two ways to operate a PFR in order to obtain kinetic data (i) differential and (ii) integral.

2.3.1 Plug flow reactor as differential reactor

A differential reactor is used commonly to determine the kinetic parameters of reactions. This is achieved by plotting the rate of reaction as a function of either concentration or partial pressure. It consists of a tube containing a very small amount of catalyst put in the middle of the tube and inert material with the same particle size put above and below the catalyst bed. The criterion for a differentially operating reactor is that the conversion of the reactants in the bed is small, less than 10%. The reason for this is to ensure that there is a small and linear gradient of the reactant concentration. As a result, the reaction rate is considered uniform within the catalyst bed. Because of the low conversion achieved in the reactor, the heat release or receipt per unit volume is small so that the reactor operates essentially in an isothermal manner. The advantage of using the differential reactor is the simplicity of the construction. Some operational difficulties, which are involved in the differential reactor, are the maintaining of the plug flow condition (no channelling or bypass of the reactants through the packed catalyst) and the accuracy of the analytical measurement of the small change of the concentrations. An example that reveals the determination of the kinetic parameters by using a differential reactor is described as follows. The reaction of A and B is an irreversible reaction.

$$A + B \rightarrow C \tag{2.13}$$

The rate law for this reaction is:

$$-r_A = k c_A^{\alpha} c_B^{\beta} \tag{2.14}$$

By utilizing the excess method maintaining B as an excess component that means the concentration of B remains essentially unchanged during the course of the reaction. As a result, the rate law can be written as:

$$-r_A = k' c_A^a \tag{2.15}$$

where

$$k' = k c_B^\beta \approx k c_{B_0}^\beta \tag{2.16}$$

The reaction rate of A can be determined directly from the experiment by using the following equation.

$$-r_A = \frac{dc_A}{dt} = \frac{c_{A_0} - c_A}{\Delta t} \tag{2.17}$$

C_{A0} is the initial concentration and C_A is the concentration at the outlet of the reactor. Δt is the contact time of the reactant flowing through the catalyst bed and can be defined as

$$Dt = \frac{V_{catalyst}}{\dot{V}} \tag{2.18}$$

$V_{catalyst}$ is the volume of the packed catalyst and $\dot{V}$ is the volume flow of the components. By varying the initial concentration of A in the experiments, a series of reaction rates can be obtained. The following equation is obtained by taking the natural logarithm of equation 2.15.

$$\ln\left(-\frac{dc_A}{dt}\right) = \ln k' + \alpha \ln c_A \tag{2.19}$$

The reaction order a and rate constant k' are then determined by plotting log r_A as a function of log C_A. The slope of the plot is equal to the reaction order α and the intercept is k'. The same experiment procedure described above can be performed to determine β where A is the excess component. The next step is to determine the reaction rate constant at different reaction temperatures. By using the Arrhenius equation written in the following, the activation energy and pre-exponential factor can be achieved.

$$k'(T) = A e^{-E/RT} \tag{2.20}$$

A= pre-exponential factor or frequency factor

E= activation energy [J mol^{-1}]

R= gas constant= 8.314 [J mol^{-1} K^{-1}]

T= temperature [K]

Equation 2.21 is obtained by taking the natural logarithm of equation 2.20,

$$\ln k' = \ln A - \frac{E}{R}\left(\frac{1}{T}\right) \qquad (2.21)$$

By plotting ln k' versus 1/T, the activation energy can be achieved from the slope of the plot and the pre-exponential factor from the intercept.

2.3.2 Plug flow reactor as integral reactor

In evaluation of an integral reactor experiments the concentration of reactants are plotted as a function of time. The measurements are usually carried out for a wide range of conversion. The integral method is used generally when the reaction order is established and it is desired to evaluate the reaction rate constants at different temperatures to determine the activation energy and the pre-exponential factor as well. An example for the determination of the kinetic parameters using integral method is described in the following.

For the reaction

$$A \rightarrow 2B + C \qquad (2.22)$$

carried out at isothermal conditions, the mole balance of A is:

$$-\frac{dc_A}{dt} = kc_A^m \qquad (2.23)$$

There are at least two methods available to achieve the reaction order m and the rate constant k. These methods are: linearization of the function or graphical fitting of the simulated curves obtained by numerical differentiation of the mole balance to the experimental data.

2.3.2.1 Linearization of the function.

After taking the integration of equation 2.23 with $c_A(t= 0)= c_{A0}$, the correlation between the concentration and time for the reaction order m = 1 is

$$\ln c_A - \ln c_{A0} = -kt \qquad (2.24)$$

By plotting ln c_A versus t, linear regression can be done through the experimental data. This method is useful to evaluate whether the assumption of the reaction order, in this case m=1, is able to describe the reaction model well or not. If that is the case, the slope of the plot of ln c_A as a function of t is the rate constant k (Figure 2.2).

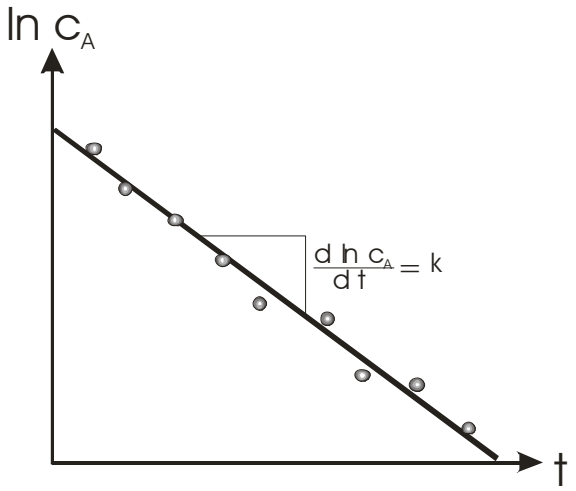

Figure 2.2: Linearization in order to determine the reaction rate

For the case that the reaction order m ≠ 1, the integral of the equation 2.23 results in

$$\left(\frac{1}{c_A}\right)^{m-1} - \left(\frac{1}{c_{A0}}\right)^{m-1} = (m-1)kt \qquad (2.25)$$

Figure 2.3 shows the plot of $(1/c_A)^{m-1}$ as a function of t. The reaction order can be determined from the intercept and the reaction rate constant from the slope of the plot.

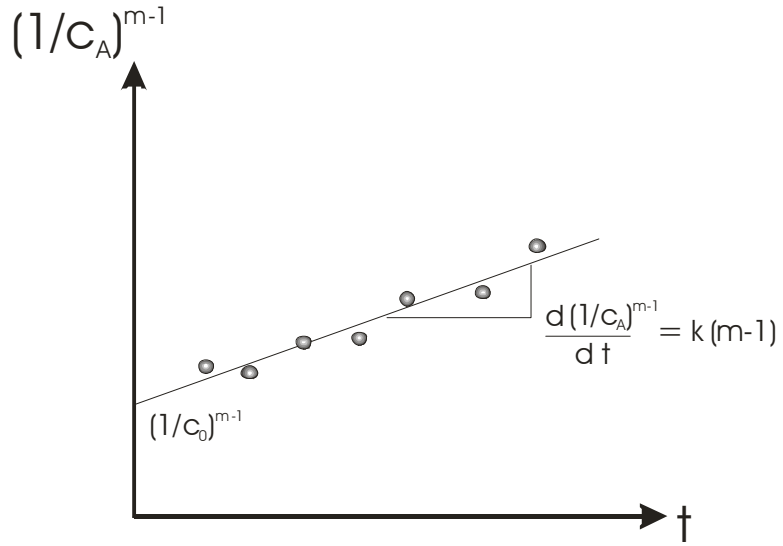

Figure 2.3: Plot of $(1/c_A)^{m-1}$ as a function of t

2.3.2.2 Graphical fitting to the experimental data.

The mole balance of all components (reactant and products) from the reaction described above can be written as follows:

$$-\frac{dc_A}{dt} = kc_A^m \tag{2.26}$$

$$\frac{dc_B}{dt} = 2kc_A^m \tag{2.27}$$

$$\frac{dc_C}{dt} = kc_A^m \tag{2.28}$$

Taking the numerical integration of these equations using e.g. the Runga-Kutta method, the curves of concentration as a function of time for all components can be achieved. The profile of the simulated curves can be changed or adjusted by changing the parameters (m and k). The reaction rate constant k and reaction order m then can be obtained after the optimal fitting between the calculated curves and the experimental data has been achieved, as shown in Figure 2.4.

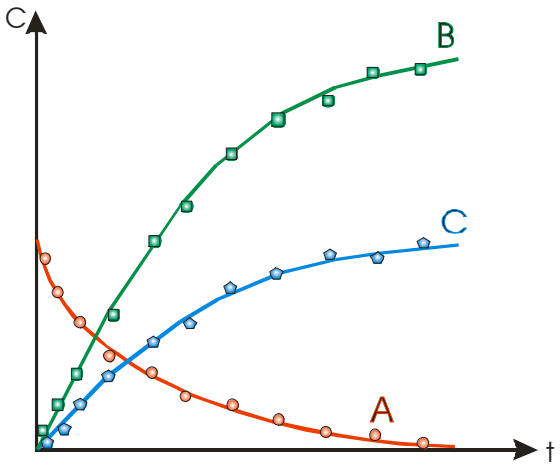

Figure 2.4: Fitting the experimental data by the simulated results

2.4 Types of multiple reactions

The reaction that occurs in a chemical reactor is seldom a process where only one product is obtained. Multiple reactions occur most commonly in chemical reactions that results in desired and undesired reactions. The minimization of undesired side reactions that occur along with the desired reaction plays an important role in the economic success of a chemical plant. Concerning the multiple reactions, there are two devices in chemical plants which impact mostly the cost of the process. They are the reaction part and separation part (responsible for the purity of the desired product), Figure 2.5.

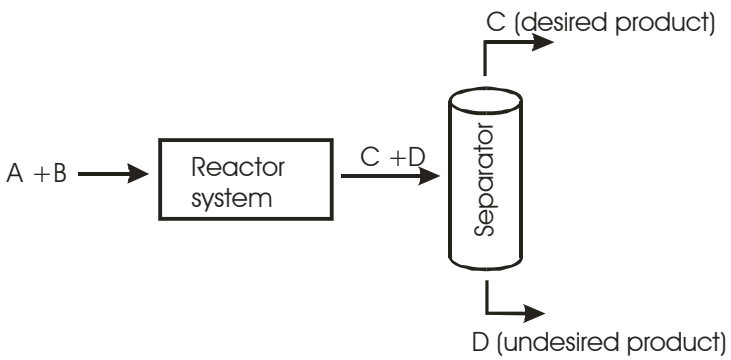

Figure 2.5: Reaction-separation devices

The way of operating the reactor for multiple reactions can influence the ratio of the desired and undesired product which correlated with the effort of the separation. This means that, the higher the selectivity (ratio of the desired product to converted reactants) obtained by the operation, the lower the energy needed for the separation, the lower cost respectively. In the multiple reactions, two or more single reactions take place at the same time. Some examples of the multiple reactions are revealed in the following.

1. Serial reaction

$$A \xrightarrow{k_1} B \xrightarrow{k_2} C \tag{2.29}$$

The differential equations with the assumption that the reactions are first order reactions which can be written as:

$$\frac{dc_A}{dt} = -k_1 c_A \tag{2.30}$$

$$\frac{dc_B}{dt} = k_1 c_A - k_2 c_B \tag{2.31}$$

$$\frac{dc_C}{dt} = k_2 c_B \tag{2.32}$$

The integration of the differential equations with the initial concentration of B and C being 0:

$$c_A = c_{A0} e^{-k_1 t} \tag{2.33}$$

$$c_B = \frac{k_1 c_{A0}}{k_1 - k_2}(e^{-k_2 t} - e^{-k_1 t}) \tag{2.34}$$

$$c_C = c_{A0}\left[1 + \frac{k_1}{k_2 - k_1} e^{-k_2 t} - \frac{k_2}{k_2 - k_1} e^{-k_1 t}\right] \tag{2.35}$$

A typical concentration-time profile of the serial reaction is showed in Figure 2.7. The concentration as a function of time for different ratios of k_1/k_2 is described in the technical chemistry handbook [2.35].

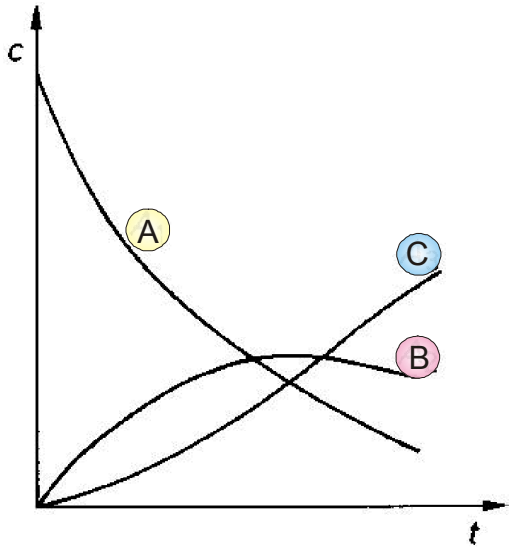

Figure 2.7: Concentration as a function of time

2. Parallel reaction (competitive reaction)

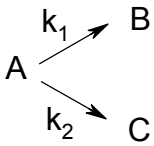

(2.36)

The differential equations for the first order reaction are:

$$\frac{dc_A}{dt} = -(k_1 + k_2)c_A \tag{2.37}$$

$$\frac{dc_B}{dt} = k_1 c_A \tag{2.38}$$

$$\frac{dc_C}{dt} = k_2 c_A \tag{2.39}$$

The integration of the differential equations gives:

$$c_A = c_{A0} e^{-(k_1+k_2)t} \tag{2.40}$$

$$c_B = c_{B0} + \frac{k_1 c_{A0}}{k_1 + k_2}\left[1 - e^{-(k_1+k_2)t}\right] \tag{2.41}$$

$$c_C = c_{C0} + \frac{k_2 c_{A0}}{k_1 + k_2}\left[1 - e^{-(k_1+k_2)t}\right] \tag{2.42}$$

A representative concentration-time profile of the parallel reaction is depicted in Figure 2.8.

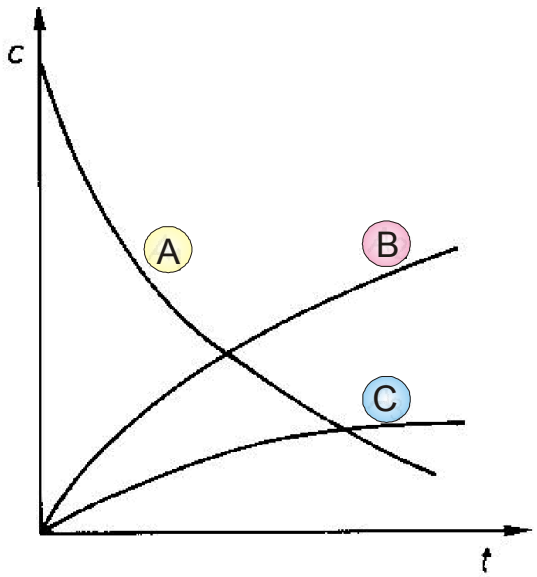

Figure 2.8: Concentration as a function of time

3. Reversible reaction

$$A \underset{k_2}{\overset{k_1}{\rightleftharpoons}} B \tag{2.43}$$

The differential equations of the reactions are:

$$\frac{dc_A}{dt} = -k_1 c_A + k_2 c_B \tag{2.44}$$

$$\frac{dc_B}{dt} = k_1 c_A - k_2 c_B \tag{2.45}$$

The equilibrium constant K can be defined as:

$$K = \frac{k_1}{k_2} \tag{2.46}$$

The integration of the differential equations results in:

$$c_A = c_A^0 - \frac{Kc_{A0} - c_{B0}}{1-K}\left[1 - e^{\left(-\frac{k_1 t(1+K)}{K}\right)}\right] \tag{2.47}$$

$$c_B = Kc_A \tag{2.48}$$

A typical concentration-time profile of the reversible reaction is shown in Figure 2.9.

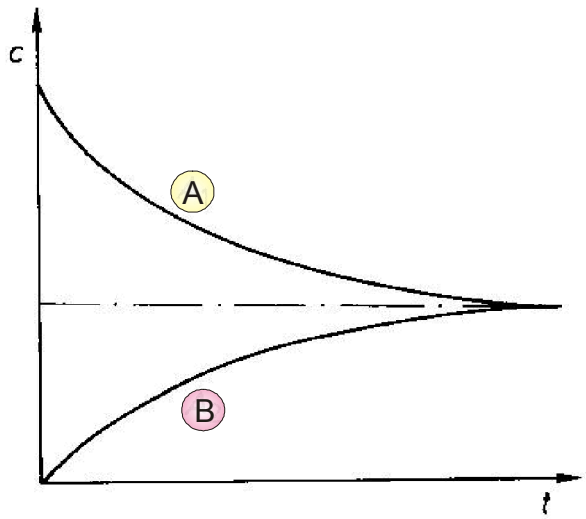

Figure 2.9: Concentration as a function of time

The profiles of concentration as a function of time for reactants and products are a very useful tool to evaluate and/or discriminate the schemes of chemical reactions. A parallel reaction is characterized through the proportional increase of the product concentrations as a function of time. For the serial reactions, the concentration of the intermediate product (B) versus time reveals a maximum and the profile of the consecutive product (C) shows a typical s-shape curve. All reaction networks can be reduced to these three simple examples of reaction networks.

2.5 Diffusion and reaction in a porous catalyst

There are two diffusion processes occurring in a heterogeneous reaction, (i) external diffusion, i.e. mass transfer of reactants from the bulk gas to the external surface of the catalyst, (ii) internal diffusion, the reactants diffuse from the external surface into the pores of the catalyst (pellet). A schematic figure for these two kinds of diffusions is shown in Figure 2.10.

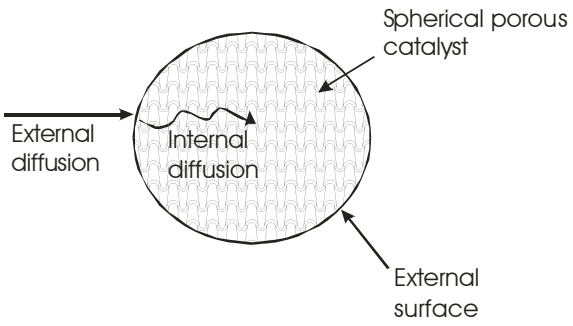

Figure 2.10: Mass transport in a spherical porous catalyst [2.36]

The mass balance of species A as it enters, leaves, and reacts in a spherical shell of the pellet can be described as:

$$\begin{pmatrix}\text{rate of}\\ \text{generation}\\ \text{of A}\end{pmatrix}=\begin{pmatrix}\text{rate of}\\ \text{input by}\\ \text{diffusion}\end{pmatrix}-\begin{pmatrix}\text{rate of}\\ \text{output by}\\ \text{diffusion}\end{pmatrix}-\begin{pmatrix}\text{rate of}\\ \text{disappearance}\\ \text{through reaction}\end{pmatrix}$$

The detailed derivation of the differential equation of the mass balance describing diffusion and reaction can be found in the book of H. Scott Fogler [2.36].
The mass balance can then be written as:

$$D_{eff}\left(\frac{d^2c}{dR^2}+\frac{2}{R}\frac{dc}{dR}\right)=kc^n \qquad (2.49)$$

D_{eff}= effective diffusion coefficient [$m^2\ s^{-1}$]
c= concentration [mol m^{-3}]
n= reaction order [-]
R= normalized sphere radius [-]
k= reaction rate constant

This equation describes a stationary condition with catalyst in spherical form. The following boundary conditions for sphere radius R_0 are considered:

$$c(R=R_0)= c_0 \tag{2.50}$$

$$\left(\frac{dc}{dR}\right)_{R=0} = 0 \tag{2.51}$$

For solving the differential equation 2.49, the dimensionless term, the *Thiele modulus Φ*, is introduced.

$$\Phi = R_0\sqrt{\frac{kc_0^{n-1}}{D_{eff}}} \tag{2.52}$$

The Thiele modulus describes the ratio between the rate of reaction and diffusion. When the Thiele modulus is large, the rate determining step is the intraparticle diffusion; when Φ is small, the surface reaction limits the overall rate of reaction. For the reaction

$$A \rightarrow B \tag{2.53}$$

the normalized concentration c_{st} as a function of sphere radius and Φ is written as

$$c_{st} = \frac{c}{c_0} = \frac{R_0}{R}\frac{\sinh(\frac{R}{R_0}\Phi)}{\sinh\Phi} \tag{2.54}$$

The concentration profile for three different values of Thiele modulus is shown in Figure 2.11.

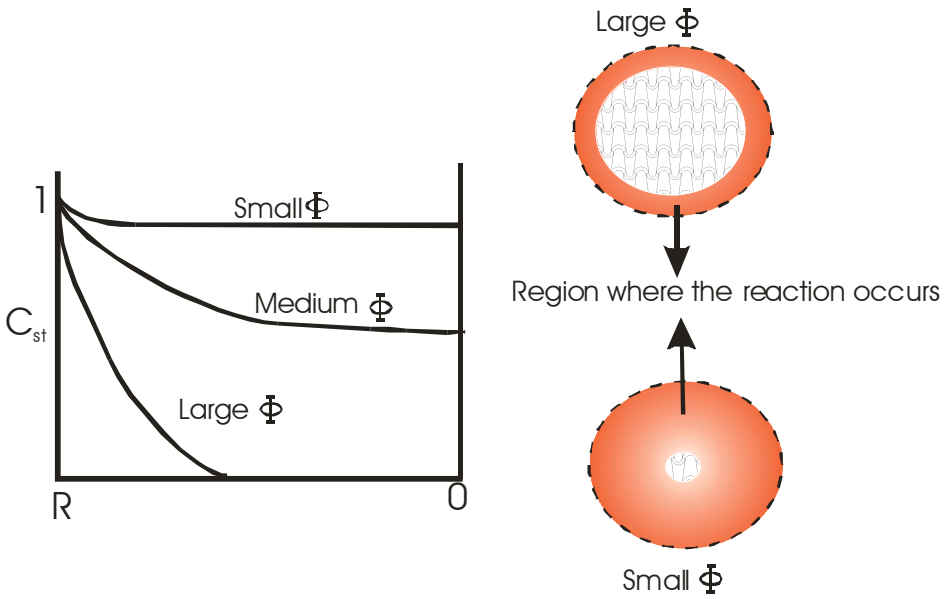

Figure 2.11: Concentration profile in a spherical porous catalyst and the reaction regions for two different values of Thiele modulus

A small Thiele modulus means that the overall reaction rate is controlled by the reaction. In another word, a significant amount of reactant diffuses well into the pellet interior without reacting. Large values of the Thiele modulus indicate that the rate of the reaction is much faster than the diffusion. The reactant is consumed closely to the external surface of the catalyst and penetrates very little into the interior of the pellet. As a consequence, the internal surface of the catalyst can not be used optimally for the reaction. This optimal use of a catalyst pellet can be described in an internal effectiveness factor η (ranging from 0 to 1). The internal effectiveness factor is defined as the ratio between the rate of the reaction in a heterogeneous and a homogenous system.

$$\eta = \frac{r_{het}}{r_{hom}} \tag{2.55}$$

The reaction rate in a homogeneous reaction is obtained where the reactants and the catalyst are in one phase. This indicates that no significant mass transport limitation occurs. The internal effectiveness factor for a reaction in a spherical pellet is:

$$\eta = \frac{3}{\Phi}\left(\frac{1}{\tanh\Phi} - \frac{1}{\Phi}\right) \tag{2.56}$$

The correlation between η and Thiele modulus Φ is depicted in the following Figure 2.12.

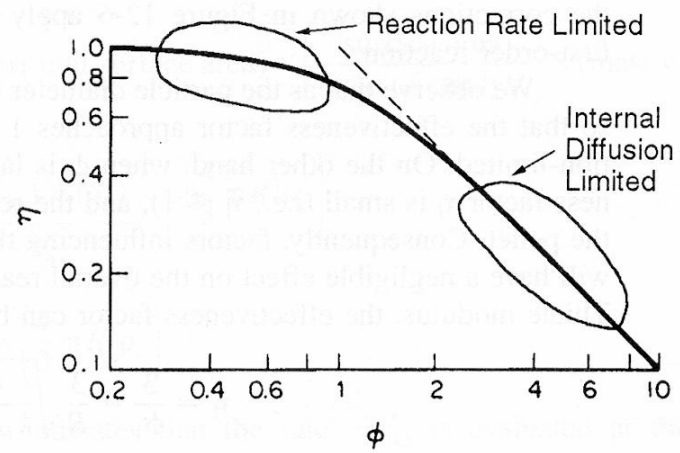

Figure 2.12: Effectiveness factor plotted as a function of Thiele modulus [2.36]

There are two areas marked in Figure 2.12 which exhibit the reaction rate controlled domain for small value of Thiele modulus and the pore-diffusion controlled domain for large value of the Thiele modulus. In order to evaluate the presence or absence of pore-diffusion resistance in catalyst particles, two available methods are described below.

1. Weisz-Prater criterion.

This method requires only a single measurement for a particle size. The rate constant and the reaction order resulting from the measurement are then introduced in equation 2.52 for calculating the value of the Thiele modulus.

- For Thiele modulus $\Phi < 0.5$, the pore-diffusion limitation is negligible.
- For Thiele modulus $\Phi > 5$, the rate is limited strongly by pore-diffusion.

2. Effect of the particle size.

In order to apply this method, the reaction rate is measured for two or more particle sizes. The reaction conditions such as temperature, pressure, flow rate, molar ratio of the reactants are kept constant for all experiments. The conversion is determined as a function of the W/F ratio (W is mass of catalyst, F is flow rate of reactants). The results that may be observed are:

(i) The rate is independent of particle size. This indicates that the pore-diffusion limitation is negligible. This result might be expected for sufficiently small particles whose diffusional path-length is very small.

A representative experimental result in which the conversion (x) as a function of W/F ratio (contact time) is plotted for two different particle sizes as depicted in Figure 2.13. There no influence of the particle size on the conversion (reaction rate) is observed.

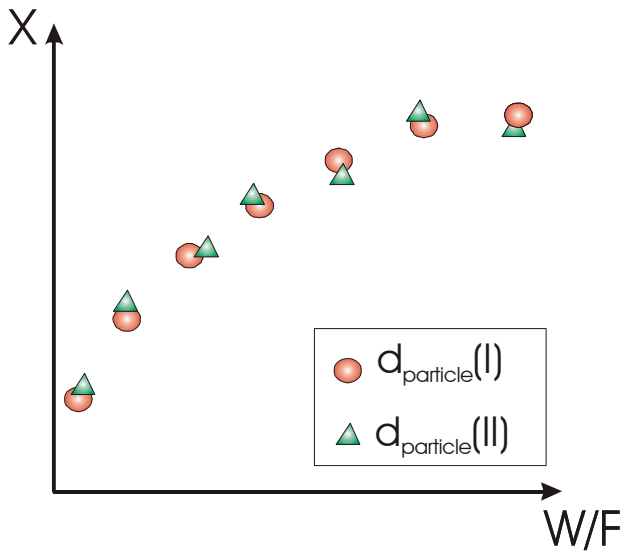

Figure 2.13: Conversion as a function of W/F ratio for two different values of particle sizes

(ii) The rate is inversely proportional to the particle size. This indicates that the presence of the pore-diffusion limitation is significant. A typical experiment result concerning the presence of the pore-diffusion limitation is plotted in Figure 2.14.

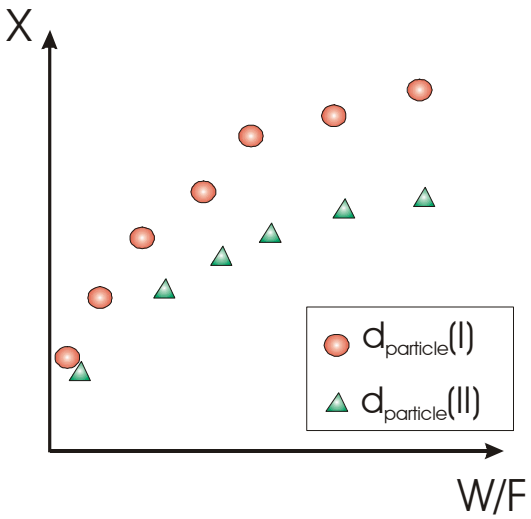

Figure 2.14: Conversion as a function of W/F ratio for two different values of particle sizes ($d_{particle}$)

Fixing the conditions (rate constant, D_{eff}, c_{A0}) the comparison of the reaction rates, effectiveness factors, Thiele modulus for two particle sizes (R_1, R_2) can be described in the following equation.

$$\frac{(r_A)_1}{(r_A)_2} = \frac{\eta_1}{\eta_2} = \frac{\Phi_2}{\Phi_1} = \frac{R_2}{R_1} \qquad (2.56.1)$$

In order to give a clear overview of the domains (poor (i) and strong (ii) pore-diffusion limitation), the reaction rate can be measured as a function of particle sizes, as shown in Figure 2.15.

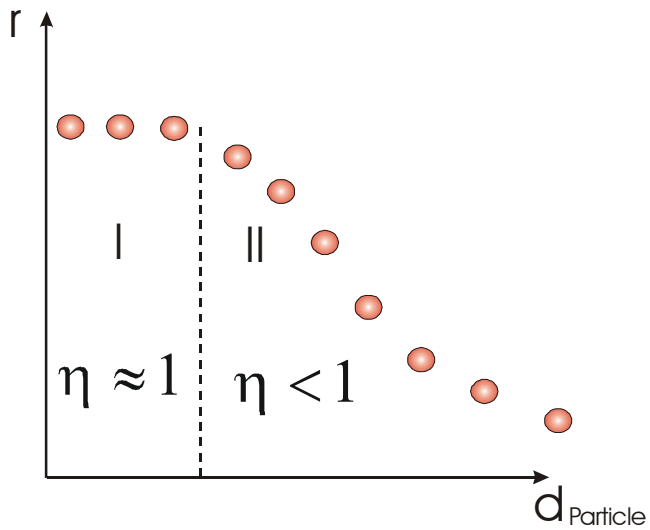

Figure 2.15: Reaction rate as a function of particle size

The diffusion limitation in the porous catalyst can affect the selectivity. In the work of Wheeler concerning the effect of the diffusion limitation to the selectivity, three types of complex reactions were investigated [2.37]. One of them is the series reaction, as described below.

$$A \xrightarrow{k_1} B \xrightarrow{k_2} C$$

Figure 2.16 exhibits the result of the experiment in which the conversion to B is plotted as a function of conversion of A for different pore sizes.

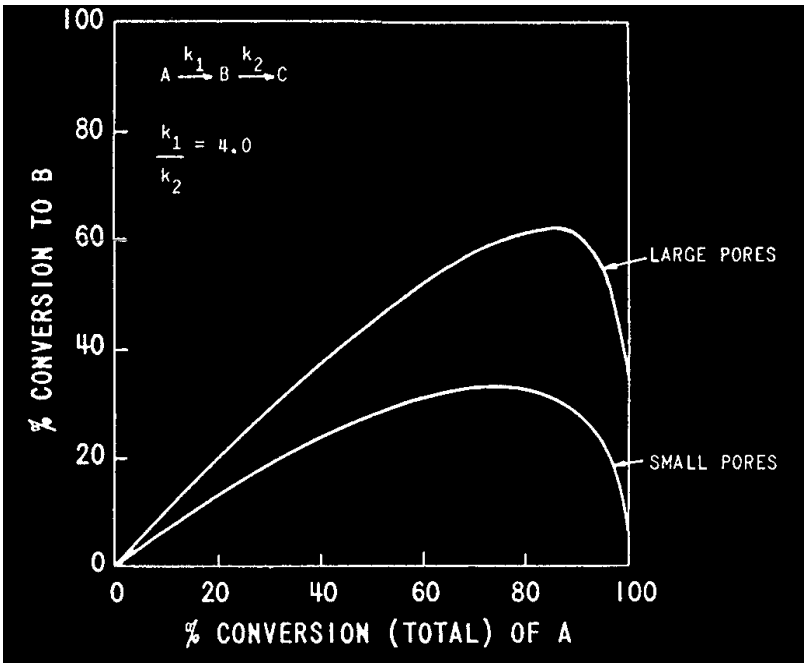

Figure 2.16: Effect of catalyst pore size on the selectivity for a first-order reaction.

The catalyst with small pores has a higher diffusion limitation than that of the large pores. The value of the conversion to B by using the small pores catalyst is significantly lower. This means that the increase of the conversion to B as well as the decrease of the formation of the component C can be minimized by reducing the diffusion limitation.

2. 6. References

[2.1] B. Bems, PhD Thesis, Berlin, Technical University, (2003).

[2.2] M. M. Günter, PhD Thesis, Berlin, Technical University, (2001).

[2.3] H. Agarás, G. Cerrella, Applied Catalysis **45** (1988) 53-60.

[2.4] J. P. Shen, C. S. Song, Catalysis Today **77** (2002) 89-98.

[2.5] W. S. Ning, H. Y. Shen, H. h. Liu, Applied Catalysis A **211** (2001) 153-157.

[2.6] Y. L. Zhang, H. Wang J. F. Deng, Chem. J. Chin. Univ. **15** (1994) 1547.

[2.7] N. Takezawa, N. Iwasa, Catalysis Today **36** (1997) 45-56.

[2.8] Y. H. Chin, R. Dagle, J. L. Hu, A. C. Dohnalkova, Y. Wang, Catalysis Today **77** (2002) 79-88.

[2.10] Y. Liu, T. Hayakawa, T. Ishii, M. Kumagai, H. Yasuda, K. Suzuki, S. Hamakawa, K. Murato, Applied Catalysis A **210** (2001) 301.

[2.11] J. P. Breen, R. H. Ross, Catalysis Today **51** (1999) 521-533.

[2.12] R. O. Idem, N. N. Bakhshi, Ind. Eng. Chem. Res. **34** (1995) 1548-1557.

[2.13] H. Kobayashi, N. Takezawa, C. Minochi, Journal of Catalysis **69** (1981) 487-494.

[2.14] Y. Y. Liu, T. Hayakawa, K. Suzuki, S. Hamakawa, Catalysis Communications **2** (2001) 195-200.

[2.15] H. Kobayashi, N. Takezawa, C. Minochi, Chemistry Letters (1976) 1347-1350.

[2.16] I. O. Bakhshi, Can. J. Chem. Res. **33** (1994) 2047-2055.

[2.17] B. Lindström, L. J. Petterson, P. G. Menon, Applied Catalysis A **234** (2002) 111-125.

[2.18] G. C. Shen, S. I. Fujita, S. Matsumoto, N. Takewawa, Journal of Molecular Catalysis **124** (1997) 123-126.

[2.19] R. O. Idem, N. N. Bakhshi, The Canada Journal of Chemical Engineering **74** (1996) 288-300.

[2.20] K. Takahashi, N. Takezawa, H. Kobayashi, Applied Catalysis **2** (1982) 363.

[2.21] C. J. Jiang, D. L. Trimm, M. S. Wainwright, N. W. Cant, Applied Catalysis A **93** (1993) 245.

[2.22] C. J. Jiang, D. L. Trimm, M. S. Wainwright, N. W. Cant, Applied Catalysis A **97** (1993) 145.

[2.24] N. Takezawa, N. Iwasa, Catalysis Today **36** (1997) 45-56.

[2.26] K. Takahashi, N. Takezawa, H. Kobayashi, Applied Catalysis **2** (1982) 383.

[2.25] H. Purnama, T. Ressler, R.E. Jentoft, H. Soerijanto, R. Schlögl, R. Schomäcker, accepted in Applied Catalysis A.

[2.27] V. Pour, J. Barton, A. Benda, Coll. Czech. Chem. Commun. **40** (1975) 2923.

[2.28] J. Barton, V. Pour, Coll. Czech. Chem. Commun. **45** (1980) 3402.

[2.29] E. Santacesaria, S. Carrá, Applied Catalysis **5** (1983) 345.

[2.30] J. C. Amphlett, M. J. Evans, R. F. Mann, R. D. Weir, Can. J. Chem. Eng. **63** (1985) 605.

[2.31] B. A. Peppley, J. C. Amphlett, L. M. Kearns, R. F. Mann, Applied Catalysis **179** (1999) 21-29.

[2.32] J. C. Amphlett, K. A. M. Creber, J. M. Davis, R. F. Mann, B. A. Peppley, D. M. Stokes Int. J. Hydrogen Energy **19** (1994) 131-137.

[2.33] J. Agrell, H. Birgersson, M. Boutonnet, Journal of Power Sources **106** (2002) 249.

[2.34] R. O. Idem, N. N. Bakhshi, Chemical Engineering Science **51** (1996) 3697.

[2.35] E. Fritzer, W. Fritz, Technische Chemie, 3. Auflage, Springer-Verlag, 1989.

[2.36] H. S. Fogler, Elements of Chemical Reaction Engineering, Third Edition, Prentice Hall International Series in the Physical and Chemical Engineering Science, New Jersey, 1999.

[2.37] A. Wheeler, “Catalysis”, ed. By P H. Emmett, Vol. II, Chap. 2, New York, Reinhold Publishing Corp., 1955.

3. Experimental Details

3.1 Materials

Following materials are used in the experiments

1. Commercial $CuO/ZnO/Al_2O_3$ catalyst (MeOH1), manufacture: Süd-Chemie
2. Methanol, for HPLC, purity ≥ 99.8% (GC), source: Sigma-Aldrich Chemie GmbH, Taufkirchen
3. Deionised water
4. Dilution material: Boron nitride (BN) (hexagonal, purity 99.5%, source: Alfa Aeser, Johnson Matthey GmbH, Karlsruhe)
5. Cooling medium: iso-Propanol
6. Inert Pyrex beads d= 0.5mm and 0.75mm, source: Th.Geyer, Berlin
7. Gas calibration, 0.5% CO, 4.5% N_2, 25% CO_2, 70% H_2, source: Messer Griesheim GmbH, Krefeld

3.2 Apparatures

1. Electro hydraulic Press PW 30 E, manufacture: Paul Weber Maschinen- und Apparatebau
2. HPLC pump P580, manufacture: Dionex
3. Condenser: ecoline RE 207, K4R electronic, manufacture: Lauda
4. Gas Chromatography: CP-3800, manufacture: Varian

Column: Carbo PLOT P7, 25 m x 0.53 mm (fused silica PLOT 25 µm)

Carrier Gas : Helium

Settings:

Front Valve Oven: 110°C

Valve 1:

Time [min]	Status
0	Fill
0.1	Inject
0.5	Fill
2	Inject

4 Fill

Front Injector Pressure : 35 psi, Column Flow: 13.8 ml/min

Front TCD Detektor : 200°C

Filament temperature : 250°C

Oven temperature programme:

T / °C	°C.min^{-1}	Hold time / min	Total time / min
30	0	7.5	7.5
80	20	2.5	12.5

6. Gas chromatography for determination of liquid composition: IGC 120 ml, manufacture: Intersmat. An Integrator 3390 A, manufacture: Hewlet Packard.

Column: CP-Wax 58 (FFAP) CB, 50 m x 0.53 mm (fused silica PLOT 2 μm)

Settings:
- Injector temperature : 145°C
- Detector temperature : 110°C
- Oven temperatur : 95°C
- Column 1(Reference) : 1.4 bar; 22.2 ml/min
- Column 2 : 2.5 bar; 20.4 ml/min

3.3 Handling of the catalysts

In order to obtain the same reaction conditions for all catalysts such as same particle size, same dilution, a standard procedure of catalyst handling was applied. The catalyst was first crushed to fine powder and then mixed with five weight amount of Boron nitride (BN). About 1.0 g of the well mixed substance was then filled in a cylinder with a diameter of 2.9 cm and pressed at 200 bar. The catalyst was pressed three times, each 4 minutes. This procedure was done on $CuO/ZnO/Al_2O_3$ catalyst which was used in the kinetic study of steam reforming of methanol. Because of the small amount of Cu/ZrO_2 catalyst obtained for the study of the catalytic behaviors, a smaller press cylinder with diameter of 1.0 cm was used. Instead of 1.0g powder, 0.4g was pressed at 200 bar three times, each 5 minutes. The pellets were then crushed carefully and the small particles were then sieved to achieve a defined particle size. The particle size used in all the experiments is 20-25 Mesh (0.75 to 1.0mm). The handling of the catalyst is shown in the following Figure 3.1.

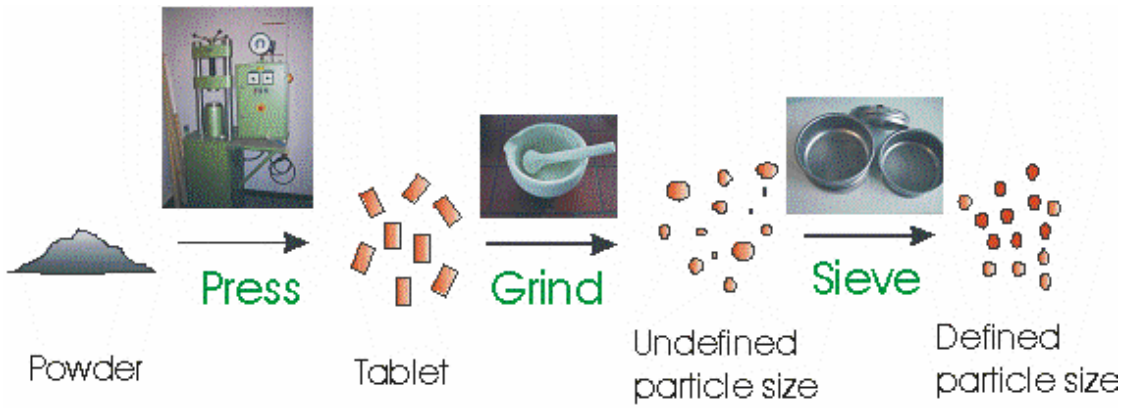

Figure 3.1: Handling of the catalyst

3.4 Experimental procedure

The catalyst with defined particle size is put into a tubular steel reactor (10mm i.d.). The catalyst is supported by a stainless steel fixed mesh grid. For flow condition, inert Pyrex beads of the catalyst's size are placed on top and below the catalyst bed. The reactor is depicted in Figure 3.2. In order to study the catalytic properties of more than one catalyst at once, three of these reactors were placed into an aluminium heating block for the heat transfer as can be seen in Figure 3.3.

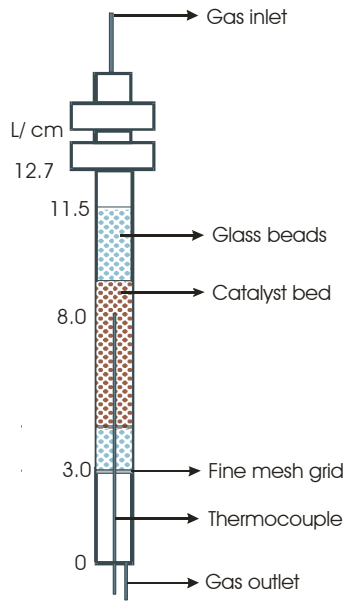

Figure 3.2: Fixed bed reactor

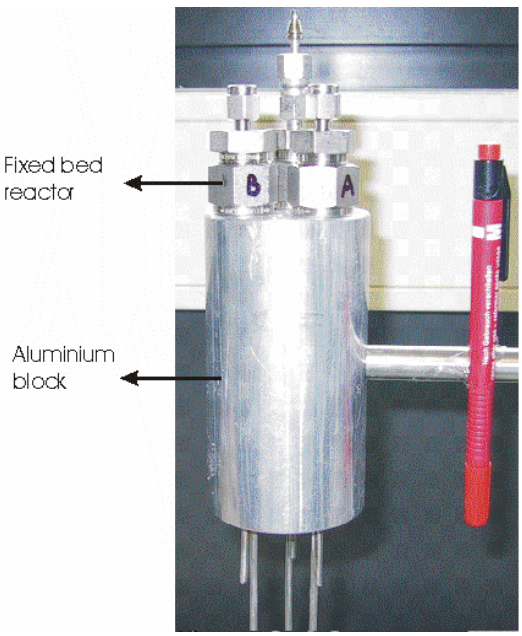

Figure 3.3 : Three channel fixed bed reactor

The advantages of using this three channels reactor with respect to the study of the catalytic properties are: direct comparison of three catalyst measurements at the same reaction conditions, changing the catalyst during the measurement, using different gases in different channels. Six cartridge heaters of 125 watt each are put inside the aluminium block. The temperature of the reactor was regulated by PID control of the cartridge heaters. Two thermocouples of type J (Fe vs. (Cu + 43% Ni)) are used, one is placed in the aluminium block, and the other one is placed in the catalyst bed. Prior to the measurement, the catalyst is reduced, activated respectively, at atmospheric pressure, 250°C by an equimolar methanol/water vapor mixture for 1h. The introduction of the reactants, water, and methanol into the reactor is done by means of an HPLC pump.

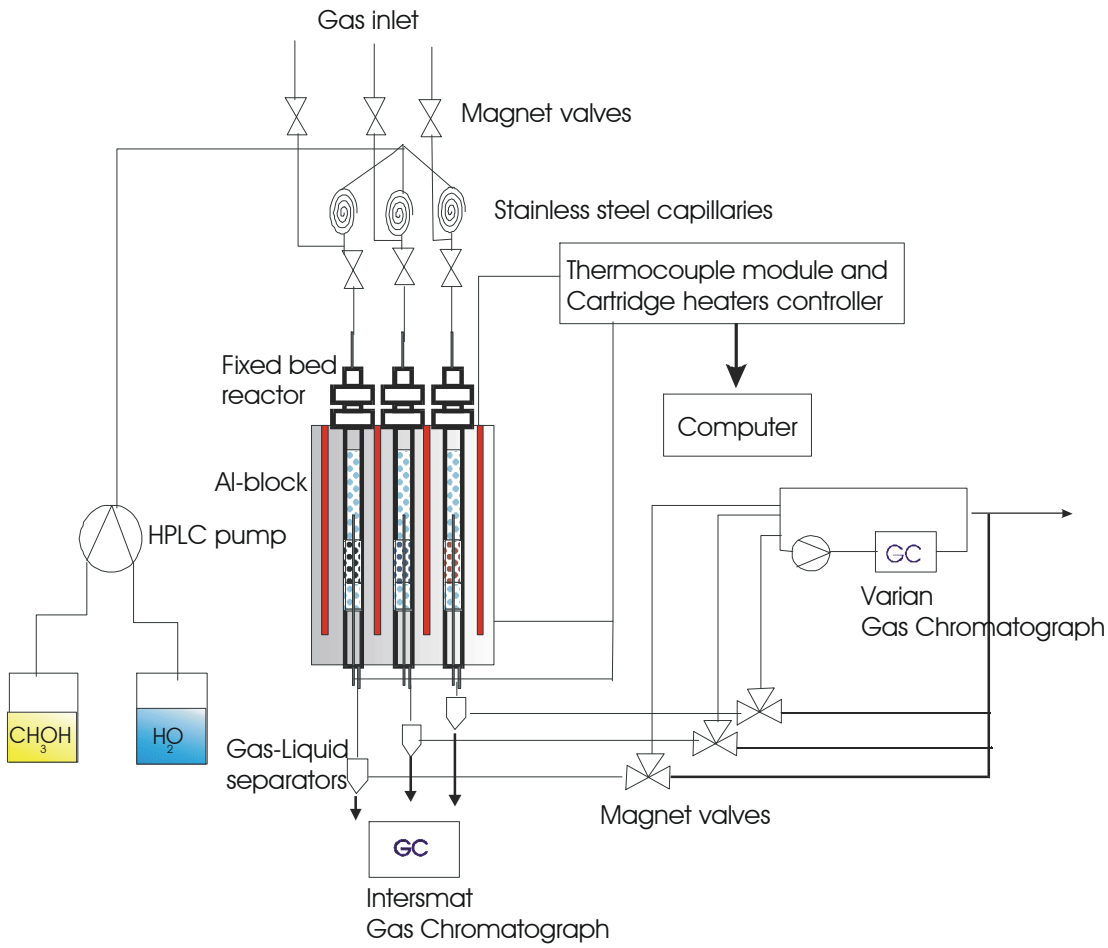

Figure 3.4: Experimental setup

By passing the exhaust gases through a series of cold traps, non-condensable product gases are separated from unreacted water and methanol. In order to obtain the dry gas, three intensive cooler with two cooling temperatures (-8°C, -8°C, -18°C) are put between the reactor and the GC. The dry effluent gases are analysed using a 25 m x 0.53 mm CarboPLOT P7 column in a Varian GC 3800 equipped with a thermal conductivity detector. Helium is used as carrier gas. The composition of the condensed mixture is analysed by a second gas chromatograph Intersmat IGC 120 ml using a 50 m x 0.53 mm fused Silica PLOT CP-Wax 58 (FFAP). The experimental setup is illustrated in Figure 3.4.

3.5 Evaluation of the experimental results

3.5.1 Determination of gas and liquid composition

In order to determine the composition of the gases produced by the reaction, a defined composition of a gas mixture is used as a calibration gas. The gas mixture contains the following gases and the volumetric content: H_2 (70%), CO_2 (25%), N_2 (4.5%), CO (0.5%). The composition of this calibration gas is chosen closely to the value that is expected from the measurements. Since TCD is used as a detector in the gas chromatograph, the calibration curve can be obtained by a linear correlation between volumetric content of the gas and the peak area plotted in the chromatogram. The volumetric content of CO and CO_2 as a function of peak area obtained by the calibration are written in equation 3.1 and 3.2.

$$\%V_{CO} = 0.0135A_{CO} \tag{3.1}$$

$$\%V_{CO_2} = 0.009A_{CO_2} \tag{3.2}$$

Due to the difference of the thermal conductivity between Hydrogen (product) and Helium (carrier gas) being small, the H_2 concentration can not be detected accurately by means of TCD detector. Hence, the determination of the volumetric content is carried out on CO and CO_2. Since the product of methanol SR process observed in our experiments contains only CO, CO_2 and H_2, the concentration of H_2 can be therefore calculated by using the mass balance showed in equation 3.3:

$$\%V_{H_2} = 1 - (\%V_{CO_2} + \%V_{CO}) \tag{3.3}$$

The composition of non converted methanol and water is determined by the second GC. In order to obtain a calibration curve depicted in Figure 3.5, a serial of methanol-water mixtures with different compositions is prepared and theirs compositions are determined by the GC.

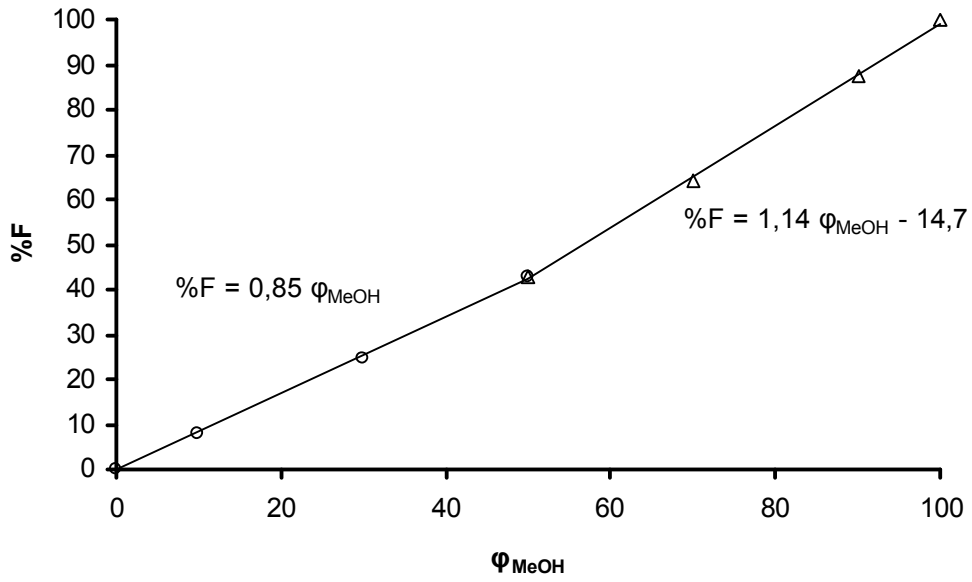

Figure3.5: GC calibration for determination of methanol composition in the mixture

%F is the relative peak area of methanol recorded by the integrator of the GC and φ_{MeOH} is the volume% of methanol in the mixture. This curve can be used to determine the volume ratio of methanol and water in a mixture. The relation between molar ratio of water to methanol, a, and the volume% of methanol and water can be described in the following equations.

$$\%V_{MeOH} = \frac{1}{(1+0.44a)} \qquad (3.4)$$

$$\%V_{H_2O} = \frac{0.44a}{(1+0.44a)} \qquad (3.5)$$

A mixture with molar ratio of 1 corresponds to the methanol volume ratio of 69.2%.

3.5.2 Determination of partial pressure of the reactants and the products

The amount of the unconverted reactants (methanol and water) can be determined as follows:

$$n_{MeOH} = n^0_{MeOH} - n^X_{MeOH} = n^0_{MeOH}(1 - X_{MeOH}) \quad (3.10)$$

$$n_{H_2O} = n^0_{H_2O} - n^X_{H_2O} = n^0_{H_2O}(1 - X_{H_2O}) \quad (3.11)$$

The amount of hydrogen is determined using the following equation.

$$n_{H_2} = 2n^X_{MeOH} + n^X_{H_2O} \quad (3.12)$$

The amount of CO and CO_2 are calculated from the amount of converted methanol and the volume ratio %V which is determined by the GC.

$$n_{CO_2} = \frac{\%V_{CO_2}}{\%V_{CO_2} + \%V_{CO}} n^X_{MeOH} \quad (3.13)$$

$$n_{CO} = \frac{\%V_{CO}}{\%V_{CO_2} + \%V_{CO}} n^X_{MeOH} \quad (3.14)$$

$$n_{total} = n_{MeOH} + n_{H_2O} + n_{H_2} + n_{CO_2} + n_{CO} \quad (3.15)$$

n^0_i is the initial amount of the component i. n^X_i is the amount of the converted reactant i. n_i is the amount of the component i after the reaction. The values of the initial moles of methanol (n^0_{MeOH}) and water ($n^0_{H_2O}$) are established. X_{MeOH} and X_{H2O} are the conversion of methanol and water. Since the reaction is performed at atmospheric pressure (P_0= 1.013 bar), the partial pressure of the component i can be defined as

$$p_i = \frac{n_i}{n_{total}} p_0 \quad (3.16)$$

3.5.3 Determination of contact time of the reactants

The contact time of the reactant mixture in the reactor can be defined as

$$\tau = \frac{V_{catalyst}}{\dot{V}_{gas}} \tag{3.6}$$

$V_{catalyst}$ is the volume of the catalyst bed in the reactor, $\dot{V}_{gas}$ is the volume flow of gaseous. The variation of the contact times is carried out by changing the flow rate of methanol and water mixture by means of HPLC pump. The determination of the contact times and conversions is done under isothermal and isobaric condition. For the calculation of the volume flow of gaseous, it is assumed that the gases behave as ideal gases. Therefore, it can be written as

$$\dot{V}_{gas} = \frac{\dot{n}_{total}\, RT}{P_{total}} \tag{3.7}$$

$\dot{n}$ is the total molar flow of the gases, R is gas constant, T is the absolute temperature and P_{total} is the total pressure. Due to the change in the number of moles in the gas as the methanol steam reforming reaction proceeds, (2 moles reactant, 4 moles product), the contact time was defined with the following equation:

$$\tau = \frac{V_{catalyst}}{\dot{V}_{gas}(1+\alpha X)} \tag{3.8}$$

α is the relative change of the gas volume in the reactor at the complete conversion, X.

$$\alpha = \frac{V_{X=1} - V_{X=0}}{V_{X=0}} \tag{3.9}$$

4. CO Formation/Selectivity for Steam Reforming of Methanol with a Commercial $CuO/ZnO/Al_2O_3$ Catalyst

4.1. Introduction

Generally, there are three possibilities to prevent CO from being introduced into the fuel cell: (i) an extra module is added between the steam reforming reactor and the fuel cell (CO clean-up unit), such as separation of hydrogen using Pd membranes or the selective oxidation of CO [4.1-4.3], (ii) a new design for the reformer reactor is employed, i.e. purification integrated in the reformer reactor [4.4-4.8], or (iii) a new catalyst is developed that is active for steam reforming, but does not produce CO. In this chapter, the formal kinetic study of methanol steam reforming over a commercial $CuO/ZnO/Al_2O_3$ catalyst has been carried out by use of differential and integral reaction data. The work is particularly focused on studying the reaction scheme of CO formation and revealing a solution to decrease CO levels in the product. As reported in the literature CO levels can be influenced by the temperature of the reactor, degree of conversion of the methanol, molar ratio of methanol and water, and addition of oxygen to the methanol-steam mixture [4.9]. As the result of the investigations, potential chemical engineering solutions for minimizing CO production are reported in this chapter.

4.2. Experimental

Measurements of the methanol steam reforming reaction were performed at atmospheric pressure in a tubular stainless steel reactor (10 mm i.d.). A commercial $CuO/ZnO/Al_2O_3$ catalyst from Süd-Chemie (approximately 50 wt% Cu) [4.14] was used in all experiments. The reactor was placed in an aluminium heating block for better heat transfer, with six cartridge heaters of 125 watt each inside the aluminium block. The temperature of the reactor was regulated by PID control of the cartridge heaters. Two thermocouples of type J (Fe vs. (Cu + 43%Ni)) were used, one was placed in the aluminium block, the other one was placed in the catalyst bed. The catalyst was supported by a stainless steel fixed fine mesh grid. For flow conditioning, inert Pyrex beads of the catalyst's size (0.85-1.0mm) were placed on top and below the catalyst bed. For steam reforming measurements the catalyst powder was first diluted with five times its weight of boron nitride (BN) and then the mixture was pressed using a cylinder stamp with a diameter of 29 mm.

One gram of the mixture was put into the cylinder stamp and was pressed at 200 bar for 4 minutes, the pressing was repeated three times for each tablet. The tablet was then crushed into smaller particles that were sieved to obtain a defined particle size. The reactants, water, and methanol (for HPLC, purity ≥ 99.8% (GC)) were introduced into the reactor in a molar ratio of 1 and at a liquid flow rate of 0.05 to 0.5 ml/min by means of an HPLC pump. Prior to the activity measurements, the catalyst was activated at 250°C in the reaction mixture.

Product analysis begins with the separation of water and methanol from the rest of the product stream. The separation is accomplished by passing the exhaust gases through a series of cold traps, non-condensed product gases (CO, CO_2, and H_2) were separated from the unreacted water and methanol. The dry effluent gases were analysed using a 25 m x 0.53 mm CarboPLOT P7 columm in a Varian GC 3800 equipped with a thermal conductivity detector. Helium was used as carrier gas. The composition of the condensed mixture was analysed by a second gas chromatograph Intersmat IGC 120 ml using a 50 m x 0.53 mm fused Silica PLOT CP-Wax 58 (FFAP). For the determination of the gas composition in the product, we used the calibrated gas von Messer Griesheim with the following composition (in % volume): CO 0.5, CO_2 25, H_2 70, the rest N_2 4.5. The peak area in the chromatogram of the 0.5 % volume of CO calculated by the GC is 520 unit. The smallest peak area that can be still counted reproducibly by the computer is about 10 unit. This indicates that the detection limit of the CO concentration is about 0.01 % volume which equals to the partial pressure of CO of 5.10^{-5} kPa. Because Helium is used as carrier gas, the concentration of N_2, CO and CO_2 can be determined accurately. By means of the mass balance calculation of the dry gas the concentration of H_2 is determined. In the work of Y. Choi et al. [4.16], they studied the methanol decomposition reaction catalyzed by a commercial $Cu/ZnO/Al_2O_3$ in the absence and presence of water (Steam reforming reaction). Their results show clearly that the by products such as methane, methyl formate and dimethyl ether are significantly detected in the reaction of methanol decomposition (in the absence of water). However, no methyl formate was detected when the feed contains 43 mol% water or greater. There was no dimethyl ether formation when the feed had more than 24 mol% water and no methane was detected after a feed of 8.6 mol% of water. Since we are working on the reaction conditions where water content in feed is 50 mol% which is much greater than that used in the work of Choi et al. The detection of the by-products under the reaction conditions applied in our experiments is therefore not necessary.

4.3. Results and Discussion

4.3.1. Activity and stability of the CuO/ZnO/Al_2O_3 catalyst

Conversion of methanol at 250 °C as a function of the W/F_m ratio (W: mass of the catalyst [kg], F_m: flow rate of methanol [mmol s^{-1}]) for the catalyst used in this study is depicted in Figure 4.1. For these measurements 200 mg of catalyst were used and the W/F_m ratio was varied by changing the flow velocity of the methanol-water mixture between 0.05 and 0.5 ml/min. The catalyst used in this work was also used in the work of Muhler and co workers [4.14] in which its composition is given. To compare the activity of this catalyst with a similar catalyst which has been reported in the literature (Süd-Chemie, G-66 MR (52 wt% Cu [11]) the methanol conversion vs. W/F_m curve for the G-66 MR catalyst at 260 °C has also been plotted in Figure 4.1.

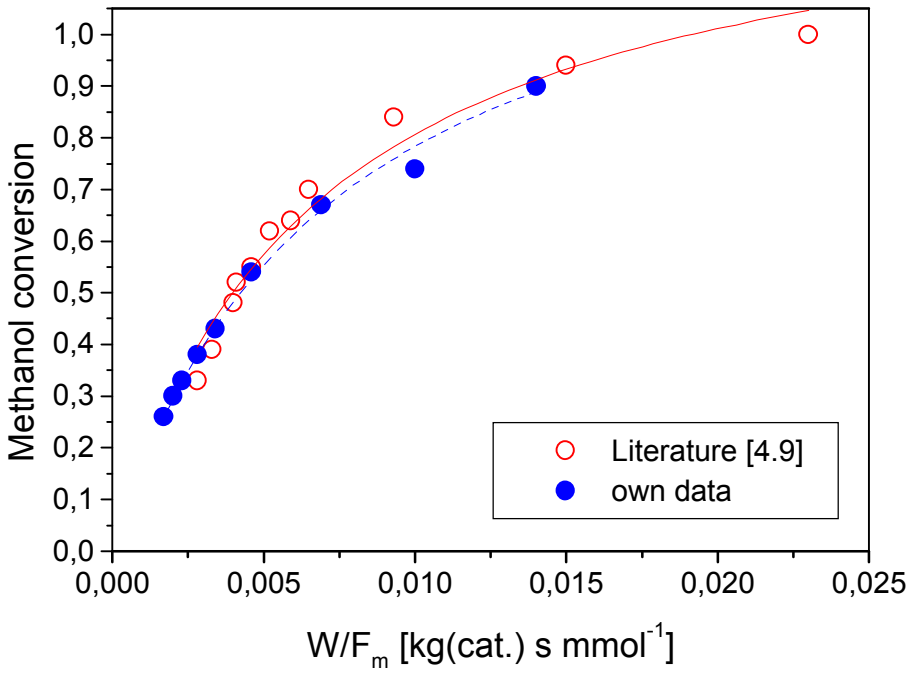

Figure 4.1: Methanol conversion as a function of W/F_m ratio for two catalysts (circle, catalyst studied in this work (T=250°C, H_2O/CH_3OH= 1.0); triangle, catalyst studied in the work of Agrell et al. [11] (T=260°C, H_2O/CH_3OH= 1.3)).

These results show little difference in methanol conversion as a function of W/F_m ratio between the two catalysts, and the catalyst studied in this work can be considered comparable to an industrial catalyst with 52 wt% Cu.

Typical runs of methanol conversion as a function of the W/F_m ratio for the $CuO/ZnO/Al_2O_3$ catalyst at reaction temperatures ranging from 230 to 300 °C are presented in Figure 4.2.

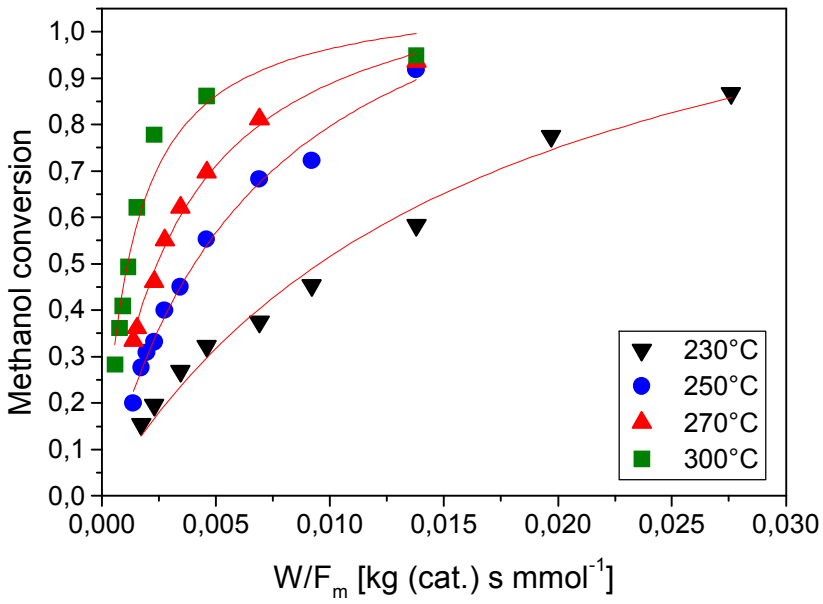

Figure 4.2: Methanol conversion as a function of W/Fm ratio at different temperatures (mass of the catalyst 200 mg).

The results show that methanol conversion increased rapidly for short contact times (0 to 0,005 kg(cat) s^{-1} $mmol^{-1}$) at all temperatures, and that the rate of the methanol conversion as function of contact time always increased with an increasing reaction temperature. Similar results have been reported in the work of Idem et al. [4.15] over a different temperature range from 170 to 250 °C. They found a dramatic change in the slope of the methanol conversion vs. W/F_m ratio curves between the reaction temperatures of 190 °C and 200 °C. Based on these results they have suggested that there are two kinetic regimes (low temperature regime $T \leq 190$ °C, high temperature regime $T \geq 200$ °C) indicating that the rate determining step for the SR reaction mechanism is different for these two temperature regimes.

The experimental results that Idem reported as being in the high temperature regime are comparable to those plotted in Figure 4.2 and we conclude that the conditions under which we have studied the SR reaction are all within the high temperature regime. The catalyst's stability over 320 h on stream is presented in Figure 4.3.

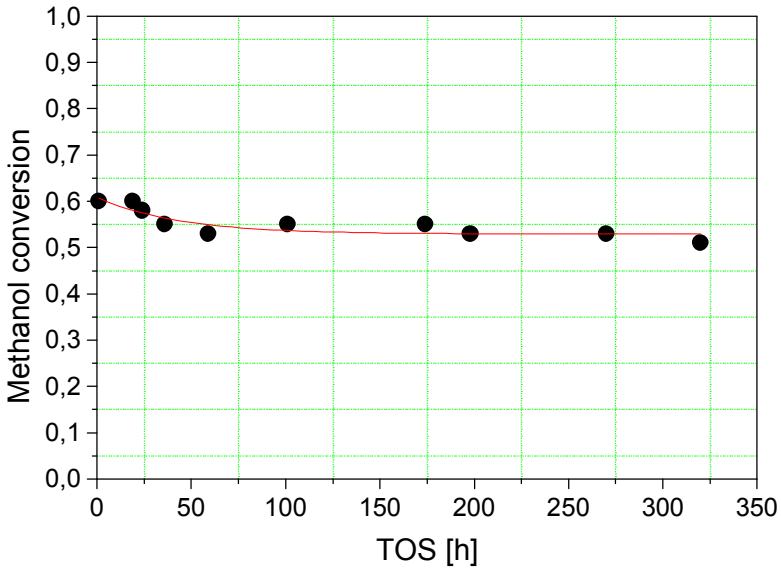

Figure 4.3: Methanol conversion as a function of time on stream at 250°C (mass of the catalyst 200mg, W/F_m ratio 0.007 [kg(cat) s mmol^{-1}]).

In the period from 0 to 100 h the conversion decreased slightly. There is little change in methanol conversion at times on stream between 100 and 320 h. This result agrees well with that reported in the literature [4.16] where the deactivation of the catalyst was measured with and without water added to methanol. It was found that in the presence of water (50%) and at 250 °C deactivation is less evident within the first 100 h on stream than with methanol alone. All measurements in this work were carried out within 100 h of the time of reduction in order to limit errors caused by catalyst deactivation.

4.3.2. Kinetic model

The reaction schemes for methanol steam reforming considered in this work are: (i) methanol steam reforming (SR) reaction and (ii) the reverse water gas shift reaction (WGS).

$$\text{(i)}\quad CH_3OH + H_2O \underset{k_{-1}}{\overset{k_1}{\rightleftharpoons}} 3H_2 + CO_2 \tag{4.1}$$

$$\text{(ii)}\quad CO_2 + H_2 \underset{k_{-2}}{\overset{k_2}{\rightleftharpoons}} CO + H_2O \tag{4.2}$$

For analysis of the kinetics of these reactions the power law was used as a model to fit the experimental data. Since both of the reactions are reversible processes, the equilibrium constant K can be defined as the ratio of the forward and backward reaction constants:

$$K_{SR} = \frac{k_1}{k_{-1}} = \frac{P_{H_2}^3 P_{CO_2}}{P_{CH_3OH} P_{H_2O}} \tag{4.3}$$

$$K_{rWGS} = \frac{k_2}{k_{-2}} = \frac{P_{CO} P_{H_2O}}{P_{CO_2} P_{H_2}} \tag{4.4}$$

where P is the partial pressure and k is the rate constant for forward (+) and reverse (-) reactions. The rate equations for the SR reaction and reverse WGS reaction can be described as follows:

$$r_{SR} = k_1 P_{CH_3OH}^m P_{H_2O}^n - k_{-1} P_{H_2}^r P_{CO_2}^s \tag{4.5}$$

$$r_{rWGS} = k_2 P_{CO_2} P_{H_2} - k_{-2} P_{H_2O} P_{CO} \tag{4.6}$$

It is clear from the low concentrations of CO formed that the rate for the reverse WGS reaction is very small with respect to that of the SR reaction. Therefore, it was necessary to assume the reaction order of the reactants and the products for the reverse WGS reaction and we have set them to 1, as in Eq. 4.6.

By inserting the reaction equilibrium constants K_{SR}, K_{rWGS} into Eqs. (4.5) and (4.6), the reaction rates can be written as:

$$r_{SR} = k_1 P_{CH_3OH}^m P_{H_2O}^n (1 - \frac{1}{K_{SR}} \frac{P_{H_2}^r P_{CO_2}^s}{P_{CH_3OH}^m P_{H_2O}^n}) \quad (4.7)$$

$$r_{RWGS} = k_2 P_{CO_2} P_{H_2} (1 - \frac{1}{K_{rWGS}} \frac{P_{H_2O} P_{CO}}{P_{CO_2} P_{H_2}}) \quad (4.8)$$

The equilibrium constant being a function of temperature can be calculated by means of the following thermodynamic descriptions:

$$\Delta G_{298}^0 = \Delta H_{298}^0 - T\Delta S_{298}^0 \quad (4.9)$$

$$\Delta G_{298}^0 = -RT \ln K_{298} \quad (4.10)$$

The reaction enthalpies ΔH^0_{298} for SR reaction and reverse WGS reaction are +49 kJ/mol and +41 kJ/mol, the reaction entropies are +177 J/mol and +42 J/mol, and the free enthalpies ΔG_{298}^0 are -3.8 kJ/mol and +28.6 kJ/mol, all respectively [4.17]. The equilibrium constant as a function of temperature is given by the van't Hoff expression:

$$\ln K = \ln K_{298} - \frac{\Delta H_{298}^0}{R} \left\{ \frac{1}{T} - \frac{1}{T_{298}} \right\} \quad (4.11)$$

The results of calculation of K_{SR}, K_{rWGS}, and the reciprocals of the constants at different temperatures are listed in Table 4.1.

Table 4.1: Equilibrium constants of SR reaction and reverse WGS reaction as a function of temperature

	SR		**r-WGS**	
T [°C]	K_1 [bar^2]	K_1^{-1} [bar^{-2}]	K_2	K_2^{-1}
230	$1{,}5\ 10^4$	$6{,}6\ 10^{-5}$	$0{,}9\ 10^{-2}$	116
250	$2{,}4\ 10^4$	$4{,}2\ 10^{-5}$	$1{,}3\ 10^{-2}$	80
270	$3{,}6\ 10^4$	$2{,}8\ 10^{-5}$	$1{,}8\ 10^{-2}$	56
300	$6{,}4\ 10^4$	$1{,}6\ 10^{-5}$	$2{,}9\ 10^{-2}$	35

Because of the very small value of the reciprocal of K_{SR}, Eq. (4.7) can be simplified as follows:

$$r_{SR} = k_1 P_{CH_3OH}^m P_{H_2O}^n \qquad (4.12)$$

Equations 4.8 and 4.12 were then used to fit the experimental reaction rate data. In order to determine the reaction parameters (reaction order, reaction rate constants, and activation energies) two experimental methods were employed. First, the differential method was used in order to determine the reaction order of methanol, and then the integral method was used to determine the total reaction order and the rate constants for the SR reaction. For the differential method determination the conversion of methanol was less than 10%, the partial pressure of water was held constant, nitrogen was used as a third component, and the reaction temperature was 250 °C. Prior to measurement, the catalyst was activated in the methanol/water feed (molar ratio of 1) at 250 °C for 1 h. Through variation of the methanol partial pressure at constant water partial pressure reaction rates with the units [mol (CH_3OH) s^{-1} $g^{-1}_{catalyst}$] were determined. A log-log plot of methanol partial pressure and reaction rate is displayed in Figure 4.4.

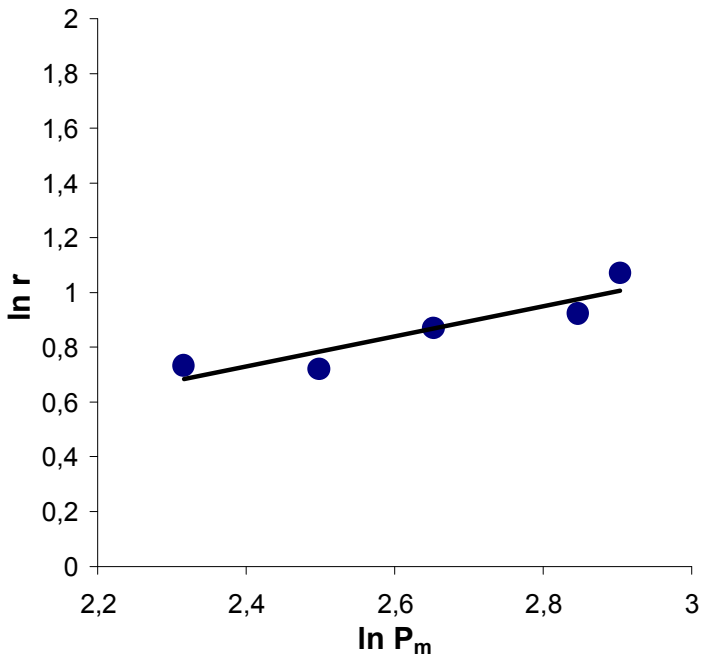

Figure 4.4: Reaction rate of methanol steam reforming as a function of methanol partial pressure at constant water partial pressure at 250°C (mass of the catalyst 40 mg, W/F_m ratio 0.33 to 0.15 [kg(cat) s mmol^{-1}]).

Linear regression of the experimental data gave a reaction order for methanol of 0.6 ± 0.1. The catalysis experiments used to obtain this value were performed using catalyst with particle sizes between 0.71 – 1.0 mm. We have determined that under these conditions there was a significant intraparticle diffusion limitation. The reaction order observed here is thus an apparent reaction order. For large values of the Thiele modulus (ratio of the surface reaction rate to the diffusion rate), i.e. for a system with significant diffusion limitation, the apparent reaction order n_{app} is related to the true reaction order n_t by [4.18]

$$n_{app} = \frac{n_t + 1}{2} \qquad (4.13)$$

The true reaction order of methanol obtained using Eq. 4.13 is 0.2. This value is comparable to that reported in the literature [4.19] of 0.26, obtained in a study of the kinetics of steam reforming of methanol over a BASF S3-85 $CuO/ZnO/Al_2O_3$ catalyst. The absence of a diffusion limitation was determined in the study of the BASF catalyst by a threefold variation in the catalyst particle size (0.15-0.59 mm).

We then determined the total reaction order and the rate constants for the SR reaction by the integral method as follows. A wide range of methanol and water conversions as a function of contact time were measured for temperatures from 230 to 300°C and these data are presented in Figures (4.5-4.8).

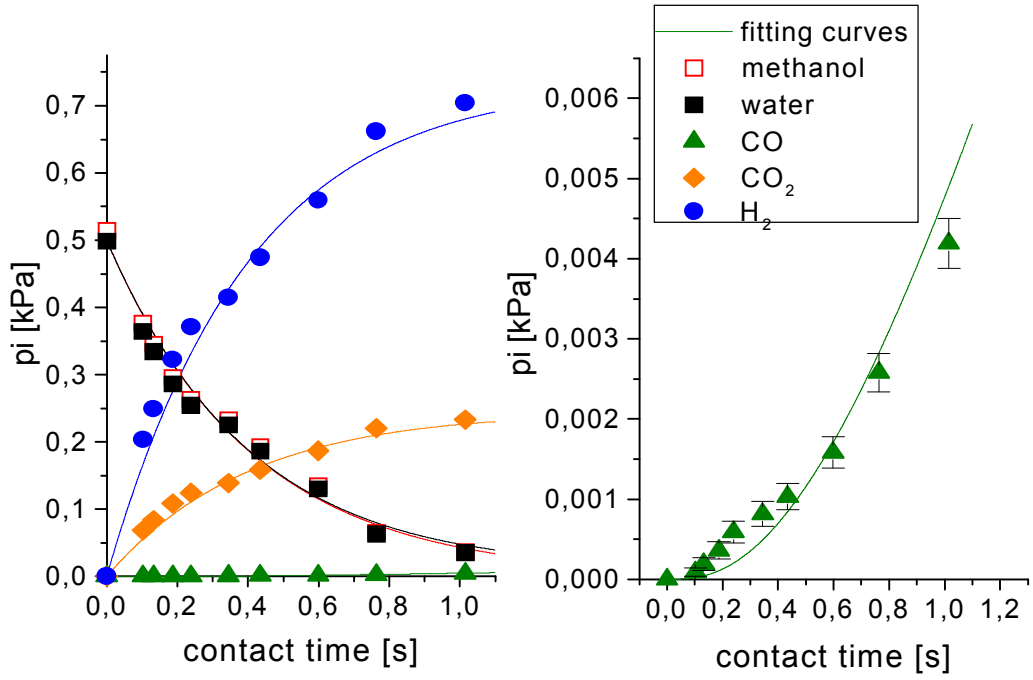

*Figure 4.5: Partial pressures of components of the product stream as a function of contact time at **230°C,** experimental data and fitting results.*

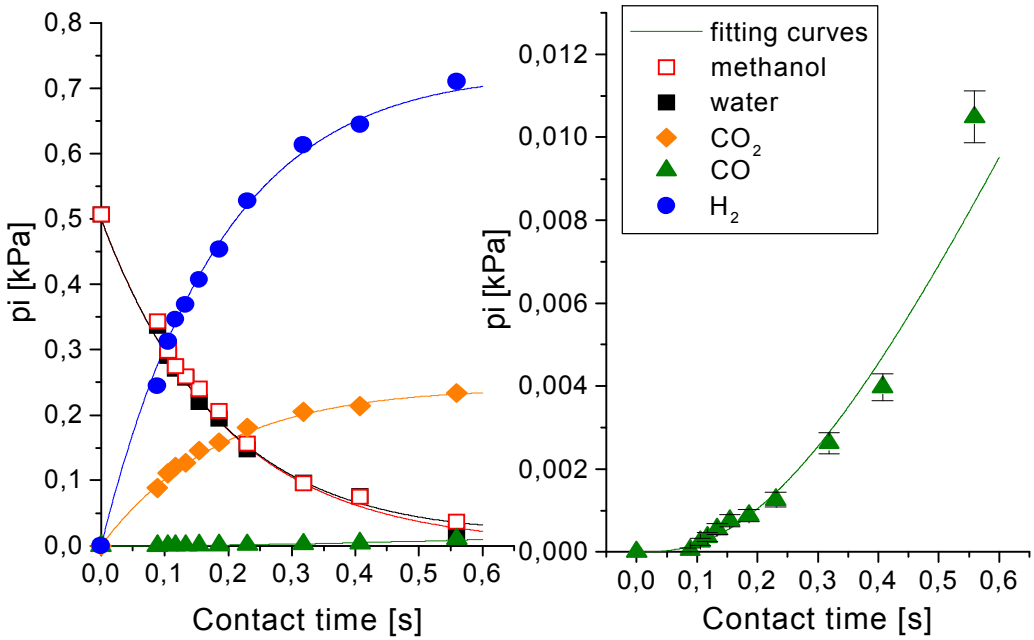

*Figure 4.6: Partial pressures of components of the product stream as a function of contact time at **250°C,** experimental data and fitting curves.*

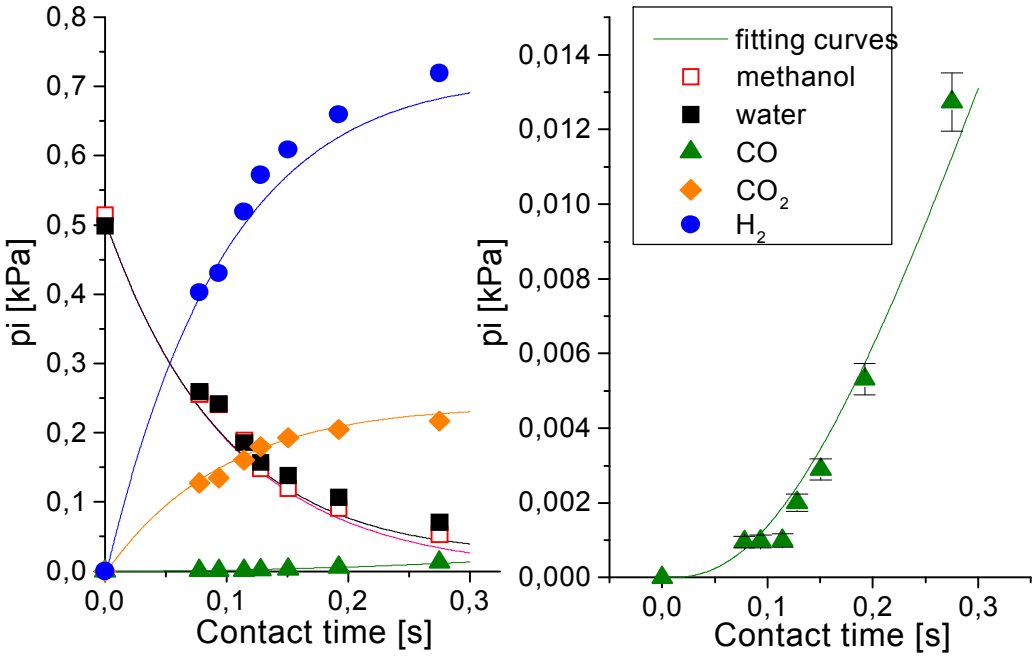

*Figure 4.7: Partial pressures of components of the product stream as a function of contact time at **270°C,** experimental data and fitting curves.*

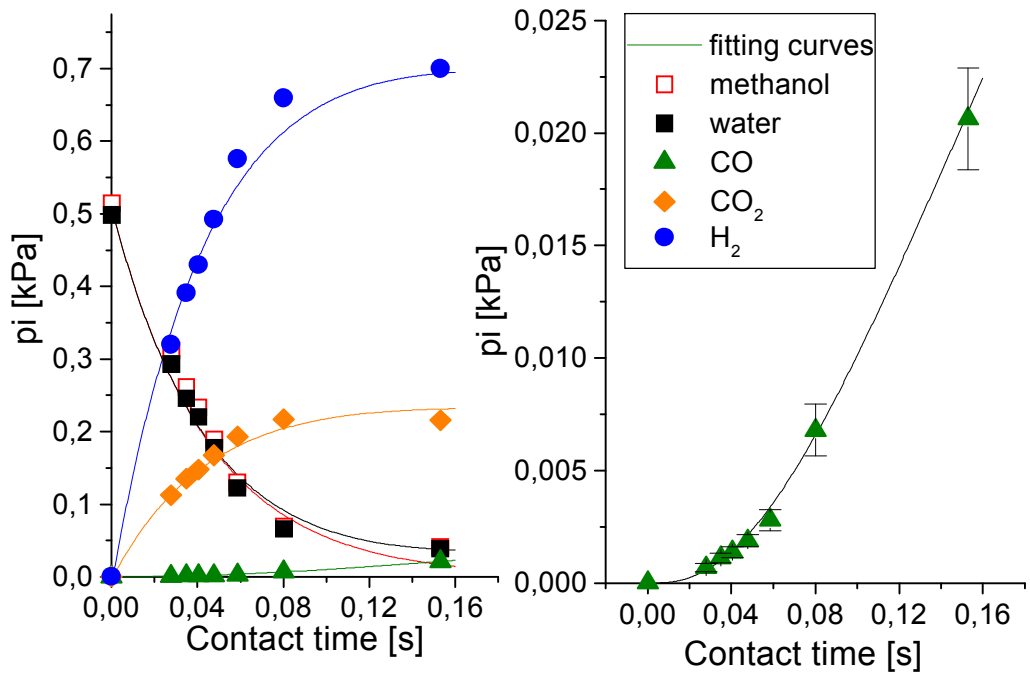

*Figure 4.8: Partial pressures of components of the product stream as a function of contact time at **300°C,** experimental data and fitting curves.*

Eqs. (4.8) and (4.12) were used to fit the experimental data for all temperature ranges. Due to the change in the number of moles in the gas as the methanol steam reforming reaction proceeds, (2 moles reactant, 4 moles product), the contact time was defined with the following equation:

$$\tau = \frac{V_{catalyst}}{\dot{V}_{gas}(1+\alpha X)} \qquad (4.14)$$

Where $V_{catalyst}$ is the volume of the catalyst bed in the reactor, $\dot{V}_{gas}$ is the volume of gaseous methanol and water, α is the relative change of the gas volume in the reactor if the conversion is complete, and X is the fractional conversion of methanol. Determination of the reaction order and rate constants was accomplished by fitting the simulation to the measured data with variation of the total reaction order and the rate constants until a good agreement is obtained. Specifically a total reaction order was chosen, and the fit was optimised by variation of the reaction rate constants. A Runge-Kutta method was used to solve the differential equations for the SR and rWGS reactions, and the experimental data was fit by means of a simplex least-square method. A new total reaction order was then selected and the data was again fit by variation of the rate constants. This procedure was repeated until an optimal fit was achieved. By this method a total reaction order for methanol and water (m + n in Eq. 4.12) of 1 was determined to fit the data well.

The reaction products were hydrogen, carbon dioxide, and a very small concentration of carbon monoxide. For all reaction temperatures measured there was no significant change in the molar ratio of methanol and water with increasing contact time. The partial pressure of hydrogen and carbon dioxide increased with increasing contact time. As expected from the SR reaction scheme, Eq. (4.1), the ratio of the partial pressures of hydrogen and carbon dioxide was about 3 at all reaction temperatures and levels of conversion. Thus, the scheme of the SR reaction as expressed by Eq. (4.12) describes well the methanol steam reforming reaction with a $CuO/ZnO/Al_2O_3$ catalyst. The small amount of CO produced increases with increasing contact time and can be described by the reaction model (i.e. Eqs. (4.8) and (4.12)). This indicates that CO is a consecutive product formed by the reverse WGS reaction from the products of the SR reaction, H_2 and CO_2. It is clear from Figure 4.5 that, although the formation of CO can be described satisfactorily with the reverse WGS reaction, the “real” reaction kinetics are more complex. Specifically, there seems to be a change in the controlling

kinetic of CO formation for conversions > 70%. This is clearly visible in the change in CO concentration with increasing contact time shown in Figure 4.5. At contact times less than 0.5 s there is more CO present than is predicted by the simulation. At higher contact times there is a distinct change in the rate of CO formation. A similar change in kinetic is discernable in Figure 4.6, also at about 70% conversion, or at a contact time of 0.15 seconds for the reaction at 250 °C. As conversion increases the changing gas phase may induce changes in the active surface. Alternatively, the change in rate law may indicate blocking of particular sites on the heterogeneous surface of the copper particles. A strained copper bulk [4.20], for instance, may result in heterogeneity in the sites active for CO formation with specific sites exhibiting a higher sticking coefficient for CO than unstrained copper metal (0.87, Cu(111)). The CO level as a function of contact time will be discussed later in more detail.

The results in Figures 4.5-4.8 show that by using the reaction schemes in Eqs. (4.8) and (4.12) the simulation agrees well with the experimental data. In addition, we did not observe any inhibition effects due high concentrations of CO_2 and H_2 produced in the SR process at high conversions. Such an effect would be expressed in the data as a decrease in the rate of reaction at higher conversion in comparison to the simulation which does not account for an inhibition effect. We did not observe such deviations indicative of product inhibitions. The reaction rate constants for the steam reforming reaction, k_1, and the reverse water gas-shift reaction, k_2, were the free parameters used in the simulation to fit the experimental data. Log(k) as a function of reciprocal temperature is presented in Figure 4.9.

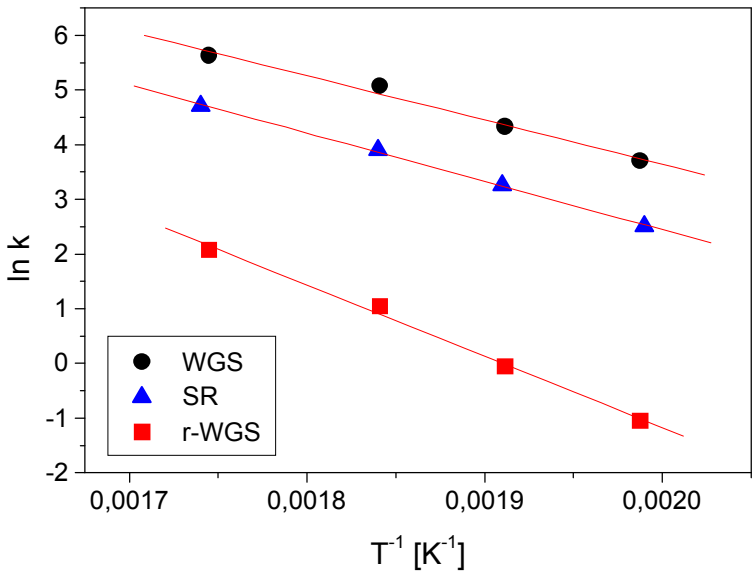

Figure 4.9: Reaction rate constants for SR reaction, reverse WGS reaction, and WGS reaction as a function of reciprocal temperatures.

The apparent activation energy and pre-exponential factor for the steam reforming reaction obtained by linear regression are:

E_a = 76 kJ/mol

$k_0 = 8.8\ 10^8$ [$s^{-1}\ g_{cat}^{-1}$]

Similarly, using data presented in Figure 4.9, E_a and k_0 were determined for the reverse WGS, and WGS reactions.

(i) reverse WGS: E_a = 108 kJ/mol $k_0 = 6.5\ 10^9$ [$bar^{-1}\ s^{-1}\ g_{cat}^{-1}$]

(ii) WGS: E_a = 67 kJ/mol $k_0 = 4.0\ 10^7$ [$bar^{-1}\ s^{-1}\ g_{cat}^{-1}$]

All reaction parameters for SR, reverse WGS, and WGS reactions obtained in this work are summarized in Table 4.2.

Table 4.2: Experimental results of reaction rate constants, activation energy and pre-exponential factor for SR reaction, reverse WGS reaction and calculated result of WGS reaction.

	SR	**r-WGS**	**WGS**
T [°C]	k [$s^{-1}\ g_{cat}^{-1}$]	k [$bar^{-1}\ s^{-1}\ g_{cat}^{-1}$]	k [$bar^{-1}\ s^{-1}\ g_{cat}^{-1}$]
230	2,5	0,07	7,8
250	5,2	0,19	14,6
270	9,8	0,57	31,7
300	22,3	1,59	54,8
Ea [kJ/mol]	76	108	67
k_0	$8,8\ 10^8$	$6,5\ 10^9$	$4,0\ 10^7$

The activation energy determined in this work is an apparent activation energy corresponding to a catalyst with particle sizes of 0.71 - 1.0 mm in which internal diffusion limitation occurred. Therefore, the activation energy is lower in comparison to that reported in the literature [4.19] which was calculated from data obtained using smaller particle sizes where mass transport limitations were absent.

4.3.3. CO formation

CO partial pressure as a function of contact time for all temperatures investigated is presented in Figures. 4.5-4.8. CO partial pressure increases monotonically with an increasing contact time. The contact time span for all the experiments was chosen to include a wide range of methanol conversions ranging up to almost 90%. The CO levels at all reaction temperatures (230 - 300 °C) are far below those predicted by equilibrium calculations based on water gas shift reaction, and this indicates that CO_2 can not be formed from CO through the WGS reaction. This result agrees well with the literature [4.9, 4.19]. The selectivity of CO and CO_2 as a function of contact time is depicted in Figure 4.10.

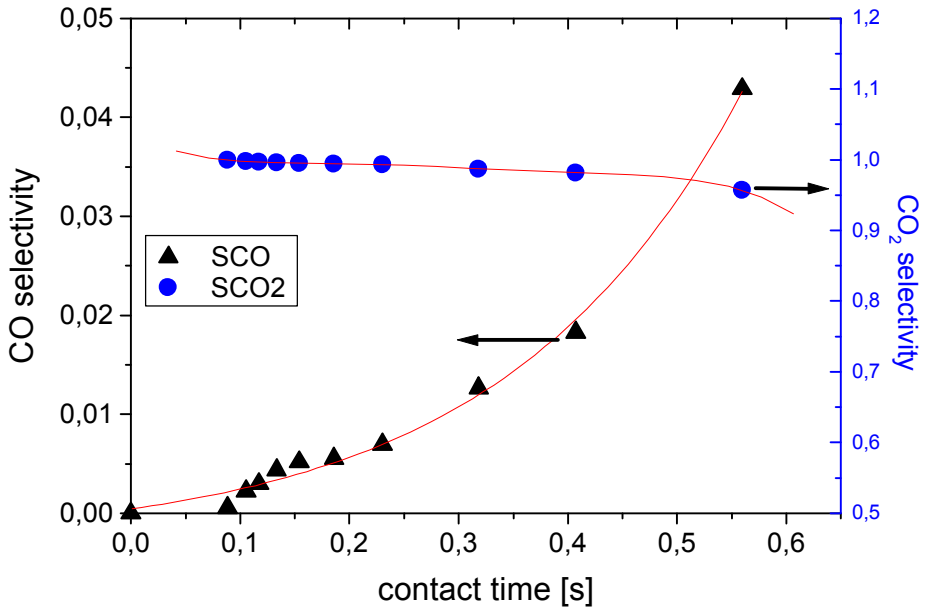

Figure 4.10: CO and CO_2 selectivity as a function of contact time at 250°C.

As contact time approaches 0, selectivity to CO goes to 0 showing that CO is a secondary product. These results show clearly that CO is produced in a consecutive reaction and that CO is not formed as a primary product of methanol decomposition. Consistent with this reaction scheme the selectivity to CO_2 is constant up to a contact time of 0.2 s and there after decreases slightly. By employing the reverse WGS reaction to describe the CO formation as a consecutive product, the experimental data have been simulated accurately.

Conversely, reaction schemes for the methanol steam reforming reaction on copper based catalysts that include the decomposition of methanol to produce CO followed by the WGS reaction [4.21-4.24] were not able to fit our experimental data. Several investigations concerning the WGS reaction on commercial ($CuO/ZnO/Al_2O_3$) catalysts have been performed under reaction conditions similar to those employed in this work. Results reported in the literature [4.19] have shown that the WGS reaction does not take place under the condition of the SR reaction, although the $CuO/ZnO/Al_2O_3$ catalyst is known to be active for the low temperature WGS reaction. In this study high concentrations of CO were added to a reactant mixture of methanol and water, and there was no significant change in the rate of hydrogen production or in the hydrogen to CO_2 ratio, the amount of CO passing through the reactor remained unchanged. One reason suggested for this minimal participation of the WGS reaction in the presence of methanol and water vapor is competitive adsorption between methanol and CO [4.19]. In an infrared spectroscopy study it was found that methanol and methyl formate adsorb more strongly on a copper surface as compared to carbon monoxide [4.25]. The blockage of the catalyst's surface through methanol and methyl formate prevents the reaction of CO and water. Takahashi et al. [4.13] have reported that the WGS reaction was also blocked in the presence of methanol for a Cu/SiO_2 catalyst.

4.3.4. Influence of intraparticle diffusion limitation to the CO formation

The study of intraparticle diffusion limitation of two different particle sizes (0.71-1.0 mm and 0.45-0.5mm), is presented in Figure 4.11. Result shows that the catalyst with smaller particle size produces the higher methanol conversion. The dependence of methanol conversion on the particle size indicates the presence of an intraparticle diffusion limitation as mentioned earlier.

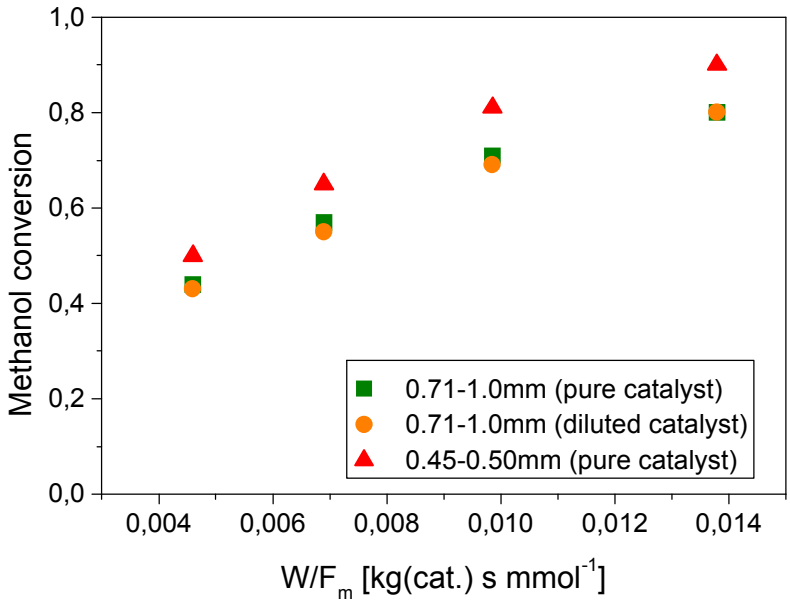

Figure 4.11: Methanol conversion as a function of W/Fm ratio carried out on different catalyst particle sizes (0.45-0.5mm(pure catalyst); 0.71-1.0mm(pure catalyst); 0.71-1.0mm (diluted with 5 fold amount of boron nitride))

CO concentration as a function of methanol conversion measured for catalysts with different particle sizes is plotted in Figure 4.12.

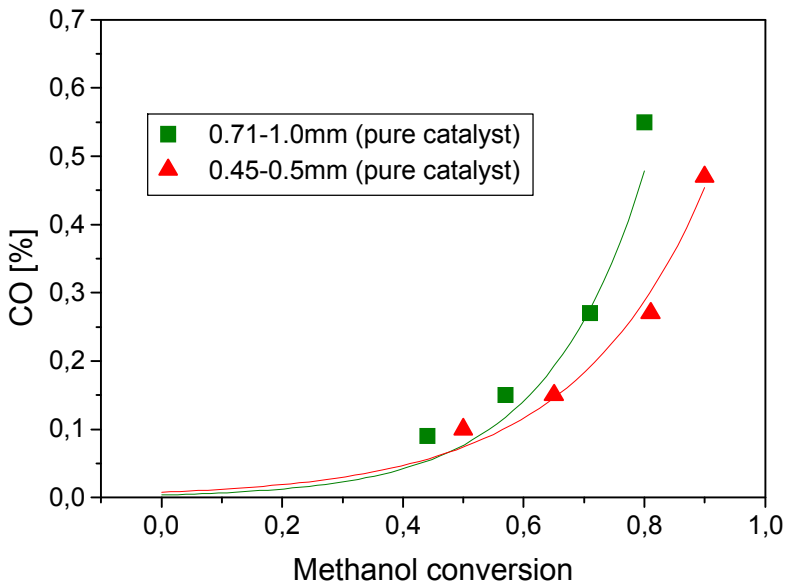

Figure 4.12: CO formation during MSR as a function of methanol conversion for catalysts with different particle sizes (0.71-1.0mm (pure catalyst), 0.45-0.5 (pure catalyst)).

At the same methanol conversion, the CO level obtained from larger particles was found to be higher than that obtained from smaller particles. The increase of the CO concentration with increasing particle size and thus, increasing diffusion limitation is again consistent with the finding that CO is formed as a consecutive product in the reverse WGS reaction. This result agrees well with our results relating to the kinetics of CO formation (CO levels as a function of contact time). CO concentration as a function of methanol conversion measured on pure and 5-fold diluted catalyst with the same particle sizes is depicted in Figure 4.13.

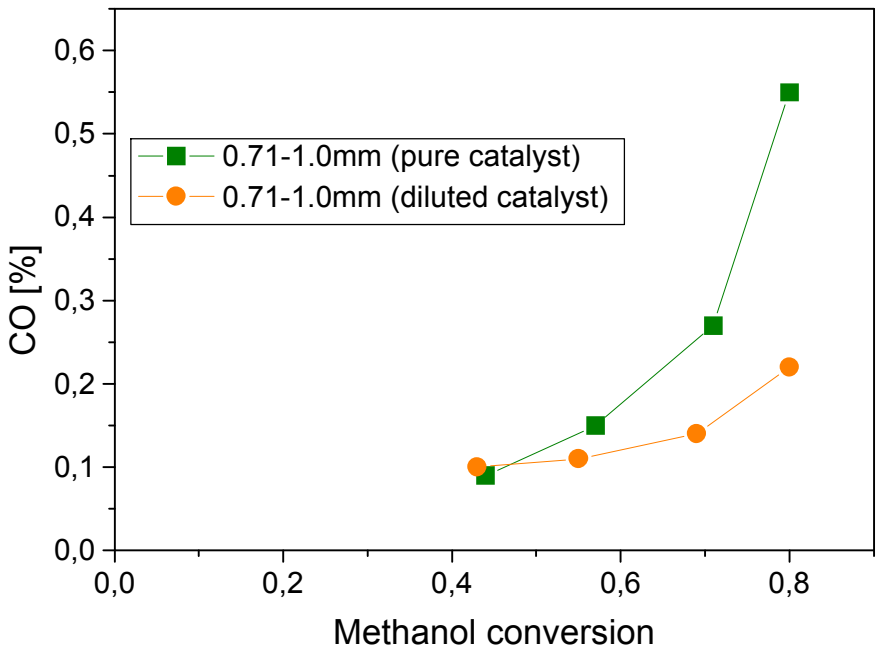

Figure 4.13: CO formation as function of methanol conversion for catalysts diluted and not diluted.

Evidently, the catalyst diluted with boron nitride produced much less CO than that without dilution. The difference becomes significant at methanol conversions higher than 0.6. The influence of diluting the catalyst with boron nitride on CO formation can be interpreted using the scheme depicted in Figure 4.14.

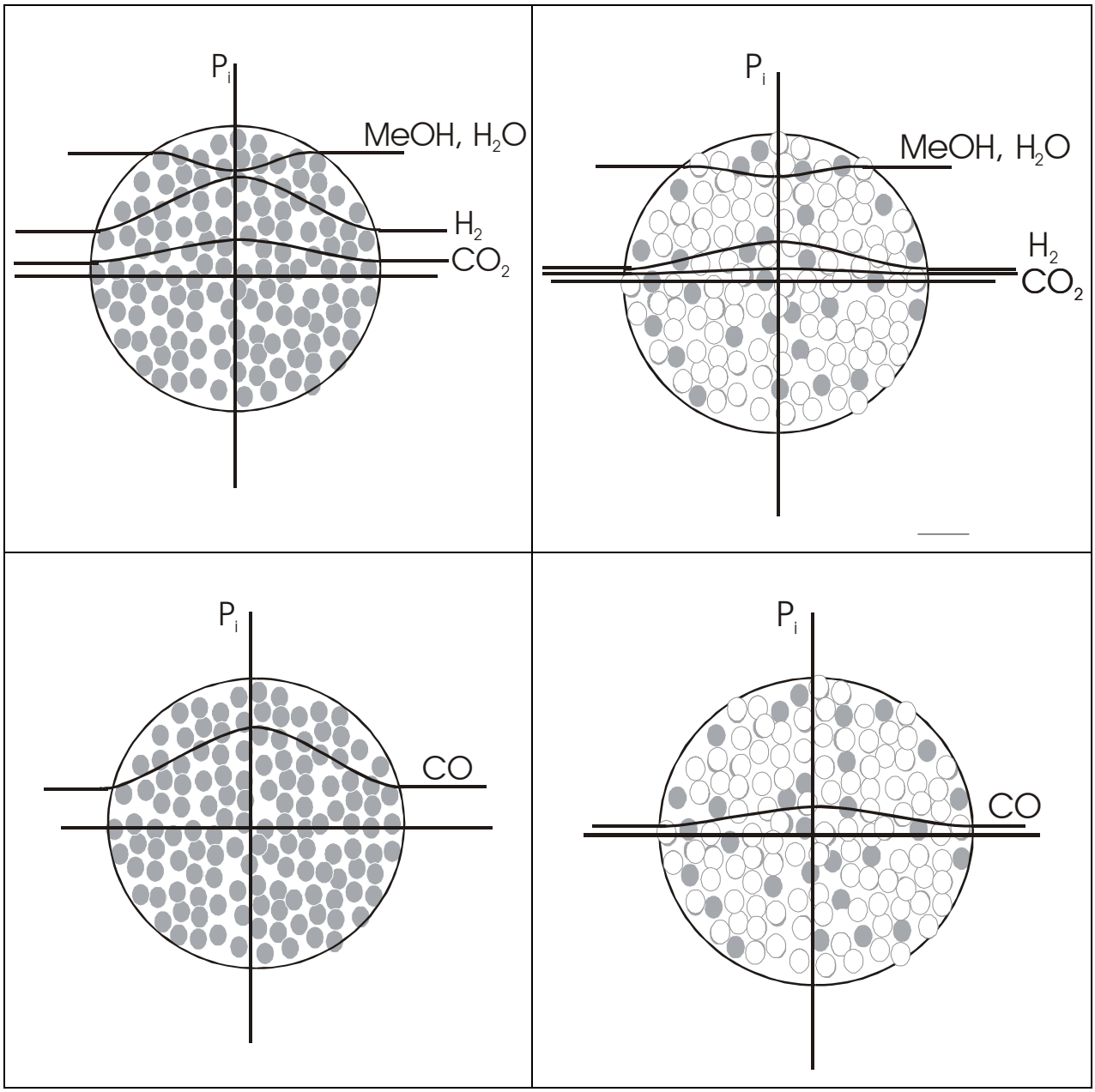

Figure 4.14: Description of the partial pressure profile of the components (reactants, products) as a function of particle radii for catalysts diluted and not diluted.

The circles with different intensities depict particles with different catalyst concentrations (dark: pure catalyst, light: inert material). Conversion in particles of the pure catalyst is much higher than that in particles of the diluted catalyst. This results in higher concentrations of hydrogen and carbon dioxide in the particle centers.

The rate of the consecutive CO formation by reverse WGS reaction is a function of the hydrogen and the carbon dioxide concentrations and so more CO is produced in the pure catalyst than in the diluted catalyst. Further studies on this subject are necessary to obtain more quantitative information. Our results clearly show that the concentration of CO formed as a consecutive product is influenced by the particle size of the catalyst which relates to the intraparticle diffusion limitation and the treatment of the catalyst, e.g. catalyst dilution with inert material. It has previously been reported that the level of CO produced in methanol steam reforming over copper based catalysts can be influenced by the following factors:

(i) reaction temperature [4.9, 4.28]
(ii) contact time, conversion of methanol respectively [4.9]
(iii) molar ratio of methanol and water [4.9, 4.16]
(iv) introducing oxygen to methanol steam mixture [4.9]

Based on this work it becomes clear that additional factors influence the formation of CO:

(v) particle size of the catalyst (intraparticle diffusion limitation)
(vi) mechanical treatment of the catalyst i.e. dilution
(vii) heterogeneity of the copper surface resulting from defects in the Cu bulk or different morphology of the copper particles.

With respect to the intraparticle diffusion limitation that influences the amount of CO formed, the objective is to minimize the diffusion path. For packed bed reactors lower levels of CO can be achieved by using a very small particle size, where intraparticle diffusion limitation is absent. In such a reactor the grain size of the catalyst in the reactor plays an important role for the flow behavior. In order to achieve plug flow behavior of the gas through the catalyst bed, the diameter of the catalyst in general should be smaller than 0.1 times the inner diameter of the reactor. However, use of excessively small particles of catalyst in a reactor can increase the pressure drop across the reactor. In order to exclude intraparticle diffusion limitations and to keep a certain particle size which obeys the plug flow criterion and produces minimal pressure drop, an egg-shell catalyst with the active component coated on the surface of a support material can be used. Using an egg-shell catalyst for methanol steam reforming over Cu catalysts may be potentially advantageous, however the ability to synthesize such a catalyst, in light of the complexity of the synthesis of Cu catalysts, would require

investigation. Alternatively, minimal levels of CO, and particle size that obeys the plug-flow criterion with less pressure drop may be achieved by diluting the catalyst with inert material. Treatment of the catalyst by dilution is a simple step which significantly influence the CO levels and will provide no substantial disadvantages to the process. Similarly, for on-board SR production of H_2, coating the walls of a micro-tube reactor with layers of catalysts sufficiently thin to exclude diffusion limitations may be feasible. Even simpler in design, if not implementation, would be to make the tubes themselves out of Cu or a Cu containing composite material which may be activatable by suitable oxidation and reduction treatments. These proposed chemical engineering solutions should be considered for implementation of the production of H_2 for fuel cells through the steam reforming of methanol. Additionally, the complex kinetics of the formation of CO, that deviate from the simplified reaction mechanism assumed here and highlights the complexity of the active surface, indicate that in addition to the engineering solutions proposed, there is room for improvement in the catalyst itself. The defect type and density in the bulk and at the surface of the copper metal and, hence, catalytic properties may be substantially improved by appropriate preparation and treatment procedures of improved copper catalysts.

4.4. Conclusions

A catalytic study of methanol steam reforming over commercial catalyst $CuO/ZnO/Al_2O_3$ has been performed at atmospheric pressure over a wide temperature range (230-300 °C). The reaction scheme used is the direct formation of CO_2 and hydrogen by the SR reaction and the formation of CO as a consecutive product by the reverse WGS reaction. The power rate law and the kinetic reaction parameters of the SR reaction and the reverse WGS reaction were used to fit the experiment data resulting in the following:

$$r_{SR} = k_1 P_{CH_3OH}^m P_{H_2O}^n$$

m= 0.6; n= 0.4

apparent E_a= 76 kJ/mol k_0= 8.8 10^8 [s^{-1} g_{cat}^{-1}]

$$r_{RWGS} = k_2 P_{CO_2} P_{H_2} - k_{-2} P_{H_2O} P_{CO}$$

apparent E_a= 108 kJ/mol k_0= 6.5 10^9 [bar^{-1} s^{-1} g_{cat}^{-1}]

Internal diffusion limitations were present for the particle size of catalyst used in this study and so only apparent activation energies for this particle size can be reported. A simulation employing the SR reaction and the reverse WGS reaction to describe the methanol steam reforming process over a $CuO/ZnO/Al_2O_3$ catalyst fit the kinetic data measured at 230 to 300 °C well. The monotonic increase of CO partial pressure as a function of contact time as well as the limit of no selectivity for CO as the contact time approaches 0, shows that CO is formed as a consecutive product. Although the majority of CO is produced as a secondary product, the deviation from a single rate law, over the broad range of conversions investigated, indicates that the complexity of the reaction kinetics, particularly at lower temperatures, is greater than described by the model given here.

In addition to the parameters that have already been reported in the literature as influencing the production of CO (reaction temperature, contact time, molar ratio of methanol and water, and addition of oxygen to the methanol-steam feed), the CO concentration can also be influenced by the particle size of the catalyst through its effect on intraparticle diffusion limitation. The greater the mass transport limitation in the catalyst particle the higher the concentration of CO in the product stream. Suppressing the CO levels by using very small

particles of pure catalyst in which internal diffusion limitations are negligible can reduce CO formation, but this solution may not be desirable due to an increased pressure drop in the reactor. Potential solutions that can be applied to reduce the CO concentration are (i) the use of egg-shell catalyst; however, this kind of catalyst is in general employed for noble metals and the synthesis route is complex, (ii) the use of a microtube reactor with either tube walls thinly coated with catalyst, or with Cu tubes which may be activatable, (iii) use of a diluted catalyst, or (iv) improve surface and bulk defect type and density by appropriate preparation and treatment procedures. Further study is needed to quantify our ability to suppress CO formation through these solutions.

4.5 References

[4.1] O. Korotkikh, R. Farrauto, Catal. Today **62** (2000) 249

[4.2] C. D. Dudfield, R. Chen, P. D. Adcock Int J. Hydrogen Energy **26** (2001)763

[4.3] Se H. Oh, R. M. Sinkevitch, J. Catal. **142** (1993) 254

[4.4] J. Han, Il-soo kim, K. S. Choi, J. Power Sources **86** (2000) 223

[4.5] Y. M. Lin, G. L. Lee, M. H. Rei, Catal. Today **44** (1998) 343

[4.6] N. Itoh, Y. Kaneko, A. Igarashi, Ind. Eng. Chem. Res. **41** (2002) 4702

[4.7] J. Han, I. S. Kim, K. S. Choi, Int J. Hydrogen Energy **27** (2002) 1043

[4.8] I. S. Wieland, I. T. Melin, I. A. Lamm, Chem. Eng. Science **57** (2002)1571

[4.9] J. Agrell, H. Birgersson, M. Boutonnet, J. Power Sources **106** (2002) 249

[4.10] R. Peters, H. G. Düsterwald, B. Höhlein, J. Power Sources **86** (2000) 507

[4.11] B. A. Peppley, J. C. Amphlett, L. M. Kearns, R. F. Mann, Appl. Catal. **179** (1999) 21

[4.12] J. P. Breen, J. R. H. Ross, Catal. Today **51** (1999) 521

[4.13] K. Takahashi, N. Takezawa, H. Kobayashi, Appl. Catal. **2** (1982) 363

[4.14] T. Genger, O. Hinrichsen, M. Muhler, Catal. Lett. **59** (1999) 137

[4.15] R. O. Idem, N. A. Bakhshi, Chem. Eng. Science **51** (1996) 3697

[4.16] Y. Choi, H. G. Stenger, Appl. Catal. B **38** (2002) 259

[4.17] P. W. Atkins, Physikalishe Chemie, VCH (1987) 859

[4.18] H. S. Fogler, Elements of Chem. Reaction Engineering, 3rd. Edition, 754

[4.19] C. J. Jiang, D. L. Trimm, M. S. Wainwright, Appl. Catal. **93** (1993) 245

[4.20] M.M Günter, T. Ressler, B. Bems, C. Büscher, T. Genger, O. Hinrichsen, M. Muhler, R. Schlögl, Catal. Lett. **71** (2001) 37.

[4.21] V. Pour, J. Barton, A. Benda, Coll. Czech. Chem. Commun. **40** (1975) 2923

[4.22] J. Barton, V. Pour, Coll. Czech. Chem. Commun. **45** (1980) 3402

[4.23] E. Santacesaria, S. Carra, Appl. Catal. **5** (1983) 345

[4.24] J. C. Amphlett, M. J. Evans, R. F. Mann, R. D. Weir, Can. J. Chem. Eng. **63** (1985) 605

[4.25] D. M. Monti, . W. Cant, D. L. Trimm and M. S. Wainwright, J. Catal. **100** (1986) 17

5. Activity and Selectivity of a Nanostructured CuO/ZrO_2 Catalyst in the Steam Reforming of Methanol

5.1. Introduction

A number of copper based catalysts promoted with different metal oxides Cu/Zn [5.1, 5.7-5.11], Cu/Cr [5.1, 5.7, 5.10, 5.12], Cu/Mn [5.7, 5.13], Cu/Zr [5.1, 5.10, 5.12, 5.14] have been investigated recently. Here, we present a study on the catalytic properties of a novel CuO/ZrO_2 catalyst. In order to improve the activity, long term stability, and reduced CO formation, a catalyst consisting of copper supported on ZrO_2 was synthesised using a polymer templating technique. The morphology and porosity of zirconia can be readily controlled by the templating procedure, resulting in a nanostructured material with high surface area. The small copper particles formed during reduction of the catalyst stay well separated by the ZrO_2 support, preventing sintering and loss of copper surface area with time on stream. The catalytic activity was determined in a fixed bed reactor using gas chromatography to measure the concentration of gases and liquids in the product stream. A commercial $CuO/ZnO/Al_2O_3$ catalyst (about 50 wt. % Cu) was employed for comparison.

5.2. Experiment

5.2.1. Catalyst preparation

The preparation of the CuO/ZrO_2 catalyst described below was performed by J. H. Schattka in the group of M. Antonietti, Max Planck Institute of Colloids and Interfaces, Golm, Germany. For the preparation of the catalyst a templating procedure was applied. At first, a porous polymer gel was formed by radical polymerization of organic monomers in a highly concentrated surfactant solution [5.15-5.18]. Subsequently, the gel was used as the template in a sol-gel nanocoating process [5.19, 5.20].

Materials. The surfactant Tween 60 ® (T60, polyoxyethylene(20) sorbitan monostearate), the organic monomers acrylamide (AA), glycidylmethacrylate (GMA) and ethylene glycol dimethacrylate (EGDMA) as well as the radical initiator potassium persulfate (KPS) were purchased from Aldrich. Zirconium(IV) propoxide (ZrP, 70 % in 1-propanol) and copper(II) acetylacetonate ($CuAcac_2$) were also obtained from Aldrich. All chemicals were used as received. The water employed during the preparation was prepared in a three-stage Millipore purification system (Milli-Q Plus 185) resulting in a resistivity higher than 18 MΩ cm.

Polymer gel preparation. For the preparation of the polymer gel 25 g of the structure directing surfactant, T60, were dissolved in 50 ml of water. The monomers (6.25 g AA and 6.25 g GMA) were added to this homogeneous solution. Upon addition of 2.51 g of EGDMA as a crosslinker, the solution became turbid. The initiator (0.63 g KPS) was dissolved in the mixture, which was then poured into test tubes. Polymerization was carried out at 60 °C. After 16 hours the resulting gel was taken out of the test tubes and cut into disks. The surfactant was removed by soxhlet extraction (ethanol, 2 days) and subsequent washing with water. Finally, the gel was transferred into 2-propanol.

Sol-gel nanocoating. 20.0 g ZrP and 2.0 g $CuAcac_2$ were stirred over night. The resulting dark blue solution was nearly saturated with the copper salt. The polymer gels were initially soaked in this solution over night and then in a hydrolysis solution for 24 h. The hydrolysis solution was prepared from equal volumes of water and 2-propanol and saturated with $CuAcac_2$ by stirring it with an excess of the salt for several hours; the undissolved salt was removed by decanting the supersaturated solution. After drying, the polymer gel was removed from the metal oxide by heating the hybrid material over 2 hours to 500 °C under a nitrogen atmosphere; then the gas was switched to oxygen and the temperature was maintained for 10 hours.

5.2.2. Structural characterisation

The X-ray diffraction (XRD) measurements were performed on a STOE STADI P diffractometer (Cu $K\alpha_1$ radiation, curved Ge monochromator) in transmission geometry with a curved position sensitive detector. X-ray absorption spectroscopy (XAS) data were collected at beamline X1 at the Hamburg Synchrotron Radiation Laboratory HASYLAB. The spectra were taken at the Cu K edge in transmission mode using a Si(111) double crystal monochromator. 10 mg of sample were mixed with 30 mg of hexagonal boron nitride and pressed with a force of one ton into a 5 mm in diameter self-supporting pellet. X-ray absorption fine structure (XAFS) analysis was performed using the software package WinXAS v2.3 [T. Ressler, *J. Synch. Rad.* **1998**, *5*, 118 – 122]. Background subtraction and normalization were carried out by fitting linear polynomials to the pre-edge and the post-edge region of an absorption spectrum, respectively. The extended X-ray absorption fine structure (EXAFS) $\chi(k)$ was extracted by using cubic splines to obtain a smooth atomic background, m0(k). The radial distribution function FT(χ(k)) was calculated by Fourier transforming the

k3-weighted experimental $\chi(k)$ function, multiplied by a Bessel window, into the R space. EXAFS data analysis was performed using theoretical backscattering phases and amplitudes calculated with the ab-initio multiple-scattering code FEFF7. [J. J. Rehr, C. H. Booth, F. Bridges, S. I. Zabinsky, *Phys. Rev.* **1994**, *B 49*, 12347 – 12350]. EXAFS refinements were performed in R space to magnitude and imaginary part of a Fourier transformed k^3-weighted experimental $\chi(k)$. Structural parameters determined by a least-squares EXAFS refinement of a Keggin model structure to the experimental spectra are (i) one E0 shift for oxygen and copper backscatterer, (ii) Debye-Waller factors for single-scattering paths, (iii) distances of single-scattering paths. Coordination numbers (CN) and S_0^2 were kept invariant in the refinement.

5.2.3. Kinetic studies

Reactor setup. Steam reforming of methanol was performed at atmospheric pressure in a tubular stainless steel reactor (10 mm i.d.). The reactor was placed in an aluminium heating block equipped with six cartridge heaters with 125 watt each. The temperature of the reactor was regulated by PID control of the cartridge heaters. Two thermocouples of type J (Fe vs. (Cu + 43%Ni)), one in the aluminium block, the other one in the catalyst bed, were used.

Catalysis measurements. For steam reforming of methanol the catalyst powder was first diluted with five times its weight of hexagonal boron nitride (BN) and then the mixture was pressed using a cylinder stamp with a diameter of 10 mm. 0.4 gram of the mixture was put into the cylinder stamp and was pressed at 200 bar for 5 minutes, the pressing was repeated three times for each pellet. The pellet was then crushed into smaller particles that were sieved to obtain a defined particle size. The catalyst was supported by a stainless steel fixed fine mesh grid. For flow conditioning, inert Pyrex beads of the catalyst's size (0.85-1.0 mm) were placed on top and below the catalyst bed. A commercial $CuO/ZnO/Al_2O_3$ catalyst from Süd-Chemie (approximately 50 wt% Cu) [5.13] was used as a reference catalyst. The reactants, water and methanol, were introduced into the reactor in a molar ratio of 1 and at a liquid flow rate of 0.07 ml/min by means of an HPLC pump. Prior to the activity measurements, the catalyst was activated at 250 °C in the reaction mixture. Non-condensable product gases were separated from unreacted water and methanol by passing the exhaust gases through a series of cold traps. The dry effluent gases were analysed using a 25 m x 0.53 mm CarboPLOT P7 columm in a Varian GC 3800 equipped with a thermal conductivity detector. Helium was used as carrier gas. The composition of the condensed mixture was analysed by a second gas

chromatograph (Intersmat IGC 120 ml) using a 50 m x 0.53 mm fused Silica PLOT CP-Wax 58 (FFAP).

5.3. Results and discussion

5.3.1. Catalyst characterisation

X-ray diffraction. The XRD pattern of an "as prepared" sample mixed with 50 wt. % corundum as internal standard is shown in Figure 5.1.

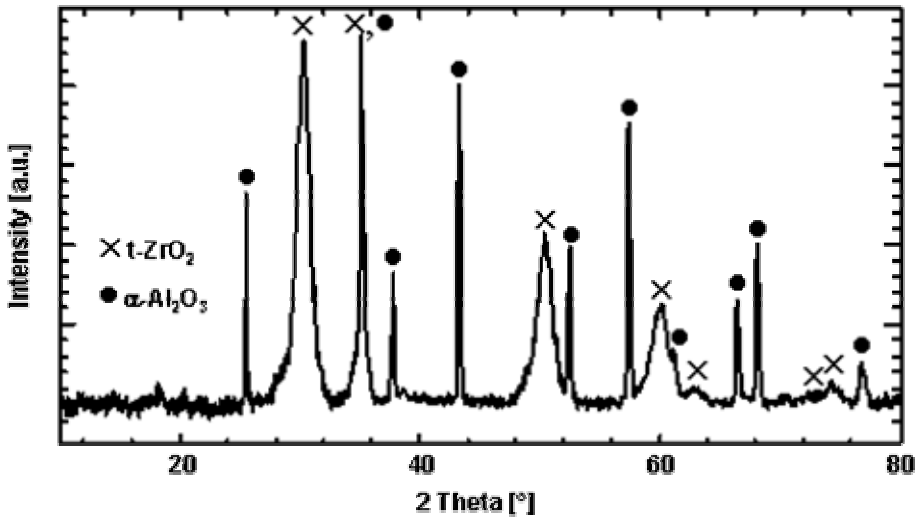

Figure 5.1: X-ray diffraction pattern of the CuO/ZrO_2 catalyst mixed with 50 wt. % corundum as internal standard.

All XRD lines detected correspond to tetragonal (or cubic) zirconia, ZrO_2. The fact that ZrO_2 crystallises as a high temperature polymorph instead of the room temperature thermodynamically stable monoclinic form could be explained by either copper doping or particle size effects. The latter explanation is adopted here because our EXAFS analysis yields no evidence for copper incorporation into the zirconia lattice (see below). The XRD lines are significantly broadened due to small crystallite sizes, making it difficult to assess the degree of tetragonality. Assuming a narrow and uniform distribution, the average crystallite size can be estimated to be in the order of ~ 60 Å based on the Scherrer formula. By comparison of the peak intensities with the internal standard, the crystallinity of ZrO_2 is close to 100%, thus excluding a significant fraction of X-ray amorphous zirconia. Furthermore, the XRD pattern exhibits no peaks belonging to monoclinic ZrO_2. Due to the low copper content of the sample, an extremely weak CuO 111 peak is the only detectable sign of a copper

containing phase. Upon reduction of the sample in 2% hydrogen at 250°C, the XRD pattern changes slightly. In addition to the ZrO_2 peaks, the strongest reflection of metallic copper (Cu 111) becomes detectable.

X-ray absorption spectroscopy. The Cu K edge spectrum of the calcined catalyst resembles that of copper(II) oxide CuO, but exhibits a pronounced reduction in amplitude (Figure 5.2).

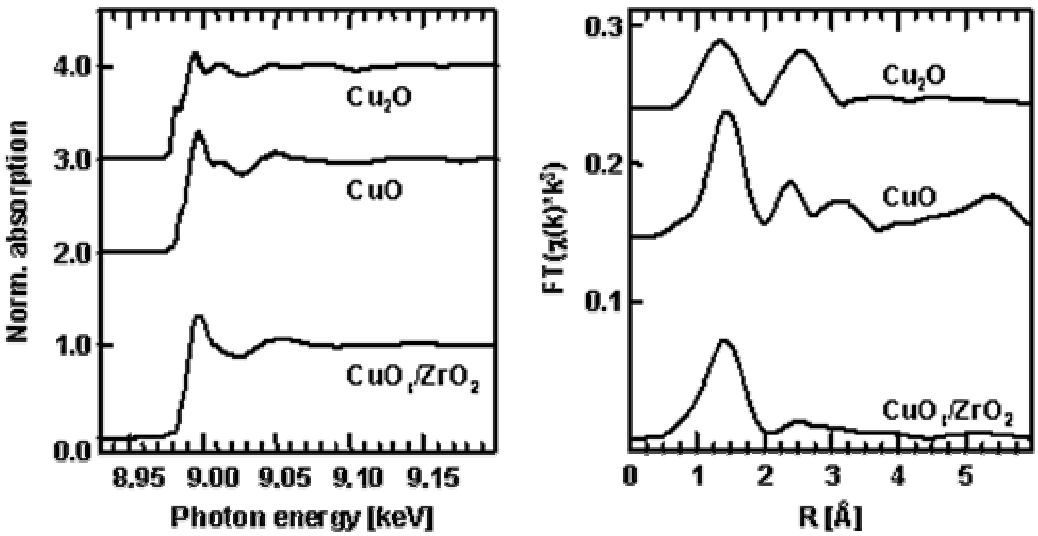

Figure 5.2: Cu K-edge X-ray absorption spectra and radial distribution functions of the calcined catalyst (CuO/ZrO_2) and two reference samples (Cu_2O, CuO)

An EXAFS refinement of a CuO model structure to the experimental spectrum resulted in a very good agreement between theoretical and experimental data, confirming that the copper containing phase of the catalyst is indeed CuO (Figure 5.3). Furthermore, the quality of the fit allows us to exclude the presence of significant amounts of other copper phases, including copper incorporated into the ZrO_2 structure. The considerable amplitude reduction of the experimental spectrum was accounted for by a small Debye temperature (corresponding to large Debye-Waller factors) for the CuO model structure. Since the spectrum was taken at room temperature, this indicates a significant amount of disorder in the CuO structure and/or very small particle sizes.

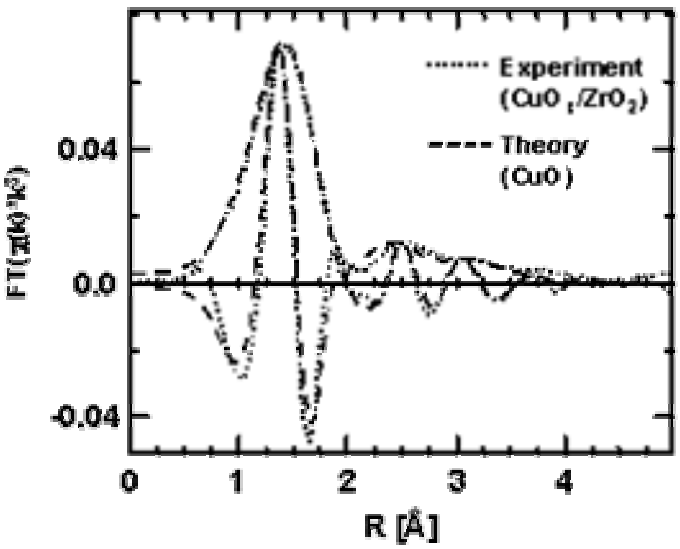

Figure5.3: EXAFS fit of a CuO structure model to the experimental fourier transformed c*(k) of* CuO/ZrO_2

The EXAFS analysis of the reduced Cu/ZrO_2 sample shows that the reduction of CuO to Cu is complete within the limit of detection, again yielding no indication for copper doping of the zirconia structure. A more detailed structural study on this catalyst system will be presented elsewhere [5.27].

5.3.2. Catalysis measurements

In order to activate the catalyst, the initially present copper(II) oxide has to be reduced to metallic copper. Possible treatments would be: (i) direct reduction by the methanol-water feedstock with methanol as the reducing agent or (ii) previous reduction in diluted hydrogen (e.g. 2%-5% H_2 in N_2). The influence of the different reduction treatments of the catalyst on the activity in methanol steam reforming has been studied by Idem et. al. [5.23]. It was demonstrated that all Cu-Al catalysts without promoter and catalysts containing the optimum promoter (Mn, Cr, Zn) achieved higher methanol conversion when reduced in a methanol-water mixture than those initially reduced in a H_2 atmosphere. In our present work, reduction of the catalysts with methanol-water vapour at 250°C was used for all experiments. The catalyst activity was evaluated in terms of methanol conversion (vol.%). In order to evaluate the activity and selectivity behaviour of the Cu/ZrO_2 catalyst, a commercial $Cu/ZnO/Al_2O_3$ methanol synthesis catalyst (Süd-Chemie, approximately 50 wt. % Cu) was examined at the same reaction conditions.

5.3.2.1. Activation behaviour

Figure 5.4 shows that the activity of the CuO/ZrO_2 catalyst can be increased significantly by temporary addition of oxygen to the feed (50 ml/min for 5 minutes).

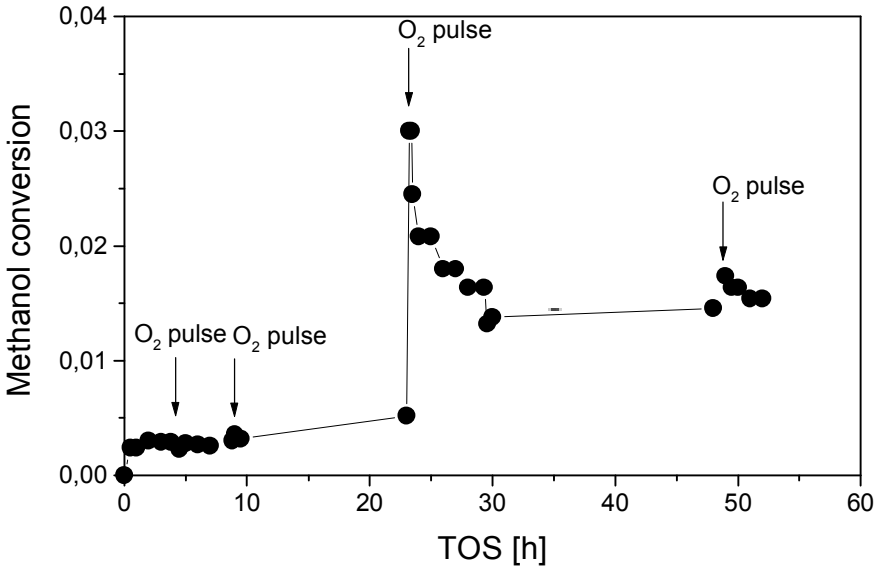

Figure 5.4: Activation of Cu/ZrO_2 catalyst by introducing O_2 into the feed. Reaction conditions: methanol/water molar ratio 1, T= 250°C, flow rate of methanol/water mixture = 0.07ml/min, mass of catalyst = 150 mg.

However, it is also apparent that the timing of the oxygen addition is an important factor. Initially, the catalyst is only slightly active after reduction in the feed. There is a slight increase in activity with time on stream. Oxygen additions during the first few hours have no apparent influence. In contrast, a drastic increase in activity is initiated by introducing oxygen after a longer time on stream. This sudden activity jump is followed by an approximately exponential decrease that ends at a higher activity level than before the oxygen addition. Another addition of oxygen several hours later causes only a small activity spike but no long term enhancement.

Because the beneficial effect of oxygen addition seems to depend on long time on stream, a similar experiment was performed on a larger time scale (more than 500 h, Figure 5.5).

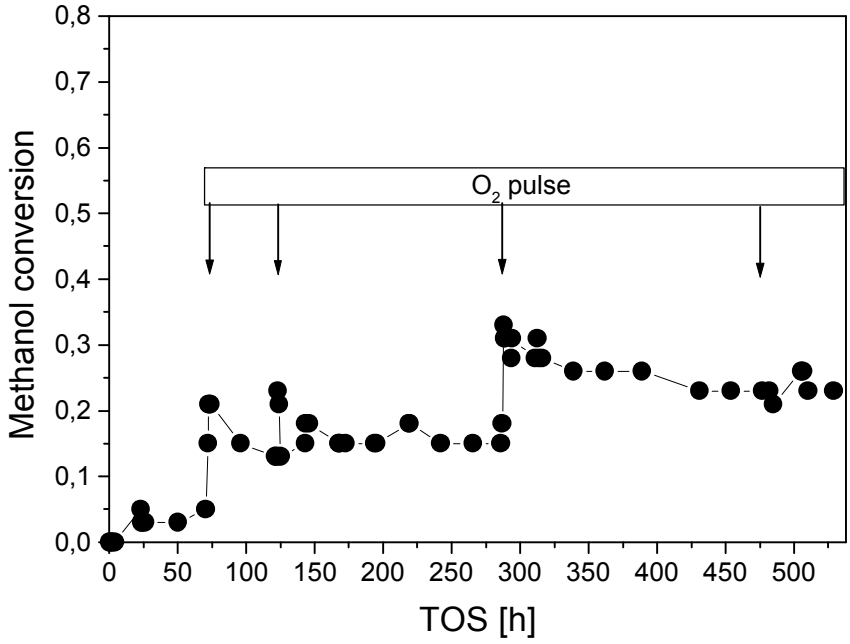

Figure 5.5: Activation of Cu/ZrO_2 catalyst by introducing O_2 into the feed. Reaction conditions: methanol/water molar ratio 1, T= 250°C, flow rate of methanol/water mixture = 0.07ml/min, mass of catalyst = 300 mg.

It seems that the necessary time intervals between "successful" oxygen treatments increase continuously. The last oxygen addition, applied about 200 h after the previous last (very effective) addition, resulted in no further improvement. We concluded that the catalyst had reached its final and stable activity. Consequently, all further experiments on Cu/ZrO_2 described in the following sections were performed with the catalyst in this final state.

In order to study whether the catalyst activation is a reversible process or not, the reactor was cooled down to room temperature and opened at the end of one experiment, exposing the catalyst to air. Several days later, the reactor was closed again and reaction conditions were applied. After a short start-up time (re-reduction in the feed), the methanol conversion returned to about the same value as before the cool-down. This indicates that the activation procedure is an irreversible process.

It seems likely that the activation via oxygen treatment includes the formation of structural defects, which results in an increased catalytic activity. In a previous study [5.21], we were able to show that the activity of the CuO/ZnO catalyst system depends strongly on defects in the copper metal bulk structure, such as strain induced by the Cu/ZnO interface, or zinc dissolved in copper due to the preparation conditions. Structure-activity correlations for the

Cu/ZrO_2 catalyst described here, particularly bulk structural changes during the oxygen treatment, are described elsewhere [5.27].

5.3.2.2. Catalytic activity

The contact time was varied by changing the liquid flow rate of the methanol water mixture between 0.02 and 0.2 ml/min. Figure 5.6 shows the methanol conversion as a function of W_{Cu}/F_m, with W_{Cu} indicating the mass of copper.

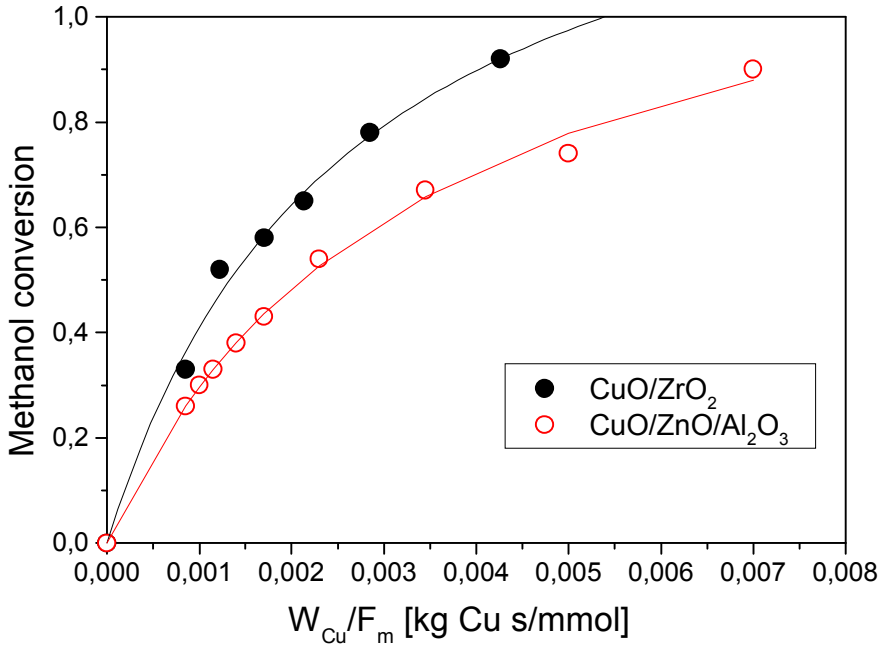

Figure 5.6: Comparison of activity between CuO/ZrO_2 catalyst and $CuO/ZnO/Al_2O_3$ catalyst. Methanol conversion vs. W_{Cu}/F_m ratio (W_{Cu}: mass of copper)

The CuO/ZrO_2 catalyst is found to be more active than the commercial $CuO/ZnO/Al_2O_3$ catalyst. Another comparison of the activity of $CuO/ZnO/Al_2O_3$ and $CuO/ZrO_2/Al_2O_3$ catalysts has been carried out by Menon et al. [5.1]. Varying the copper loading from 3 to 12 wt%, they found that the $CuO/ZrO_2/Al_2O_3$ catalysts were significantly less active than the corresponding $CuO/ZnO/Al_2O_3$ catalysts. This discrepancy between our result and those reported by Menon and co-workers can be attributed to (i) the difference in the preparation methods of the CuO/ZrO_2 catalysts (polymer templating technique vs. wet impregnation [5.24] and (ii) the activation procedure described above.

5.3.2.3. Stability of the catalyst

One of the main problems using a $CuO/ZnO/Al_2O_3$ catalyst in SRM is the deactivation with time on stream. The experiment presented in Figure 5.7 shows the methanol conversion as a function of time on stream for both CuO/ZrO_2 and $CuO/ZnO/Al_2O_3$.

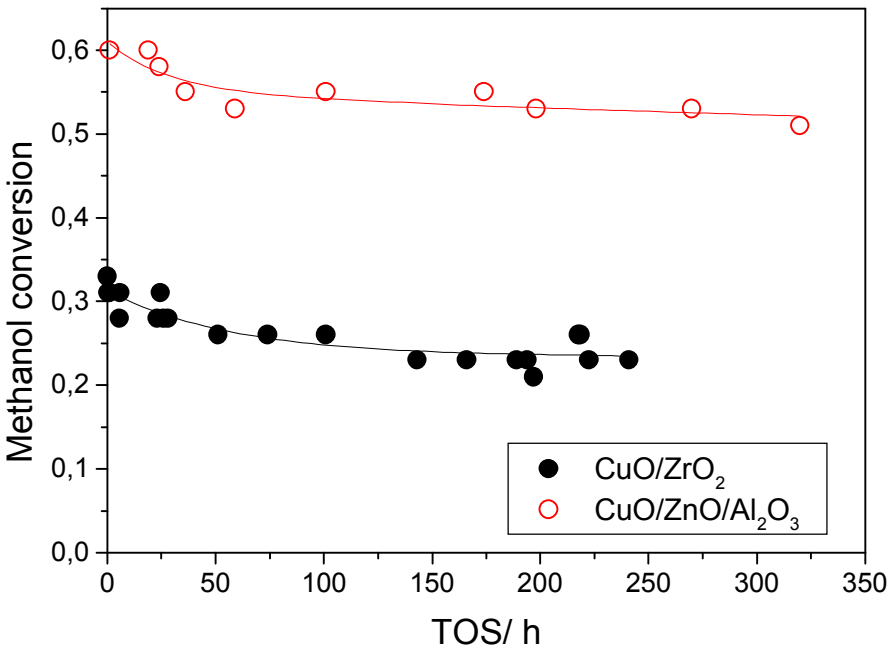

Figure 5.7: Deactivation experiment with CuO/ZrO_2 catalyst and $CuO/ZnO/Al_2O_3$ catalyst at comparable reaction conditions.

In order to compare the stability of both catalysts, the measurement was performed at similar reaction conditions, i.e. dilution of the catalyst with inert material and loading of the catalyst in the reactor. The deactivation of the catalysts with time on stream can be divided into two sections, (i) 0-100 h, the methanol conversion is decreasing exponentially, (ii) >100 h linear behaviour. At the initial period (0-100 h), the deactivation of the CuO/ZrO_2 catalyst looks similar to that of the $CuO/ZnO/Al_2O_3$ catalyst. However, after more than 150 h, the methanol conversion is decreasing steadily for the $CuO/ZnO/Al_2O_3$ catalyst, while it appears to be constant for the CuO/ZrO_2 catalyst. The initial exponential decay of activity observed for both catalysts agrees with observations made by Löffler et. al. on $CuO/ZnO/Al_2O_3$/graphite [5.26]. The authors studied the deactivation of several commercial water-gas shift catalysts in the methanol steam reforming reaction over more than 2000 h time on stream. Two simplified models for the deactivation rate were derived, based on (i) deactivation by metal sintering,

and (ii) deactivation by feed poisoning, respectively. With the time dependence of the two models being significantly different, the exponential decay observed for several catalysts was attributed to metal sintering. Following this interpretation, the smaller extent of deactivation of our CuO/ZrO_2 catalyst compared to commercial $CuO/ZnO/Al_2O_3$ seen in Figure 5.7 indicates that the copper particles in the zirconia catalyst are less prone to sintering.

5.3.2.4. CO formation

The presence of CO in the product stream of SRM is a crucial problem for the use of the resulting hydrogen gas in a fuel cell, because adsorption of CO on the Pt electrode will deteriorate the polymer electrolyte fuel cell performance [5.22]. In a previous report, we have shown that during the steam reforming of methanol over a commercial $CuO/ZnO/Al_2O_3$ catalyst, CO is formed as a consecutive product by the reverse water-gas shift reaction [5.25]. In addition, we were able to propose practical solutions for minimising the formation of CO. Figure 5.8 shows the CO production as a function of W_{cat}/F_m ratio for the CuO/ZrO_2 catalyst. The CO concentration, measured as volume content in the dry product stream, increases monotonically with increasing W_{cat}/F_m ratio for all temperatures.

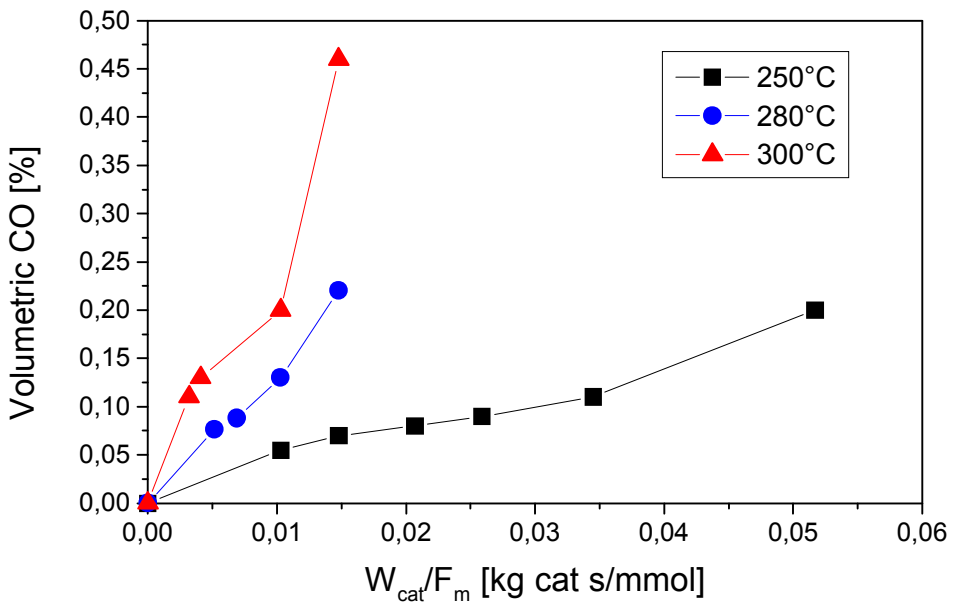

Figure 5.8: CO concentration as a function of W_{cat}/F_m ratio. Mass of the catalyst (CuO/ZrO_2)= 300mg.

The S-shape of the curves indicates that CO, again, is formed as a consecutive product. Therefore, the reaction pathway of CO formation may be the same for copper based catalysts independent of the support type or synthesis method. Figure 5.8 also shows that the CO concentration increases with higher reaction temperatures at constant contact time. When the CO concentration is plotted as a function of the methanol conversion, an exponential increase is obtained in the observed temperature range (Figure 5.9).

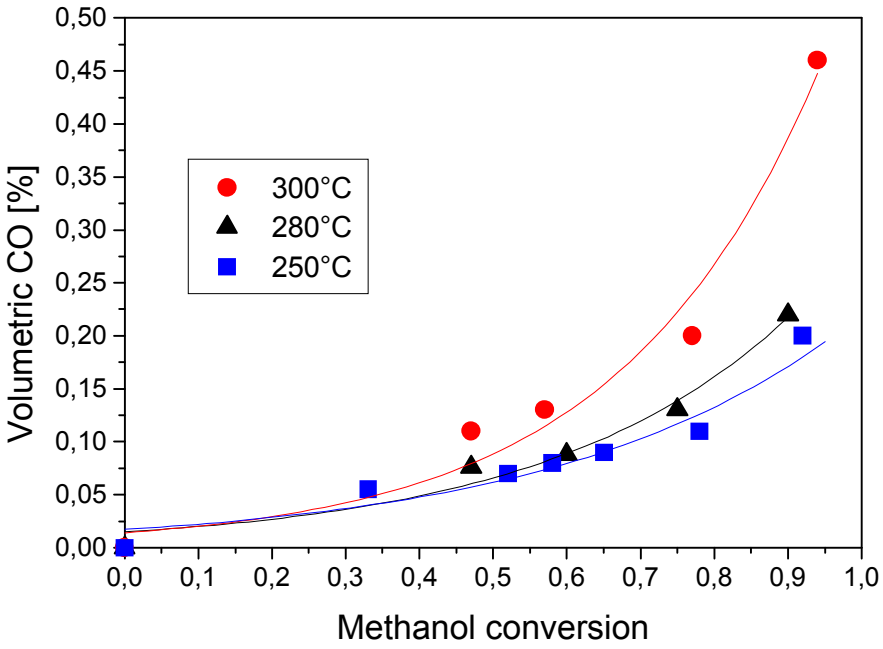

Figure 5.9: CO concentration as a function of methanol conversion. Mass of the catalyst (CuO/ZrO_2)= 300mg.

In Figure 5.10, the same representation is used to compare the CuO/ZrO_2 catalyst with $CuO/ZnO/Al_2O_3$ at 250°C. It can be seen that CuO/ZrO_2 produces significantly less CO than the commercial catalyst at high conversions.

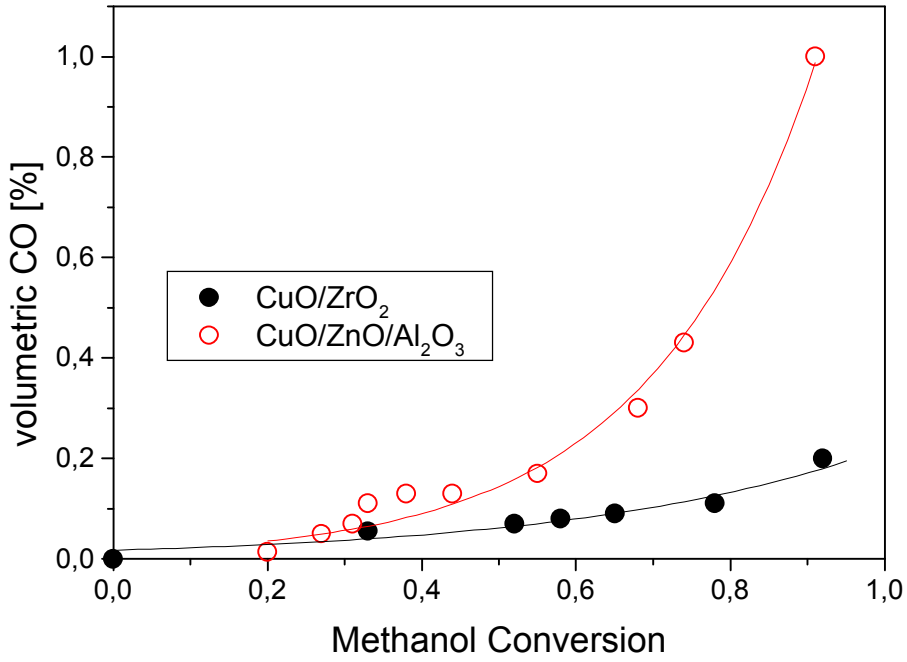

Figure 5.10: CO concentration in dependence on methanol conversion at 250°C.

5.4. Conclusion

The catalytic properties of a novel CuO/ZrO_2 catalyst in the methanol steam reforming process were investigated at a temperature range from 250°C to 300°C at atmospheric pressure. The XRD and XAS results revealed that the CuO/ZrO_2 sample consists of small and/or disordered CuO particles and small particles of crystalline, tetragonal ZrO_2. The CuO/ZrO_2 catalyst can be activated by introducing oxygen (50 ml/min) for a short time (5 min) into the feed at reaction condition. The data obtained from contact time variation reveals that CO is produced as a consecutive product, as already has been demonstrated for $CuO/ZnO/Al_2O_3$. The new CuO/ZrO_2 catalyst, which was prepared by a polymer template sol-gel method, exhibits the following enhanced catalytic properties in comparison to the commercial $CuO/ZnO/Al_2O_3$ catalyst: (i) higher activity in terms of methanol conversion as a function of W_{Cu}/F_m, (ii) increased long term stability (i.e., less deactivation), probably because the macroporous zirconia support is more effective than ZnO/Al_2O_3 in preventing copper particle sintering, and (iii) reduced CO formation, especially significant at high methanol conversion. The work described here clearly shows that a knowledge-based preparation of heterogeneous catalysts is feasible permitting the rational design of materials exhibiting an improved catalytic performance. Elucidating structure-activity relationships is a

necessary prerequisite for a rational catalyst design, however, detailed knowledge about appropriate preparation and treatment conditions resulting in the right target structure of the heterogeneous catalyst is equally important.

5.5. References

[5.1] Lindström, B.; Petterson, L. J.; Govind Menon, P. Applied catalysis **234** (2002) 111-125.

[5.2] Cubeiro, M. L.; Fierro, J. L. G. Applied Catalysis **168** (1998) 307-322.

[5.3] Choi, Y.; Stenger, H. G. Applied Catalysis B: Environment **38** (2002) 259-269.

[5.4] Ning, W.; Shen, H.; Liu, H. Applied Catalysis A: General **211** (2001) 153-157.

[5.5] Gasteiger, H. A.; Markovic, N.; Ross, P. N.; Cairs, E. J. Phys. Chem. **98** (1994) 617.

[5.6] Schmidt, V. M.; Brocherhoff, P.; Hohlein, B.; Menzer, R.; Stimming, U. Journal of Power Sources **144** (1994) 175.

[5.7] Idem, R. O.; Bakhshi, N. N. The Canadian Journal of Chemical Engineering **74** (1996) 288.

[5.8] Agrell, J.; Hasselbo, K.; Jansson, Kjell; Järas, S. G.; Boutonnet, M. Applied Catalysis A: General **211** (2001) 239-250.

[5.9] Shen, G. C.; Fujita, S.; Matsumoto, S.; Takezawa, N. Journal of Molecular Catalysis A: Chemical **124** (1997) 123-136.

[5.10] Lindström, B.; Pettersson, L. J. *International* Journal of Hydrogen Energy **26** (2001) 923-933.

[5.11] Jiang, C. J., Trimm, D. L.; Wainwright, M. S. Applied Catalysis A: General **93** (1993) 245-255.

[5.12] Lindström, B.; Pettersson, L. J. Journal of Power Sources **106** (2002) 264-273.

[5.13] Idem, R. O.; Bakhshi, N. N. Chemical Engineering Science **51** (1996) 3697.

[5.14] Breen, J. P.; Ross, J. R. H. Catalysis Today **51** (1999) 521-533.

[5.15] Antonietti, M.; Hentze, H. -P. Colloid Polym. Sci. **274** (1996) 696-702.

[5.16] Antonietti, M.; Hentze, H.-P. Adv. Mater. **8** (1996) 840-844.

[5.17] Antonietti, M.; Caruso, R. A.; Göltner, C. G.; Weissenberger, M. C. Macromolecules **32** (1999) 1383-1389.

[5.18] Hentze, H.-P.; Antonietti, M. Curr. Opin. Solid St. Mater. Sci. **5** (2001) 343-353.

[5.19] Caruso, R. A.; Giersig, M.; Willig, F.; Antonietti, M. Langmuir **14** (1998) 6333-6336.

[5.20] Schattka, J. H.; Shchukin, D.G.; Jia, J.; Antonietti, M.; Caruso, R. A. Chem. Mater. 2002, *accepted*.

[5.21] Günter, M. M.; Ressler, T.; Jentoft, R. E.; Bems, B., Journal of Catalysis **203** (2001) 133-149.

[5.22] K. Narusawa, M. Hayashida, Y. Kamiya, H. Roppongi, D. Kurashima, K. Wakabayashi, JSAE Review **24** (2003) 41

[5.23] R. O. Idem, N. N. Bakhshi, Ind. Eng. Chem. Res. **34** (1995) 1548

[5.24] E. D. Guerreiro, O. F. Gorriz, G. Larsen, L. A. Arrúa, Applied Catalysis *A* **204** (2000) 33

[5.25] H. Purnama, T. Ressler, R. E. Jentoft, H. Soerijanto, R. Schlögl, R. Schomäcker, accepted in Applied Catalysis *A*.

[5.26] D.G. Löffler, S.D. McDermott, C.N. Renn, Journal Power of Sources (2002) 5063

[5.27] A. Szizybalski et al., in preparation.

6. Catalytic study on novel Cu/ZrO_2 catalysts prepared with different methods for steam reforming of methanol

6. 1. Introduction

Beside the CuO/ZnO catalysts, other copper based catalysts which are also active and maintain high CO_2 selectivity in the steam reforming of methanol are CuO/ZrO_2 catalysts [6.2-6.5]. However, most of the studies on CuO/ZrO_2 catalysts reported in the literature were performed for methanol synthesis. Generally, the catalysts used in the methanol synthesis are also active catalysts in its reverse reaction. For the CuO/ZrO_2 catalysts, the structure of ZrO_2 is found to play an important role for the activity of the catalyst. To obtain highly active Cu/ZrO_2 catalyst, the amourphous nature of zirconia should be maintained under calcinations and reaction conditions [6.6].

The objective of this work is to study the catalytic behaviour of the copper based catalysts which were prepared on a variety of ZrO_2 materials. These catalysts are expected to give superior long term stability with time on stream and low formation of CO in comparison to the commercial $CuO/ZnO/Al_2O_3$ catalyst. There were three types of ZrO_2 materials used in the preparation of the Cu/ZrO_2 catalysts: (i) nanopowder (ii) mesoporous and (iii) macroporous. In order to compare the catalytic of the catalysts at the same reaction conditions, a three channel fixed bed reactor with same geometric and size of each channels was used. The determination of specific area of the catalysts is carried out by using BET. Reaction Frontal Chromatography method (N_2O titration) was used to determine the copper surface area for as prepared catalysts and used catalysts.

6.2. Experiment

6.2.1. Catalyst preparation

The synthesis of the CuO/ZrO_2 catalysts described in the following was carried by Y.Q. Wang and J.H. Schattka (Macro) in Max Planck Institute of Colloids and Interfaces, Golm, Germany.

6.2.1.1. Preparation of CuO/ZrO_2 powders (Nanopowder method)

Two methods were used to prepare these samples. One was the in-situ (INS) preparation: in this method (10 wt% Cu in the sample), 5 ml $Zr(OPr)_4$ was added dropwise to an aqueous solution of TMAOH (2.5 mmol), and stirred for 1 h. Then a calculated amount of an 0.5 M $Cu(NO_3)_2$ aqueous solution was added according to the molar ratio of copper to zirconium, making a final volume of 50 ml. The mixture was stirred for another 1 h at room temperature, and then heated at 80 °C for 20 h. The sample was collected by centrifugation, washed with water and then ethanol, dried overnight (60 °C), and finally calcined at 500 °C for 12 h under air. The sample is called Nano-INS. The other method was the step-by-step (SBS) preparation: in this method (10 wt% Cu in the sample, Nano-SBS-10 and 30 wt% Cu in the sample, Nano-SBS-30), the aqueous solution of $Cu(NO_3)_2$ (0.5 M) was added after the aqueous TMAOH/zirconia precursor suspension had been heated at 80 °C for 20 h. Heating at 80 °C continued for another 6 h, the following steps were kept identical to those used in the in-situ method.

6.2.1.2. Preparation of mesoporous CuO/ZrO_2

Materials: The zirconia precursor, zirconium propylate ($Zr(OPr)_4$, 70 % in propanol), was modified with acetylacetone (AcacH). The triblock copolymer (poly(ethylene-oxide)-poly(propylene-oxide)-poly(ethylene-oxide), $EO_{20}PO_{70}EO_{20}$) was used as the porogen. Post-treatment of the zirconia materials was carried out with hexamethyldisilazane (HMDS, $[Si(CH_3)_3]_2NH$). For the incorporation of copper within the zirconia materials the salts copper acetate ($Cu(Ac)_2 \cdot 2H_2O$) or copper nitrate ($Cu(NO_3)_2 \cdot 2H_2O$) and ammonium hydroxide (NH_4OH) were used. All the chemicals were purchased from Aldrich and used without further purification. Absolute ethanol and deionised water were used as solvent.

Synthesis of ZrO_2-block copolymer mesostructured composites: The modified zirconia precursor was mixed with the block copolymer in a mixture of ethanol and deionised water. In a typical preparation, 4.94 g $Zr(OPr)_4$ (0.01 moles) was dissolved in 10 mL absolute ethanol, 1.00 g AcacH (0.01 moles) was added, and then 5 mL deionised water was added dropwise to the stirred solution forming a slightly yellow liquid. This solution was continuously stirred at room temperature for 3 h. The copolymer, 1.16 g $EO_{20}PO_{70}EO_{20}$ (0.002 moles), was dissolved in a mixture of 10 mL ethanol and 50 mL deionised water under stirring. This surfactant solution was then slowly added to the zirconia precursor solution and heated at 80 °C for 90 h, resulting in a transparent gel. This was dried at 60 °C over 3 days, and is referred to as the as-prepared product.

Post-treatment of mesostructured materials: The as-prepared mesostructured material was treated with HMDS. Typically, 5 mL HMDS was added to 1.0 g as-prepared material and heated to 150 °C, then maintained at this temperature for 1 h under stirring. It can be seen that the bubbles of NH_3 released after heating to 150 °C and then stopped releasing after reaction for 1h. After washing with acetone, the sample was dried at 60 °C overnight, and then calcined at 400 °C for 12 h under air (ramp 2 °Cmin^{-1}). (TGA profile shows that the polymers were completely removed at 350 °C). A light yellow monolithic product was obtained. For comparison, the as-prepared mesostructured material (i.e., without the HMDS post-treatment) was also calcined under the same conditions.

Incorporation of CuO in the mesoporous ZrO_2: Two methods were used to incorporate CuO in the mesoporous ZrO_2. One was the chemisorption-hydrolysis method. In this method, the aqueous solution of $[Cu(NH_3)_4(H_2O)_2]^{2+}$ was obtained by mixing a suitable amount of copper nitrate with an excess of ammonia, and the pH of the final solution was 10.5. 1.0 g of the calcined ZrO_2 samples were soaked in an aqueous solution (5 mL) containing $[Cu(NH_3)_4(H_2O)_2]^{2+}$ (0.45 M, pH=10.5) for 5 h, then diluted with cooled deionised water (0 °C), washed three times with deionised water and ethanol, and finally calcined at 450 °C for 2 h (ramp, 2 °Cmin^{-1}) under air after being dried at 60 °C overnight. The sample is called Meso-post. The other method used to synthesize Meso-pre sample was the in-situ preparation of mesoporous CuO/ZrO_2. In this method, 0.22 g $Cu(Ac)_2$ (1.1 mmol, 10 mol.% Cu) was dissolved in the solution of block copolymer, then reacted with the zirconium precursor solution. Following treatment of these copper-containing samples was the same as that described for the ZrO_2 mesostructure preparation. (i.e. This sample was calcined at 400 °C for 12 h).

Preparation of the Macro is described in chapter 5.2.1.

6.2.2. N_2O titration

The determination of the copper surface area has been described by Chinchen et al. [6.7]. The copper surface area was calculated assuming $1.47*10^{19}$ copper atoms per m^2. In our work, N_2O decomposition was used to determine the copper surface areas of fresh catalysts and used catalysts (after the reaction and after the oxygen pulses). After the activation in feed (methanol/water mixture with molar ratio 2:1, heated to 523K for 1 h at a rate of 6K/min), the sample was purged for 1 h in He at 523 K with a flow of 50 ml/min to remove any adsorbed molecules and the cooled at 313 K. The measurements were performed at 40 °C with a

mixture of 0.5 % N_2O/He at 15 ml/min. The catalysts were diluted with boron nitride to establish a sample bed of about 1.5 cm height and to guarantee, that the thermocouple is located directly in the powder. The material was placed onto a quartz frit in a quartz tube reactor, which was heated via an electrical resistivity heating wire.

6.2.3. Catalytic studies

The measurement of the steam reforming reaction was carried out at atmospheric pressure in a tubular stainless steel reactor (10 mm i.d.). In order to study the catalytic properties of more than one catalyst at once, three of these reactors were placed into an aluminium heating block for the heat transfer. The advantages using this three channels reactor to study the kinetic properties of the catalysts are: direct comparison of the measurements in the same reaction conditions, possibility of changing the catalysts during the measurement, availability of using different gases. For steam reforming measurements the catalyst powder was first diluted with five times its weight of boron nitride (BN) and then the mixture was pressed using a cylinder stamp with a diameter of 10 mm. 0.4 g of the mixture was put into the cylinder stamp and was pressed at 200 bar three times each 5 minutes. The tablet was then crushed to small particles and sieved to obtain a defined particle size (0.71-1.0mm). The mass of the CuO/ZrO_2 catalysts used in all experiments is 0.3g which corresponds to 1.8 g (catalyst + BN). The further experimental details concerning temperature controller, the pump device and analytical measurements are the same as that described in 5.2.1. A commercial $Cu/ZnO/Al_2O_3$ catalyst from Süd-Chemie (approximately 50 wt% Cu) [6.8] was used as a reference.

6.3. Result and discussions

6.3.1. Copper content and copper surface area of the catalysts

The copper content (Cu metal molar %) and the copper surface area of fresh samples are shown in Table 6.1. The copper content of all the catalysts was determined by XRF (X-ray fluorescence). Nano-SBS-30 catalyst has the highest Cu content and followed by Macro-sample. The lowest copper content is found in the catalyst prepared by the mesoporous method (Meso-post). The specific surface areas of the fresh catalysts are depicted in Table 6.1.

Table 6.1: The properties of the Cu/ZrO_2 catalysts

Sample	Cu [metal Cu mol %]	S_{Cu} [$m^2/g_{cat.}$]	BET [m^2/g_{cat}]
Nano-INS	9.0	0.63	72
Nano-SBS-10	9.0	0.14	110
Nano-SBS-30	20.6	1.59	168
Meso-pre	9.6	0.15	157
Meso-post	5.8	0.77	226
Macro	15.5	0.18	67

There is no correlation observed between the copper content and the specific area. The catalyst prepared in the mesoporous ZrO_2 (Meso-post) provides the highest specific surface area. The specific copper surface area, S_{Cu}, (surface area of copper per gram catalyst) of the fresh catalysts determined by means of N_2O titration can also be seen in Table 6.1. The Nano-SBS-30 with the highest Cu content in the sample is found to have the highest S_{Cu}. The S_{Cu} plotted as a function of copper content is shown in Figure 6.1. There is no correlation observed within the six samples. This indicates that there are different sizes of copper particles obtained in the samples. According to this assumption, Meso-post sample is found to have the smallest particle size among the samples.

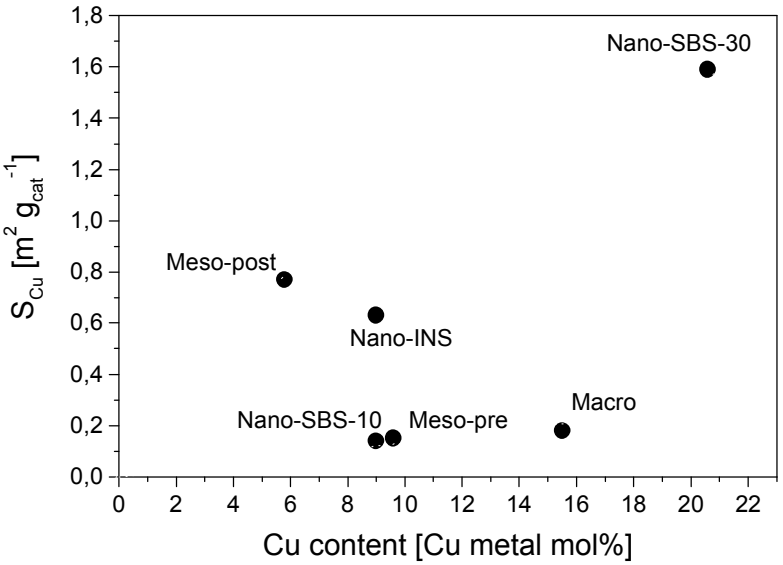

Figure 6.1: Specific copper surface area of CuO/ZrO_2 catalysts as a function of copper content [mol %]

6.3.2. Activation behavior

Figure 6.2 shows the conversion of methanol of the Nano-SBS-10 and the Meso-pre as a function of time on stream.

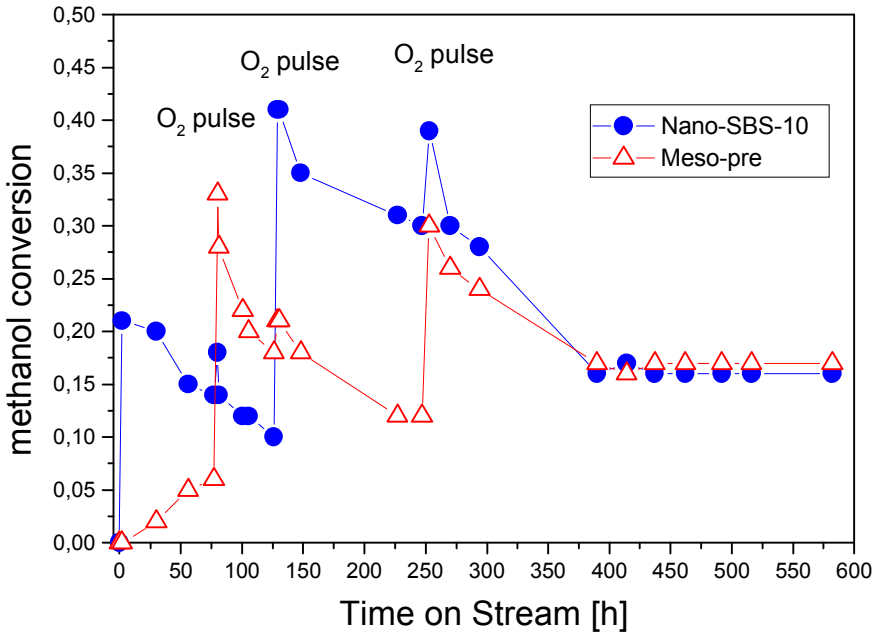

Figure 6.2: Activation of Cu/ZrO₂ catalysts (Nano-SBS-10, Meso-pre) by introducing O₂ into the feed. Reaction conditions: methanol/water molar ratio 1, T= 250 °C, flow rate of methanol/water mixture = 0.07 ml/min, mass of catalyst = 300 mg.

The initial activity of Meso-pre was significantly lower than Nano-SBS-1, although the specific copper surface area of the both catalysts is almost the same (S_{Cu} (Meso-pre)= 0.15; S_{Cu} (Nano-SBS-10)= 0.14). The activity of catalyst Meso-pre in term of methanol conversion increased monotonically from 0 to 0.06 with time on stream (TOS) from the beginning to 75 h. In contrast, the activity of catalyst Nano-SBS-10 decreased from 0.21 to 0.14 within the same period on stream. The rate of the increase and the decrease of the activity with TOS are almost the same. In order to activate the catalysts through the redox treatment, oxygen (50 ml/min, 5 min) was introduced into the feed. After the first introduction of O_2, the activity of both catalysts increased. The activity of Meso-pre is now higher than that of Nano-SBS-10. By the next introduction of the oxygen, the increase in the activity of both catalysts is observed. At this time the jump of the activity of the Nano-SBS-10 is much higher than Meso-pre and therefore its activity is correspondingly higher. After the last introduction of the

oxygen in this experiment, the activity of the both catalysts increased but decreased rapidly with time on stream and reached the same conversion of methanol. Afterwards, the activities of the both catalysts were found constant for about 200 h on stream. We assumed that the catalysts have reached the stable conditions. Next, Figure 6.3 shows the activation behaviour of another three samples, Nano-INS, Meso-post, Nano-SBS-30.

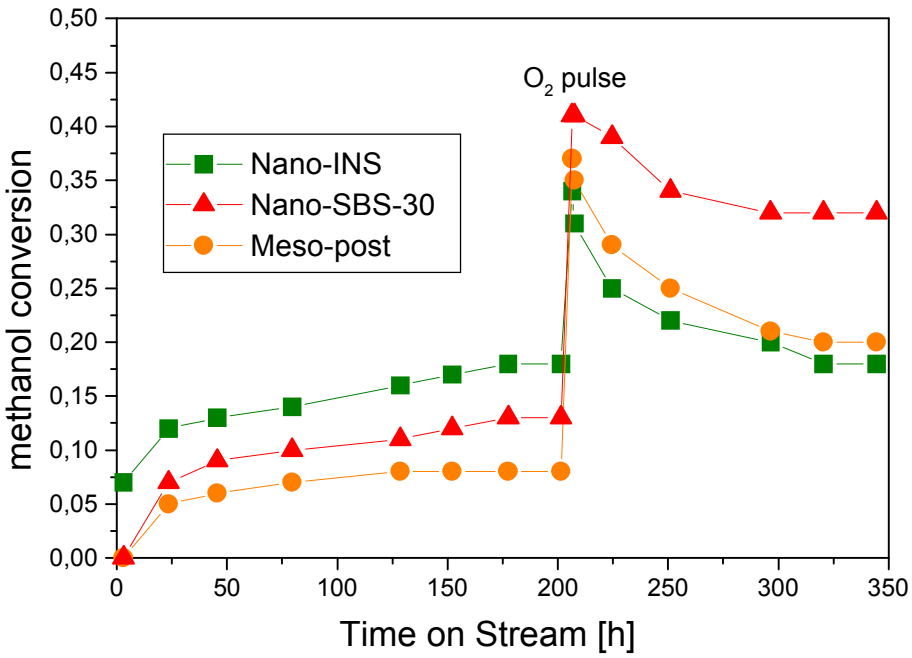

Figure 6.3: Activation of Cu/ZrO_2 catalysts (Nano-INS, Meso-post, Nano-SBS-30) by introducing O_2 into the feed. Reaction conditions: methanol/water molar ratio 1, T= 250 °C, flow rate of methanol/water mixture = 0.07 ml/min, mass of catalyst = 300 mg.

This measurement was carried out in the three channels reactor in order to provide a similar reaction condition for all the catalysts with TOS for almost 350 h. The aim of this experiment is to study the influence of the oxygen pulse on the enhancement of the activity. Thus, the activity of the catalysts was measured against the time on stream and introduction of the oxygen was performed after the activity has already reached the steady state. The experiment can be divided into two sections: (i) from the beginning to the stable state before the oxygen introduction, (ii) from the introduction of the oxygen to the reach of the stable conversion. The activity of all the catalysts increased slowly from the initial and reached a constant methanol conversion at 175 h. At the first section, Nano-INS is found to be the most active catalysts followed by Nano-SBS-30 and then Meso-post. Nano-SBS-30 is less active than

Nano-INS, although the value of the Cu content of Nano-SBS-30 (18.1%) is more than twice times higher than Nano-INS (7.8%). No linear correlation was observed between the activity (Nano-INS>Nano-SBS-30>Meso-post) and the Cu content (Nano-SBS-30>Nano-INS>Meso-post).

In the second section, the activity of all the catalysts increased immediately after the oxygen was added to the feed. Nano-SBS-30 becomes the most active catalyst, followed by Meso-post and then Nano-INS. The activity decreased continuously with TOS and reached a stable state at 325 h. At the stable conditions, the activities of Nano-SBS-30 and Meso-Post are found to be higher compared to their activities measured before the oxygen addition. However, no change of Nano-INS was observed at the stable conditions, before and after the treatment of the oxygen. It can be concluded from this experiment that the improvement of the activity can be obtained through the long period activation in feed (methanol/water mixture) and through the introduction of the oxygen. The study of the activation behaviour of the Macro-sample is reported in chapter 5.

6.3.3 Specific copper surface area of fresh and used catalysts

The determination of the specific copper surface area per gram catalyst performed by means of N_2O titration was done on fresh and used catalysts, Table 6.2. The used catalysts are the catalysts that have been applied in the experiments corresponding to Figure 6.2, 6.3 and 5.5.

Table 6.2: Specific copper surface area of fresh and used catalysts.

Sample	S_{Cu}, fresh [$m^2/g_{cat.}$]	S_{Cu}, used [$m^2/g_{cat.}$]	realtive change of S_{Cu} [%]
Nano-INS	0.63	1.69	168
Nano-SBS-10	0.14	1.79	1178
Nano-SBS-30	1.59	3.43	116
Meso-pre	0.15	1.26	769
Meso-post	0.77	0.77	0
Macro-sample	0.18	0.71	294

The specific copper surface area (S_{Cu}) of the used catalysts is higher than that of the fresh catalysts with the exception of Meso-post. The increase of the copper surface area of the used catalysts compared to the fresh catalysts is between 116% and 1178%. This result indicates

that the activation of the catalyst (long time in feed and the addition of oxygen sequentially to the feed) have a significant influence to the increase of the copper surface area. For the Meso-post, there no change of the S_{Cu} was observed. The quantification of the influences between the activation in feed and the activation by the oxygen treatment to the increase of the copper surface area is the present object of our study. The study of the geometric structure of these catalysts (fresh and used catalysts) in correlation with their copper surface area has been carried out by Szizybalski et al. [6.9].

6.3.4 Activity of the CuO/ZrO_2 catalysts

The activities of the catalysts as a function of the specific copper surface area (used catalysts) are shown in Figure 6.4.

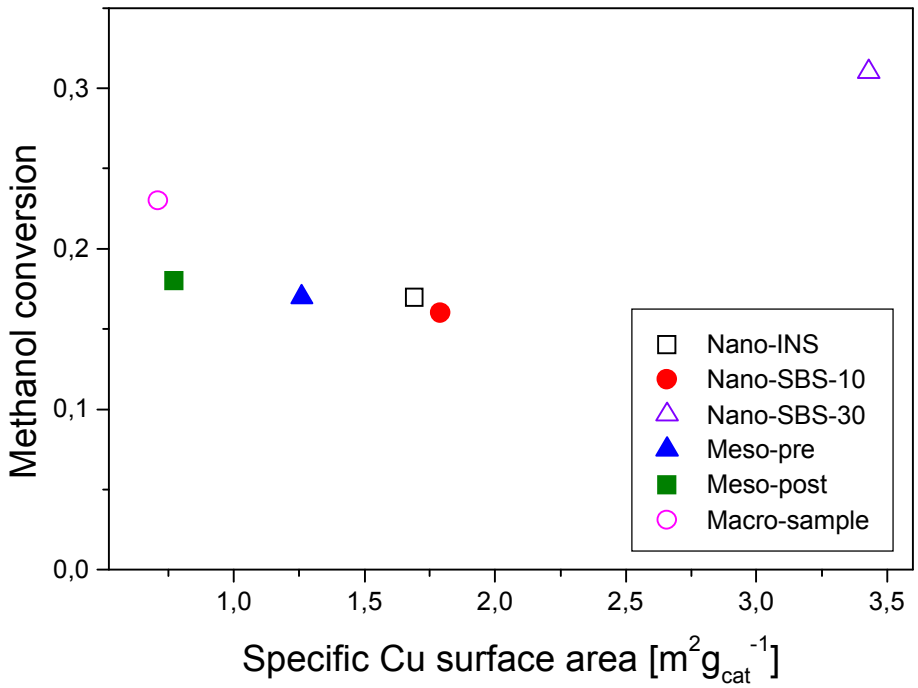

Figure 6.4: Methanol conversion as a function of specific copper surface area of CuO/ZrO_2 catalysts.

The result reveals clearly that there is no linear correlation between the catalyst activity and S_{Cu}. This finding agrees well with those reported in the literature [6.10, 6.11]. The studies of the activities of the Cu/ZnO catalysts in methanol steam reforming process done by Günter [6.10] show that there is no linear correlation between activity in term of TOF (turn over frequency) and the copper surface area. In addition, Bartley et al. reported the same result

with respect to the study of methanol synthesis. The authors, Bartley et al. said that the activity of the copper catalyst is strongly dependent on the choice of support. The copper area determined with nitrous oxide is not necessarily a reliable measure of the active copper surface. This means that a global measurement of surface area using N_2O titration will not count the number of active centers correctly. They proposed, therefore, that the morphology of the copper rather than the total surface area may be the important factor for the activity. In order to compare the activity of the six CuO/ZrO_2 catalysts and the commercial $CuO/ZnO/Al_2O_3$ catalyst with each other, the activity is defined as in term of x_s (ratio of methanol conversion and copper surface area) and can be written as:

$$x_s = \frac{x}{m_{Cat} S_{Cu}} \ [m^{-2}] \qquad (6.1)$$

x is the conversion of methanol [-], m_{Cu} is the mass of the catalyst [g] and S_{cu} (used catalysts) is specific copper surface area [$m^2 g_{cat}^{-1}$]. The methanol conversion was measured at the stable state after the oxygen treatment. The value of the x_s of the catalysts is listed in the following table and plotted in Figure 6.5.

Table 6.3: Activity, x_s, of the six CuO/ZrO_2 catalysts and the $CuO/ZnO/Al_2O_3$ catalyst.

Sample	Methanol conversion	S_{Cu}, used [$m^2/g_{cat.}$]	Mass [g]	x_s [m^{-2}]
Nano-INS	0.17	1.69	0.3	0.030
Nano-SBS-10	0.16	1.79	0.3	0.027
Nano-SBS-30	0.31	3.43	0.3	0.027
Meso-pre	0.17	1.26	0.3	0.041
Meso-post	0.18	0.77	0.3	0.070
Macro-sample	0.23	0.71	0.3	0.097
$CuO/ZnO/Al_2O_3$	0.74	8.3*	0.2	0.018

** S_{Cu} from $CuO/ZnO/Al_2O_3$ is measured on the fresh catalyst.*

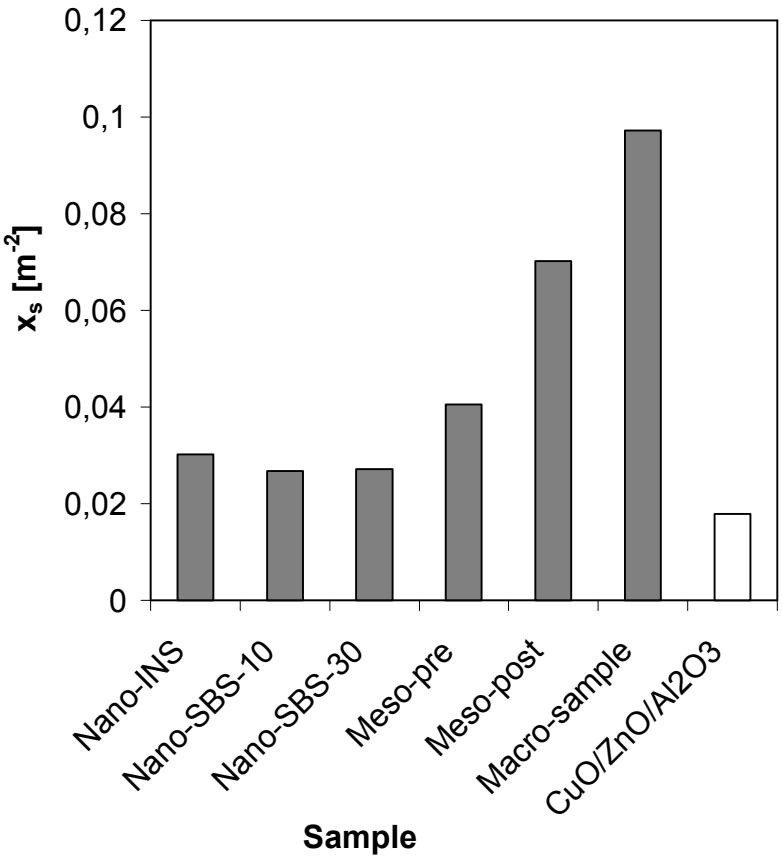

Figure 6.5: x_s *of the six* CuO/ZrO_2 *catalysts and the* $CuO/ZnO/Al_2O_3$ *catalyst.*

Due to the significant decrease of the activity of the $CuO/ZnO/Al_2O_3$ catalyst which relates directly to the decrease of the copper surface area with time on stream [6.1], the value of S_{Cu} is therefore determined from the fresh catalyst. The comparison to the CuO/ZrO_2 catalysts admits more conviction.

The preparation methods of the Cu/ZrO_2 catalysts studied in this work can be generally divided into three groups. They are: (i) Nanopowders which include in-situ method (Nano-INS) and step-by-step method (Nano-SBS-10, Nano-SBS-30), (ii) Mesoporous which include pre-support-formation (Meso-pre) and post-support-formation (Meso-post), (iii) Macroporous (Macro-sample). Concerning the result plotted in Figure 6.5, the catalysts prepared on macroporous ZrO_2 (Macro-sample) is the most active catalyst followed by the catalysts prepared on mesoporous ZrO_2 (Meso-post, Meso-pre). The catalyst prepared by post-support formation (Meso-post) is significantly more active than that prepared by pre-support formation (Meso-pre). The catalysts prepared using the nanopowder method (Nano-INS, Nano-SBS-10, Nano-SBS-30) have the lowest activity. No significant difference in the

activity was observed for the three catalysts prepared by nanopowders methods. As a conclusion, there is a relation between the activity and the preparation methods. Concerning the comparison to the commercial catalyst, all CuO/ZrO_2 catalysts provide higher activity. The value of the x_s of the Macro is five times greater than that from the commercial catalyst. The enhancement of the activity in term of x_s of the CuO/ZrO_2 catalysts compared to the commercial catalyst can be caused by the following reasons: (i) difference in the morphology of the copper particles, (ii) difference in the particle sizes. The study of the structure and activity of copper/zinc oxide catalysts using XRD and XAS has been carried out by M. M. Günter [6.10]. The activity of the Cu/Zn catalyst is correlated with the structure (strain) and size of the copper particles.

The following Figure 6.6 shows the comparison of the activity between the Macro and the commercial catalyst, methanol conversion is plotted as a function of A_{Cu}/F_m ratio. A_{Cu} is the surface area of copper [m^2]. F_m is the molar flow rate of methanol (mmol/s). The result reveals that the Macro-sample catalyst is more active than the commercial $CuO/ZnO/Al_2O_3$ catalyst over the whole range of the A_{Cu}/F_m ratio.

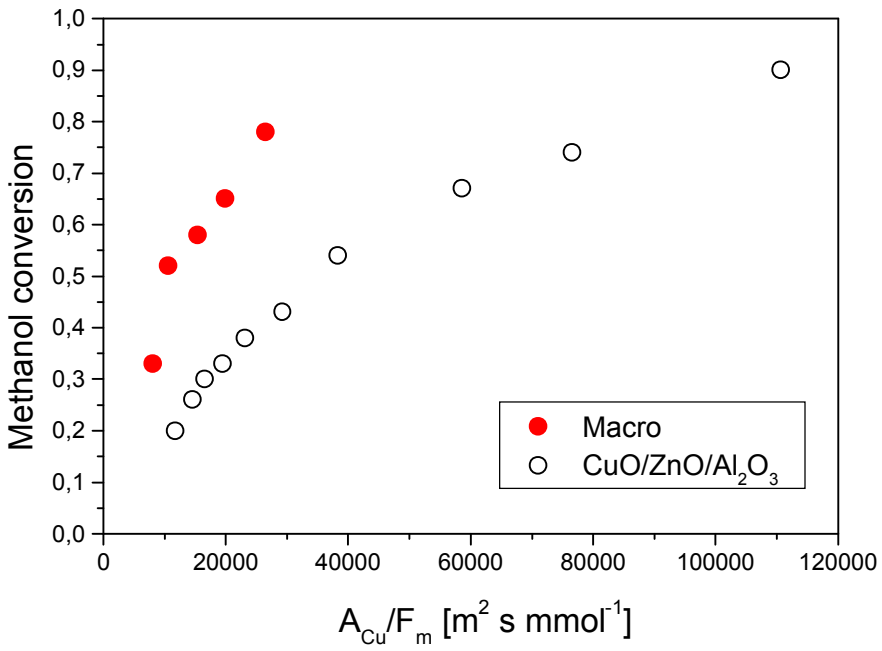

Figure 6.6: Methanol conversion versus A_{Cu}/F_m [m^2 s $mmol^{-1}$]

6.3.5 CO formation

The study of CO formation over CuO/ZrO_2 catalysts and commercial $CuO/ZnO/Al_2O_3$ catalyst is depicted in Figure 6.7.

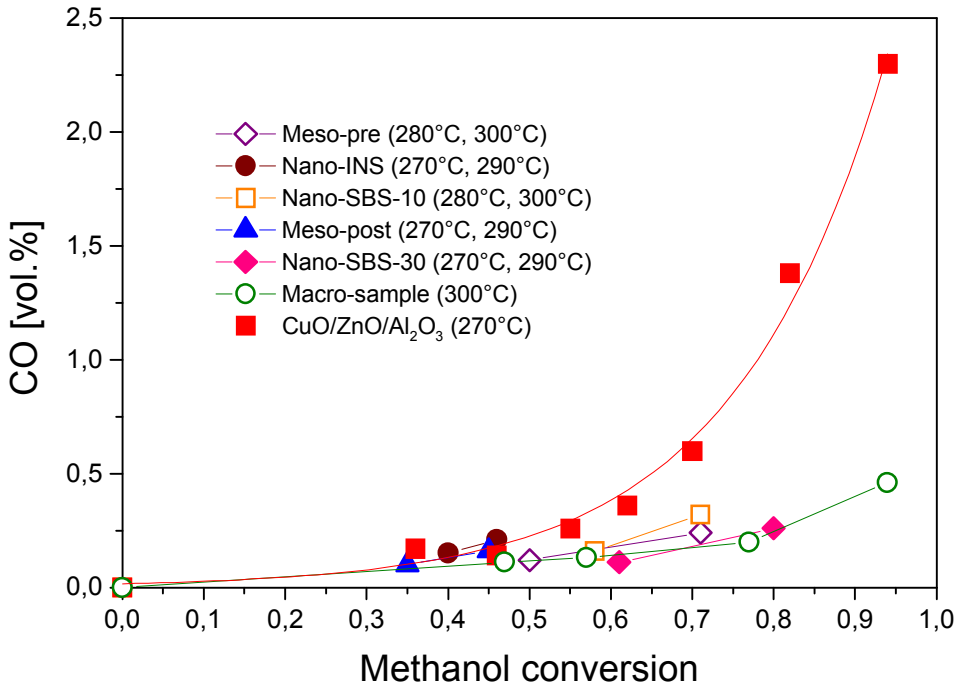

Figure 6.7: CO concentration as a function of methanol conversion, a comparison between the CuO/ZrO_2 catalysts and the commercial $CuO/ZnO/Al_2O_3$ catalyst.

The CO concentration was plotted as a function of methanol conversion. The measurements of the CO concentration of the CuO/ZrO_2 catalysts (with exception of Macro-sample) have been carried out at different reaction temperatures. The higher conversions were obtained at higher temperatures. However, the CO concentration of the Macro-sample was measured at 300 °C. In order to compare the catalytic properties of the CuO/ZrO_2 catalyst concerning the formation of CO as a function of the methanol conversion, the measurement of CO concentration versus methanol conversion of the $CuO/Zn/Al_2O_3$ catalyst was performed at 270 °C (lowest temperature in this experiment). As reported in our early work [6.12, 6.13], the CO concentration of the SRM process increases with the increase of the reaction temperature. The result depicted in Figure 6.7 shows that the CuO/ZrO_2 catalysts measured at

the same or even higher temperatures (>270°C) than that performed on the $CuO/ZnO/Al_2O_3$ catalyst, less CO concentration was obtained in the product stream over these catalysts than the commercial catalyst. The difference becomes significant at conversion higher than 0.5. In the following Figure 6.8, the CO concentration versus methanol conversion of the Macro and $CuO/ZnO/Al_2O_3$ catalyst was measured at the same reaction temperature, 300 °C. Significantly less CO is formed by using the Macro than the commercial catalyst measured over the wide range of the methanol conversion (0.28-0.94).

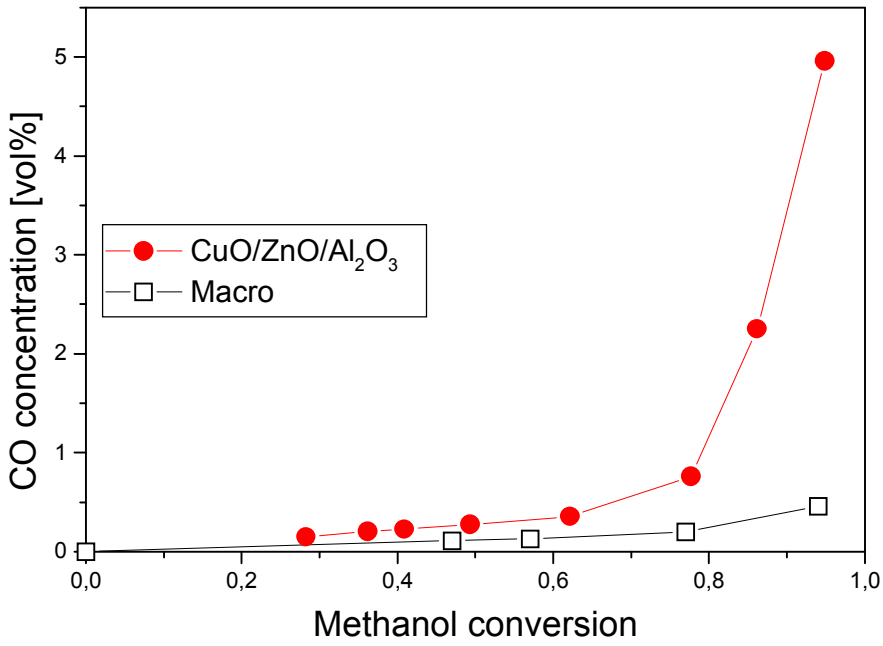

Figure 6.8: CO concentration versus methanol conversion of Macro-sample and $CuO/ZnO/Al_2O_3$ catalyst measured at 300°C.

6.4. Conclusion

The study of the catalytic behaviour of steam reforming of methanol over the novel CuO/ZrO_2 catalysts which were prepared by method of various kinds has been performed at 250 °C and at atmospheric pressure. The activity of all these CuO/ZrO_2 catalysts can be improved by the activation for a long period in feed and introducing oxygen for a short time into the feed at reaction condition. The investigation of the activity in term of x_s among the CuO/ZrO_2 catalysts reveals that there is a correlation between the activity and the preparation methods. The catalysts prepared on macroporous ZrO_2 (Macro) is the most active catalyst followed by the catalysts prepared on mesoporous ZrO_2 (Meso-post, Meso-pre). However, the catalysts prepared using the Nanopowder method (Nano-INS, Nano-SBS-10, Nano-SBS-30) have the lowest activity. The three catalysts prepared by means of Nanopowder method result in a similar activity. The enhanced catalytic properties of novel CuO/ZrO_2 catalysts compared to the commercial $CuO/ZnO/Al_2O_3$ catalyst are exhibited as follows: (i) The increase of the copper surface of the used catalysts compared to the fresh catalysts from the CuO/ZrO_2 catalysts with exception of Meso-post, is observed in this study. Contrary, the copper surface area of the commercial $CuO/ZnO/Al_2O_3$ catalyst is decreased after the catalyst was used in the reaction. This indicates that the new CuO/ZrO_2 catalysts provide much higher stability with respect to the sintering of metal particles in comparison to the commercial $CuO/ZnO/Al_2O_3$ catalyst. (ii) The value of the x_s shows that all of the CuO/ZrO_2 catalysts are more active. (iii) Less CO is formed over CuO/ZrO_2 catalysts, especially significant at methanol conversion higher than 0.5.

In this work we are able to show that the preparation method plays an important role to achieve catalysts with enhanced properties. Another crucial point which can also have a strong influence to the behaviours of the catalyst is the structure of the copper, as well as ZrO_2 as support materials. The study of the correlation between structure and activity of these catalysts is still under investigation. The knowledge of the relation among synthesis, structure and catalytic properties is the key to successful rational design catalysts with superior properties.

6.5. References

[6.1] D.G. Löffler, S.D. McDermott, C.N. Renn, Journal Power of Sources (2002) 5063.

[6.2] Breen, J. P.; Ross, J. R. H. Catalysis Today **51** (1999) 521-533.

[6.3] Lindström, B.; Petterson, L. J.; Govind Menon, P. Applied catalysis **234** (2002) 111-125.

[6.4]Lindström, B.; Pettersson, L. J. International Journal of Hydrogen Energy **26** (2001) 923-933.

[6.5] Lindström, B.; Pettersson, L. J. Journal of Power Sources **106** (2002) 264-273.

[6.6] R.A. Koeppel, A. Baiker, Ch. Schild, A. Wokaun, Sud. Surf. Sci. Catal. A 84 (1992) 77.

[6.7] Chinchen et al., Journal of Catalysis **103** (1987) 79-86.

[6.8] T. Genger, O. Hinrichsen, M. Muhler, Catal. Lett. **59** (1999) 137.

[6.9] Szizybalski et al., in preparation

[6.10] M. M. Gunter, PhD Thesis, Berlin, Technical University, (2002).

[6.11] G.J.J. Bartley, R. Burch, Applied Catalysis 43 (1998) 141.

[6.12] H. Purnama, T. Ressler, R.E. Jentoft, H. Soerijanto, R. Schlögl, R. Schomäcker, accepted in Applied Catalysis A.

[6.13] H. Purnama, F. Girgsdies, T. Ressler, J.H. Schattka, R.A. Caruso, R. Schlögl, submitted to Catalysis Letters.

7. Summary and Perspectives

The object of this thesis is the study of the catalytic behaviour of copper based catalysts in methanol steam reforming for on board production of hydrogen. In order to study the catalytic properties, an experimental setup which consists mainly of pump device for methanol and water, reactor, separator units for liquid and gas and analytical instruments was established. The investigations were performed by means of a three channel fixed-bed reactor. Due to the poor long term stability and high CO formation of the commercial $CuO/ZnO/Al_2O_3$ catalysts in the methanol steam reforming, a series of novel CuO catalysts supported on ZrO_2 has been prepared and their catalytic properties are investigated in this work. These catalysts were synthesized with different preparation methods, such as CuO on nanopowder ZrO_2, on mesoporous ZrO_2 and on macroporous ZrO_2. In order to compare the catalytic properties of these catalysts, the commercial $CuO/ZnO/Al_2O_3$ catalyst was used as a reference. The results of this thesis can be divided into three sections (chapter 4, 5 and 6). In chapter 4 the study of the commercial $CuO/ZnO/Al_2O_3$ catalyst was focused on the formation of CO. In the next chapter the study of the catalytic properties of the CuO catalyst supported on macroporous ZrO_2 was performed and compared to those of the commercial $CuO/ZnO/Al_2O_3$ catalyst. In chapter 6 the catalytic behaviour of the six CuO/ZrO_2 catalysts was studied and the catalysts are compared to each others.

The main results of these three chapters are summarized in the following:

In chapter 4 the kinetic study of methanol steam reforming over commercial $CuO/ZnO/Al_2O_3$ catalyst has been performed at atmospheric pressure over a wide temperature range (230-300 °C). The reaction scheme used is the direct formation of hydrogen and carbon dioxide by steam reforming reaction and the formation of CO as a consecutive product by the reverse water-gas shift reaction. A simulation employing these schemes to describe methanol steam reforming process over a $CuO/ZnO/Al_2O_3$ catalyst fit the experimental data measured at 230 to 300°C well.

The monotonic increase of CO partial pressure as a function of contact time measured at the temperature range from 230°C to 300°C as well as the limit of no selectivity for CO as the contact time approaches 0, proves that CO is formed as a consecutive product.

A new finding reported in this work concerns the parameters influencing the formation of CO. It was found that the CO concentration can be influenced by the particle size of the catalyst through its effect on intraparticle diffusion limitation. This parameter can be added to those reported in the literature as influencing the production of CO, i.e. reaction temperature, contact time, molar ratio of methanol and water, and addition of oxygen to the methanol-steam feed. The greater the mass transport limitation in the catalyst particle the higher the concentration of CO in the product stream.

In Chapter 5 the catalytic properties of the CuO/ZrO_2 catalyst which was prepared using a polymer template sol-gel method (CuO on macroporous ZrO_2) have been examined. After the reduction in a methanol/water mixture at 250°C for 1h the catalyst showed a very poor activity. After several hours of time on stream, the catalyst can be activated by introducing oxygen. The CO concentration observed as a function of contact time reveals that CO is formed as a consecutive product. The enhancement of the catalytic properties of the CuO/ZrO_2 catalyst in comparison to the commercial $CuO/Zn/Al_2O_3$ catalyst is described as follows:

(i) higher activity in term of methanol conversion as a function of W_{Cu}/F_m,

(ii) more stability in time on stream (i.e. less deactivation), probably due to the higher effectivity of macroporous zirkonia support than ZnO/Al_2O_3 in preventing sintering of copper particles,

(iii) lower CO formation, especially at high methanol conversion.

In Chapter 6 the catalytic properties of the six CuO/ZrO_2 catalysts prepared by different synthesis methods have been studied at the same reaction conditions as employed in chapter 4 and chapter 5. The activity of the catalysts can be improved by introducing oxygen to the feed at reaction condition. The study of the activity of the CuO/ZrO_2 catalysts as a function of the copper surface area reveals a relation between the activity and the synthesis. The CuO catalyst prepared on macroporous ZrO_2 is the most active followed by the CuO catalysts prepared on mesoporous ZrO_2. The CuO catalysts on nanopowder ZrO_2 have the lowest activity. There is no significant difference with respect to the formation of CO as a function of methanol conversion determined over all the CuO/ZrO_2 catalysts.

The comparison of the catalytic properties between the CuO/ZrO_2 catalysts and the commercial $CuO/ZnO/Al_2O_3$ catalyst gives the following results:
(i) the measurement of the activity described in term of x_s (ratio of methanol conversion and copper surface area) shows that in comparison to the commercial $CuO/ZnO/Al_2O_3$ catalyst, all of the six CuO/ZrO_2 catalysts exhibit higher activity.
(ii) The CuO/ZrO_2 catalysts provide a higher long term stability than the $CuO/ZnO/Al_2O_3$ catalyst. This can be seen in the increase of the copper surface area after the catalysts were measured for a long time on stream and with the treatment of oxygen. In contrast, as reported in the literature the activity of the commercial $Cu/ZnO/Al_2O_3$ catalyst decreases with oxygen introduction into the feed. This is because of the sintering of the copper particle.
(iii) There is less CO formed in the product stream by using the CuO/ZrO_2 catalysts. The difference is becoming more significant at high methanol conversion.

The following paragraphs describe the perspectives with respect to the results presented in this thesis.

The formation of CO as a consecutive product (in case of the commercial catalyst) correlated with the finding that CO concentration increases with the increase of the intraparticle diffusion limitation in the catalyst particle permits potential solutions that can be applied with respect to the chemical engineering process to minimize CO formation are the application of the following methods:
(i) The use of a membrane reactor
(ii) The use of a microtube reactor
(iii) The use of a monolith reactor
(iv) The use of an egg-shell catalyst
(v) Dilution of the catalyst.

Referring to the main results in chapter 5 and 6 which describe that the novel CuO/ZrO_2 catalysts prepared with various kinds of methods exhibit significantly enhanced catalytic properties (more stability with time on stream, higher activity and less CO formation) in comparison to the $CuO/ZnO/Al_2O_3$ catalyst, a knowledge-based preparation of heterogeneous catalysts is feasible permitting the rational design of materials exhibiting an improved catalytic performance.

Furthermore, in order to accomplish a rational design of catalyst, the study of the structure of the catalyst is an important prerequisite bridging synthesis and catalysis. The relation between the synthesis, the structure and the catalytic properties is illustrated in the following Figure. The treatment condition (e.g. introduction of oxygen), however, is an additional tool to improve the catalyst activity which in turn can influence the catalyst structure.

Figure 7.1: Relationship between synthesis, structure and catalysis.

8. Appendix

8.1 Simulation program with Madonna Software

```
{ 1: Methanol+Water <--> 3Hydrogen+Carbondioxide }
    RXN1 = K1f*Methanol^0.6*Water^0
    K1f = 12
    K1r =0

    INIT Methanol       = 0.5
    INIT Water          = 0.5

    d/dt(Methanol) = -RXN1
    d/dt(Water) = -RXN1+RXN2


{ 2: Carbondioxide+Hydrogen <--> Carbonmonoxide+Water }
    RXN2 = K2f*Carbondioxide*Hydrogen - K2f*K*Carbonmonoxide*Water
    K2f = 0.21
    K =80
    INIT Carbonmonoxide = 0
    d/dt(Carbonmonoxide) = +RXN2

Ppro=1-Methanol-Water-Carbonmonoxide

Carbondioxide = 0.25*Ppro
Hydrogen=0.75*Ppro
METHOD RK4

STARTTIME = 0
STOPTIME=0.6


DT = 0.001
```

8.2 Curriculum Vitae

Name:	Herry Purnama
Date of Birth:	14. August 1971
Place of Birth:	Medan, Indonesia
Nationality:	Indonesia

Graduate School

since April 2000	PhD Thesis in Fritz-Haber-Institut of Max-Planck-Society (MPG), Prof. Dr. R. Schlögl, Department of Anorganic Chemistry. Title: *"Catalytic study of copper based catalysts in the Steam Reforming of Methanol"*
since July 2000	Member of Graduiertenkolleg „Synthetische, mechanistische und reaktionstechnische Aspekte von Metallkatalysatoren"

University

1992-2000	Study at the Technische Universität Berlin Diploma Thesis at Institut für Technische Chemie, Prof. Dr. Schomäcker, TU-Berlin Major: Chemical Engineering Title: *"Herstellung von Porenmembranen aus Polyacrylsäurepartikeln verschiedener Größe"*.

Preparation course

1991-1992	Studienkolleg, Berlin

Education

1985-1991	High school, Jakarta
1978-1984	Primary school, Medan and Jakarta

Research experiences

1998-2000	Assistant at SFB 448 (Sonder-Forschungsbereich) part-project A7 "Mesokopische Verbundsysteme", Berlin Specifics: Synthesis and study of porous polymer Membranes used in heterogenous catalytic processes.
1996-1998	Assistant at Fraunhofer Institute for Silicium Technology (ISiT), Berlin Specifics: Investigations of Chemo and Biosensors used in the clinical medicine (HIV-Test system). Worked on different electrochemical

Publications

1. Synthesis and characterisation of porous polymere membrane produced by interparticle crosslinking.
   U. Mähr, H. Purnama, E. Kempin, R. Schomäcker, K.-H. Reichert, *J. Membrane of Science* **171,** (2000), 285

2. CO formation/selectivity of steam reforming of methanol with a commercial $CuO/ZnO/Al_2O_3$ catalyst.
   H. Purnama, T. Ressler, R. E. Jentoft, R. Schlögl, R. Schomäcker, (accepted in *Applied Catalysis A*)

3. Activity and Selectivity of a Nanostructured Cu/ZrO_2 Catalyst in the Steam Reforming of Methanol.
   H. Purnama, F. Girgsdies, T. Ressler, J. H. Schattka, R. Caruso, R. Schomäcker, R. Schlögl (submitted to *Catalysis Letters*)

German Patent Application

„Aktivierung und Langzeitstabilität von nanostrukturierten Kupfer-Zirkoniumdioxid-Katalysatoren für die Dampfreformierung von Methanol zur Gewinnung von Wasserstoff“, 4. March 2003

Poster and Oral presentation

1. Kinetische Untersuchung zum Steam-Reforming von Methanol (Poster)
   H. Purnama, R. Schomäcker, S. Winter, B. Bems, M. M. Günter, R. Schlögl
   „Deutscher Katalytiker“ annual conference, **Weimar**, March 2001

2. Kinetische Untersuchung zum Steam-Reforming von Methanol (Talk)
   H. Purnama
   Project meeting „ZEIT-Foundation“, **Berlin**, 23 Nov. 2001

3. Cu/ZrO_2 Catalysts for Methanol Steam Reforming (Poster)
   F. Girgsdies, H. Purnama, A. Szizybalski, T. Ressler, J. H. Schattka, Y. Q. Wang, R. Caruso
   „Deutscher Katalytiker“ annual conference, **Weimar**, 20-22 March 2002

4. Kinetische Untersuchung zum Steam-Reforming von Methanol (Poster)
   H. Purnama, R. Schomäcker, H. Soerijanto, M. M. Günter, T. Ressler, R. Caruso, M. Antonietti, R. Schlögl
   „Dechema“ annual conference, **Wiesbaden**, 11-13 June 2002

5. Kinetische Untersuchung zum Steam-Reforming von Methanol (Talk)
   H. Purnama
   Project meeting „ZEIT-Foundation”, **Hamburg**, 15 Nov. 2002

6. A Catalytic Study on Cu/ZrO_2 Catalysts for Methanol Steam Reforming (Poster)
   H. Purnama, R. Schomäcker, J. H. Schattka, R. Caruso, T. Ressler, R. Schlögl
   „Deutscher Katalytiker“ Annual conference, **Weimar**, 19-21 March 2003

7. Aktivitäts- und Selektivitätsuntersuchung von Cu/ZrO_2 Katalysatoren (Talk)
   H. Purnama
   Project meeting „ZEIT-Foundation”, **Mülheim**, 11 April 2003

Supervision of a Diploma Thesis

2002	„Kinetische Untersuchungen zum Reforming von Methanol“ by H. Soerijanto, **Berlin**